# SPECULAR SCATTERING OF ACOUSTIC WAVES FROM A ROUGH SURFACE IN THE FRAUNHOFER AND FRESNEL APPROXIMATIONS

APPROVED BY SUPERVISORY COMMITTEE:

C. W. Horton

Herbert A. Craig

Thomas G. Giuffre

F. W. de Wolf

J. D. Dawson

(6) SPECULAR SCATTERING OF ACOUSTIC WAVES FROM A ROUGH SURFACE IN THE FRAUNHOFER AND FRESNEL APPROXIMATIONS

(9) Doctoral Thesis

(11) Jan 69

(12) 144 p.

by

(10) DANIEL RAYBURN MELTON, B.S. in Physics, M. S. in Physics

(14) DRL-TM-68-20

(15) N00024-68-C-1112

DISSERTATION

Presented to the Faculty of the Graduate School of

The University of Texas at Austin

in Partial Fulfillment

of the Requirements

for the Degree of

DOCTOR OF PHILOSOPHY



THE UNIVERSITY OF TEXAS AT AUSTIN

January 1969

107 500

ACKNOWLEDGEMENTS

The success achieved in writing this dissertation is the result of the effort and cooperation of many people and organizations. The author wishes to express his appreciation to Dr. C. W. Horton, Sr., Chairman of the dissertation committee, for his suggestion of this topic and for his guidance and assistance during the progress of this work.

Appreciation is extended to The Texas Company, Bellaire Research Laboratories for granting a leave of absence so that the author could participate in both the academic and research programs of The University of Texas at Austin. During the past four years the author has been pleased to be the recipient of a Texaco Fellowship in Physics.

I wish to express my thanks to Mr. Garland Barnard, Special Research Associate and Supervisor of the Sonar Research Division of Applied Research Laboratories, for affording me the opportunity to engage in research at the Laboratory during my academic pursuit at the University of Texas at Austin. The goal of the experimental part of this dissertation could not have been achieved without the use of the equipment provided by the Applied Research Laboratories. Also, gratitude is due to members of the Reflection and Scattering Section of Applied Research Laboratories for lending their electronic skills and for their stimulating discussions of the theoretical aspects. Appreciation is expressed to Barbara Schulze and her staff of Technical Reports Office of Applied Research Laboratories for the final preparation of the dissertation.

Finally, the author wishes to offer his very special thanks to his wife for her patience and endurance.

Daniel Rayburn Melton

Austin, Texas
October, 1968

## ABSTRACT

This ~~dissertation~~ presents the results obtained in an experimental and theoretical study of the scattering of underwater acoustic waves from a rough surface. Four rough surfaces 32 in. by 32 in. in size were made of a pressure-release material. The reliefs of these surfaces were approximately Gaussian and were characterized by an exponential covariance function. The amplitude and relative phase of a pulsed wave scattered in the specular direction were measured at a frequency of 95.8 kHz for grazing angles from 6 deg to 80 deg. Both the directional source with a beamwidth of 9 deg measured at the half-power points and the omnidirectional receiver were placed at a slant-line distance of 60 in. from the scattering surface for all measurements. The measurements were used to calculate the amplitude fluctuations, the phase fluctuations, and the scattering coefficient. Theoretical formulas were developed for the fluctuations and the scattering coefficient in the Fraunhofer and the Fresnel approximations for the specular direction.

The theoretical approach of Gulin was used successfully in the Fresnel approximation to predict the observed amplitude fluctuations for values of the Rayleigh parameter less than 0.6. The experimental amplitude fluctuations reached a maximum at a Rayleigh parameter of 2.5 and for values between 4.5 and 7.4 the fluctuations disclosed a spread of 33 - 65 percent (relative to the average amplitude).

Gulin's theory in both the Fraunhofer and Fresnel approximations agreed with the experimental phase fluctuations to within 6 percent (relative to a radian) for values of the Rayleigh parameter less than 0.6. The experimental phase fluctuations varied from 12 to 250 percent (relative to a radian) over a range of values of Rayleigh parameters from 0.2 to 7.4.

The theoretical development in the Fraunhofer approximation had to be extended to the Fresnel approximation in order to obtain values for the scattering coefficient that were in good agreement with the measured

values in the specular direction. As the value of the Rayleigh parameter increased the difference between the theoretical values and the measured values of the scattering coefficient increased in both the Fraunhofer and Fresnel approximations. For values of the Rayleigh parameter near 1.8 the Fresnel theory predicted values within 2 dB of the experimental values of the scattering coefficient. When the Rayleigh parameter for the surface was 3.6 (7.2), the theoretical value for the scattering coefficient was 5 dB (10 dB) smaller than the experimental value. The need for the Fresnel theory was evident in that for values of the Rayleigh parameter near 7.2 the Fraunhofer theory predicted values that were 22 dB smaller than the experimental scattering coefficient.

TABLE OF CONTENTS

TABLE OF CONTENTS

## LIST OF TABLES

## LIST OF FIGURES

LIST OF FIGURES

LIST OF FIGURES

# CHAPTER I

# INTRODUCTION

The problem of the scattering of waves from a rough surface has interested physicists ever since Rayleigh (1896) first predicted the scattered field from a sinusoidal surface. His solution was limited to normal incidence and was applicable only when the wavelengths of the surface and the incident radiation were much larger than the surface amplitude. It was 67 years later before an exact solution for the problem of the reflection of a plane sound wave from a pressure-release corrugated surface was obtained by Uretsky (1963). He made no simplifying assumptions concerning the frequency of the incident radiation or the geometrical parameters of the sinusoidal surface. Uretsky (1965) has published an expanded paper in which he gives more details regarding his solution of this problem. Barnard, Horton, Miller, and Spitznogle (1966) have given experimental results which show that Uretsky's theory provides a satisfactory prediction of scattered sound field from a pressure-release sinusoidal surface when the amplitude of the sinusoid is comparable to the wavelength of the incident radiation.

The number of papers published in the area of underwater acoustics in the last 15 years has shown the growing interest in understanding the scattering of underwater sound by the sea bottom and the sea surface. The topography of these surfaces is neither periodic nor deterministic; in practice they can only be described by their statistical properties. The first general theory which predicted the field scattered by a perfectly reflecting statistically rough surface, the irregularities being large compared with the wavelength, was presented by Isakovich (1952). The problem was solved in the Kirchhoff approximation; that is, it was assumed that the field at each point of the surface could be represented as the sum of the incident wave and a wave reflected from the plane tangent to the surface at the given point. In addition, the Fraunhofer (farfield) approximation was used throughout the paper. The rough surface that

was studied by Isakovich was isotropic and characterized by a Gaussian covariance function.

Eckart (1953) presented a theory which predicted the field scattered by a pressure release or rigid surface that was randomly rough and isotropic. His theory for a directional source leads to useful expressions for two limiting cases:

(1) when the wavelength of the incident radiation is much greater than the largest values of the surface relief, and

(2) when the wavelength is much less than the surface relief.

The Kirchhoff and the Fraunhofer approximations were employed throughout the paper. Eckart did not consider any specific covariance functions.

Apparently, the first theory in the Fresnel approximation (as opposed to the Fraunhofer approximation) was presented by Feinstein (1954). The method of physical optics (Kirchhoff approximation) was used to predict the field scattered from a randomly rough surface characterized by a Gaussian covariance function. Also, he employed the exponential covariance function to describe the field scattered from a one-dimensional rough surface. All formulas were restricted to the specular direction.

Clay (1960) extended the theory of Eckart (1953) to include an omnidirectional source. A Gaussian covariance function for the rough surface was assumed for the calculations. Considering only the long wavelength case, Clay compared his theoretical results for the amplitude fluctuations to the fluctuations of the sound reflected from the sea surface measured by Brown and Ricard (1960). The numerical calculations of scattered sound had the same dependence on the source-receiver separation as the experimental data.

Formulas for the amplitude and phase fluctuations of a sound wave reflected from a statistically uneven surface were derived by Gulin (1962). His theoretical approach was similar to that of Eckart (1953) except that all calculations were made in the Fresnel approximation and were confined to the specular direction. Only the long wavelength case in the Kirchhoff approximation was considered. The

details were given for the derivation of the fluctuations of a spherical wave scattered from a rough surface characterized by a one-dimensional quasi-harmonic Gaussian covariance function. The details in the development using a two-dimensional Gaussian covariance function were omitted. The theoretical results for the amplitude fluctuations obtained with the one-dimensional quasi-harmonic Gaussian covariance function were compared with the results of an experimental investigation made by Gulin and Malyshev (1962) of the amplitude fluctuations of sound signals reflected from the undulating surface of the sea. The experimental amplitude fluctuations increased linearly with the Rayleigh parameter up to values of the latter equal to approximately 0.7 and corresponded to the theoretical law over this range of Rayleigh parameters. For Rayleigh parameters between 0.7 and 3.5 there was a well defined alternation of experimental amplitude coefficient of variation between maximum and minimum values. This saturation effect at large values of the Rayleigh parameter could not possibly be explained by means of the theoretical analysis, as the region of applicability of the analytical formulas was limited by the condition that the Rayleigh parameter must be less than one. It was stated by these authors that the conclusion of the maxima and minima in the saturation region of the coefficient of variation should be considered as a tentative result and in need of further verification. No experimental data were given for the phase fluctuations.

The problem of the scattering of waves from a rough surface has been the subject of at least one monograph written by Beckmann and Spizzichino (1963). This book provides an excellent survey of the literature. Beckmann's approach to the problem is more general than that of Isakovich (1952) and that of Eckart (1953) in that it is not restricted to the special cases of a short wavelength or a long wavelength assumption. Beckmann employed both the Kirchhoff and the Fraunhofer approximation throughout the theoretical analysis. A rough surface characterized by a Gaussian covariance function was investigated. Later, Beckmann (1965) discussed the scattering of a wave from a rough surface characterized by an exponential covariance

function. Medwin (1966) modified Beckmann's theory to account for the error inherent in the common assumption of uniform insonification over a fixed area.

Horton and Muir (1967) have employed the theory of Eckart (1953) to study the scattering from isotropically rough surfaces whose covariance functions are exponential, Gaussian, and sinusoidal. The effect of the radiation pattern of the source upon the scattered intensity was discussed by inserting an analytical expression for the transducer pattern. In a companion paper Horton, Mitchell, and Barnard (1967) produced surprising experimental evidence of the validity of a modified form of Eckart's theory in the short wavelength case. These experimental studies were performed on a model surface whose covariance function was exponential. The theory was developed in the Kirchhoff and the Fraunhofer approximations.

Of the references quoted here only two, Feinstein (1954) and Gulin (1962), have studied the problem of scattering from a rough surface in the Fresnel approximation. Neither have compared their results with the corresponding solutions in the Fraunhofer approximation. One might question whether or not the extension of the mathematical analysis of the problem from the Fraunhofer to the Fresnel approximation would give better agreement between the theoretical and experimental results. No one to the author's knowledge has presented a solution in the Fresnel approximation to the problem of scattering from a randomly rough surface whose statistical properties are given by an exponential covariance function. One is further motivated to investigate the scattering of acoustic waves from this type of surface since there are available model surfaces that are characterized by an exponential covariance function. Those model surfaces whose statistical properties were analyzed by Horton, Hoffman, and Hemkins (1962) give an excellent means of experimental verification of the theoretical results.

The plan of study will be the following. In Chapter II general expressions are derived for the amplitude and phase fluctuations of an acoustic wave scattered in the specular direction from a randomly

rough surface. The theoretical approach is that of Gulin (1962). In the same chapter general expressions are obtained for the scattering coefficient derived in a manner similar to that presented by Beckmann (1963). Throughout Chapter II there is a parallel presentation of the integral expressions obtained in the Fraunhofer and Fresnel approximation. The expressions for the amplitude and phase fluctuations will be valid only for Rayleigh parameters less than one whereas the formulas for the scattering coefficient should be correct for any value of the Rayleigh parameter. The calculations in this initial study shall be confined to the specular direction where the mathematical analysis is less cumbersome.

In Chapter III the problem is specialized to the case where the statistical properties of the rough surface are described by an exponential covariance function. The integral expressions occurring in Chapter II are solved giving formulas for the amplitude fluctuations, phase fluctuations, and scattering coefficient that can be used to describe the experimental results.

The statistical properties of the model surfaces used in the experimental work are discussed in Chapter IV. This section presents a list of the experimental equipment and gives an explanation of the experimental procedures used to measure the fluctuations and the scattered intensity.

The experimental data are compared with the theoretical formulas in Chapter V, a general discussion is presented in Chapter VI, and the conclusions of this study are stated in Chapter VII.

The theory presented in Chapters II and III and in Appendixes A and C can best be followed by referring to the block diagrams in Figs. 1 and 2.

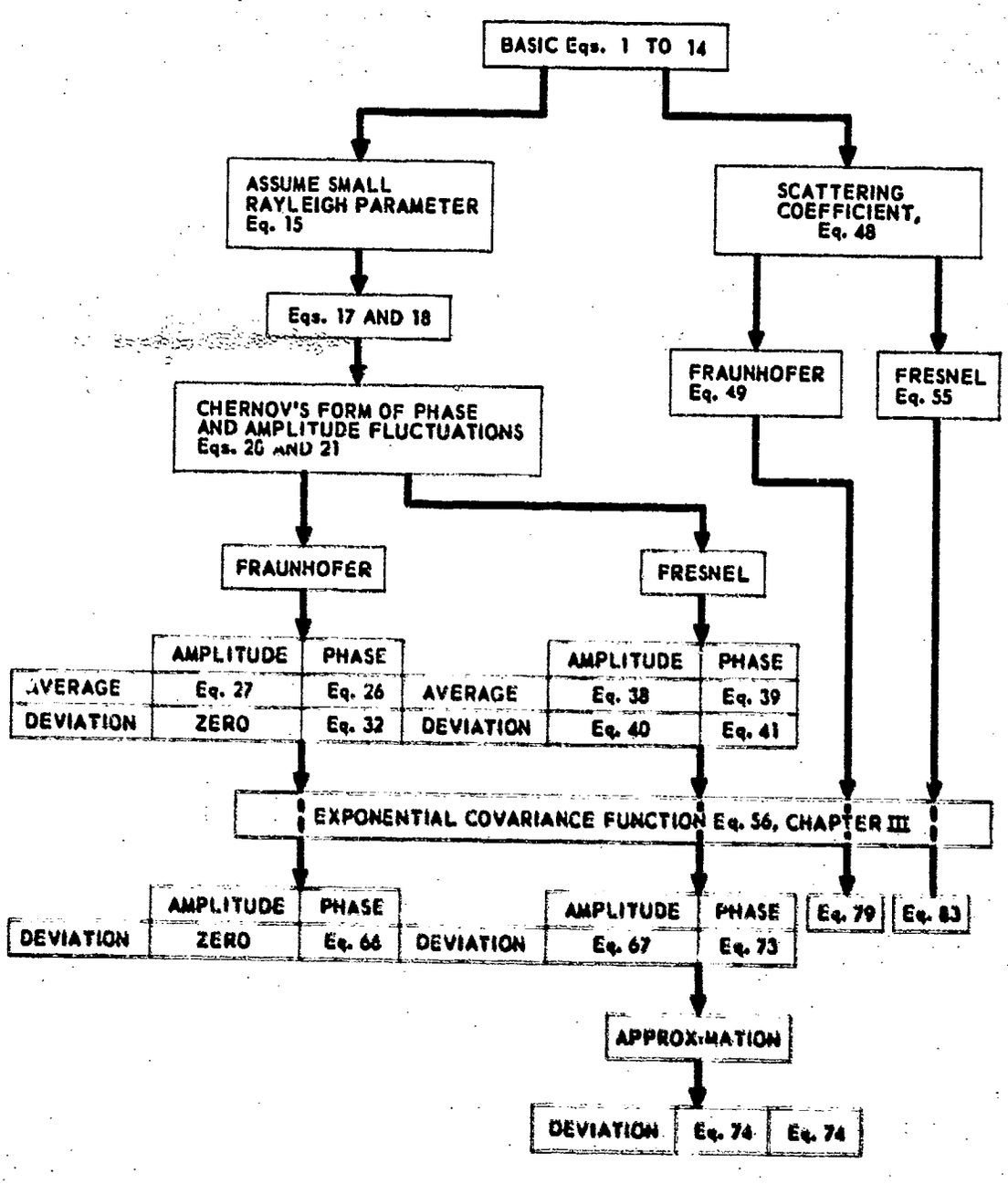


FIGURE 1
PRIMARY CALCULATIONS

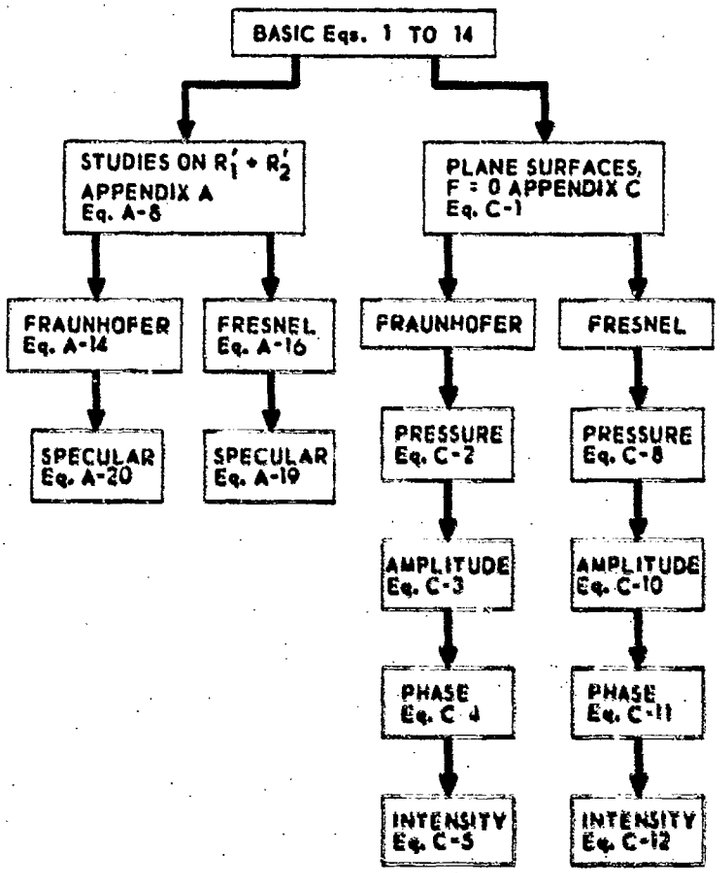


**FIGURE 2**
**AUXILIARY CALCULATIONS**

## CHAPTER II

## THEORETICAL APPROACH

General expressions are derived for the amplitude and phase fluctuations, and for the scattering coefficient in the specular direction for an acoustic wave scattered from a randomly rough surface. The theoretical approach that is used is the method presented by E. P. Gulin (1962). Gulin's notation will be maintained in this paper.

### A. The Pressure Field

The coordinates of the source $(0,0,z_1)$ and the receiver $(L,0,z_2)$ are illustrated in Fig. 3. $\psi_1$ is the grazing angle. $\psi_2$ is the receiving angle measured with respect to the x-axis. The axis of the directional source is directed toward the point on the surface labeled O'. The x-y plane is oriented so that the average height of the interface above this plane is zero. $R_{10}$ is the distance from the source to the point O' which is located on the x-y plane. $R_1$ is the distance from the source to any arbitrary point on the randomly rough surface. $R_1'$ is the distance from the source to a point on the x-y plane directly above or below the arbitrary point on the scattering surface. The distances $R_{20}$, $R_2$, and $R_2'$ to the receiver are defined in the same way.

The total pressure field p of a sound wave reflected from an uneven surface can be written in terms of the Helmholtz integral, Baker and Copson (1939),

$$p = \frac{1}{4\pi} \iint_S \left[ -p \frac{\partial}{\partial n} \left( \frac{e^{ikR_2}}{R_2} \right) + \frac{e^{ikR_2}}{R_2} \frac{\partial p}{\partial n} \right] dS \quad , \qquad (1)$$

where $\underline{n}$ is the outward normal to the surface (in a direction away from source and receiver). The wave incident on the surface is assumed to be a sperical wave given by

$$p_o' = \frac{e^{ikR_1}}{R_1} \qquad (2)$$

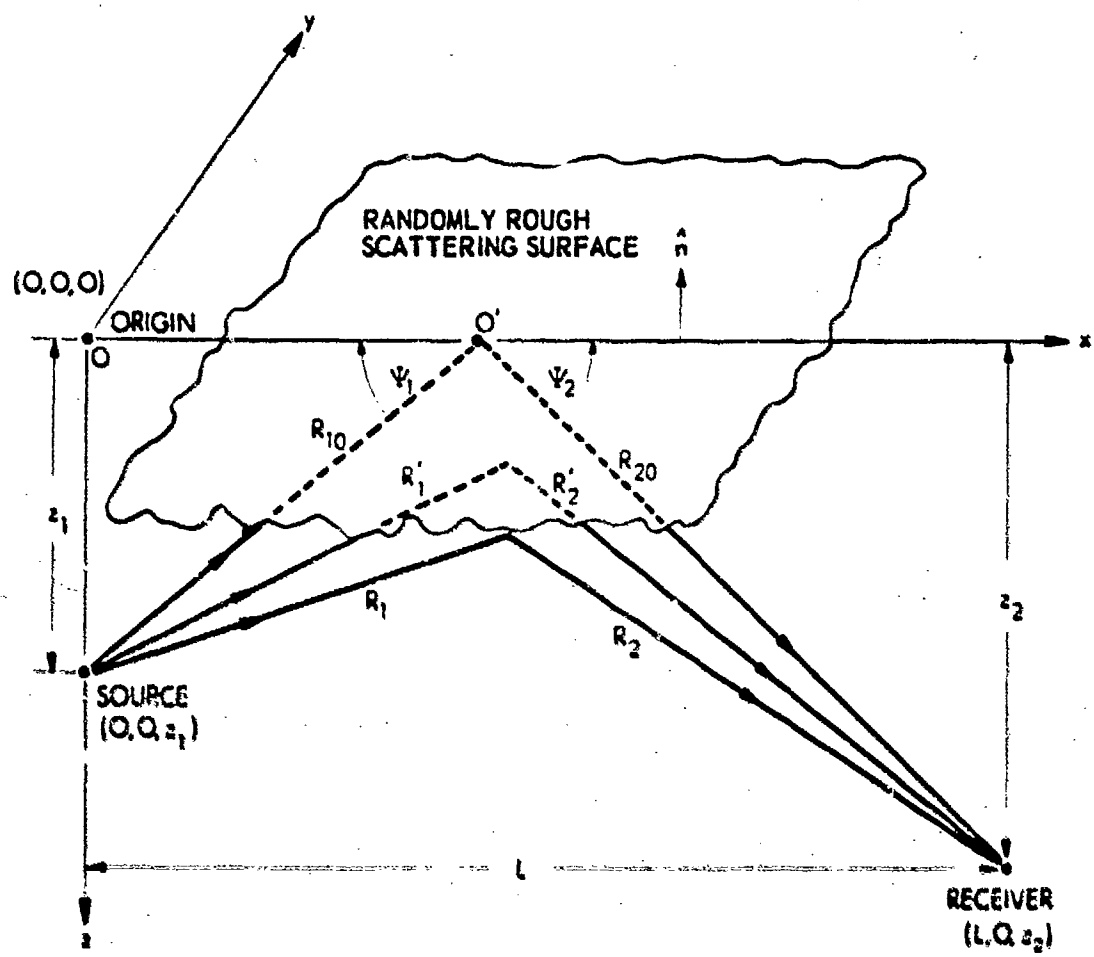


**FIGURE 3**
**COORDINATE SYSTEM**

The field at the surface S is specified after the example of Eckart (1953) for the special case of a "pressure release" surface. The boundary conditions at the surface S are

$$p'_o + p = 0 \quad , \text{ and} \tag{3}$$

$$\frac{\partial p'_o}{\partial n} = \frac{\partial p}{\partial n} \quad . \tag{4}$$

The application of these boundary conditions corresponds to the Kirchhoff approximation in the problem of sound scattering by rough surfaces. The applicability of this approximation has been formulated by Brekhovskikh (1952) and Isakovich (1952), and has been discussed by Beckmann (1953).

Substituting Eqs. (2), (3), and (4) into Eq. (1) one obtains

$$p = \frac{ik}{4\pi} \iint_S \left[ \left( \frac{\partial R_1}{\partial n} + \frac{\partial R_2}{\partial n} \right) + \left( \frac{i\lambda}{2\pi R_1} \frac{\partial R_1}{\partial n} + \frac{i\lambda}{2\pi R_2} \frac{\partial R_2}{\partial n} \right) \right] \frac{e^{ik(R_1+R_2)}}{R_1 R_2} \, dS \quad , \tag{5}$$

where $\lambda$ is the wavelength of the incident radiation. If it is assumed

$$R_1 \gg \lambda \quad , \text{ and} \tag{6}$$

$$R_2 \gg \lambda$$

the second group of terms can be neglected, which reduces Eq. (5) to

$$p = \frac{ik}{4\pi} \iint_S \frac{1}{R_1 R_2} \left( \frac{\partial R_1}{\partial n} + \frac{\partial R_2}{\partial n} \right) e^{ik(R_1+R_2)} dS \quad . \tag{7}$$

In the case of irregularities of sufficiently small slope differentiation along the normal can be approximately replaced by

differentiation along the negative z-axis, and integration over the rough surface by integration over the x-y plane.† Thus, Eq. (7) becomes

$$p = -\frac{ik}{4\pi} \iint \frac{1}{R_1 R_2} \left( \frac{\partial R_1}{\partial z} + \frac{\partial R_2}{\partial z} \right) e^{ik(R_1+R_2)} dxdy \quad . \tag{8}$$

Introducing the new terms $z_1'$, $z_2'$, and F which are depicted in Fig. 4, one can show that

$$\frac{\partial R_1}{\partial z} = -\frac{z_1'}{R_1} \quad , \quad \frac{\partial R_2}{\partial z} = -\frac{z_2'}{R_2} \quad .$$

Eq. (8) becomes

$$p = \frac{ik}{4\pi} \iint \frac{1}{R_1 R_2} \left( \frac{z_1'}{R_1} + \frac{z_2'}{R_2} \right) e^{ik(R_1+R_2)} dxdy \quad . \tag{9}$$

F is the deviation of the surface relief from the average height. If it is assumed that $|F|$ is much less than the minimum of $z_1$ and $z_2$, then

$$R_1 = \left[ x^2 + y^2 + (z_1 - F)^2 \right]^{1/2}$$

can be written as

$$R_1 = \left( x^2 + y^2 + z_1^2 \right)^{1/2} \left( 1 - \frac{Fz_1}{x^2 + y^2 + z_1^2} \right) \quad .$$

† Beckman (1963) inserts the "local" scattering geometry of the normal derivative at the surface in his theoretical approach. This method introduces the term

$$\frac{1 + \sin\psi_1 \sin\psi_2 - \cos\psi_1 \cos\psi_2}{\sin\psi_1 (\sin\psi_1 + \sin\psi_2)} \quad ,$$

which reduces to one in the specular direction ($\psi_1 = \psi_2$).

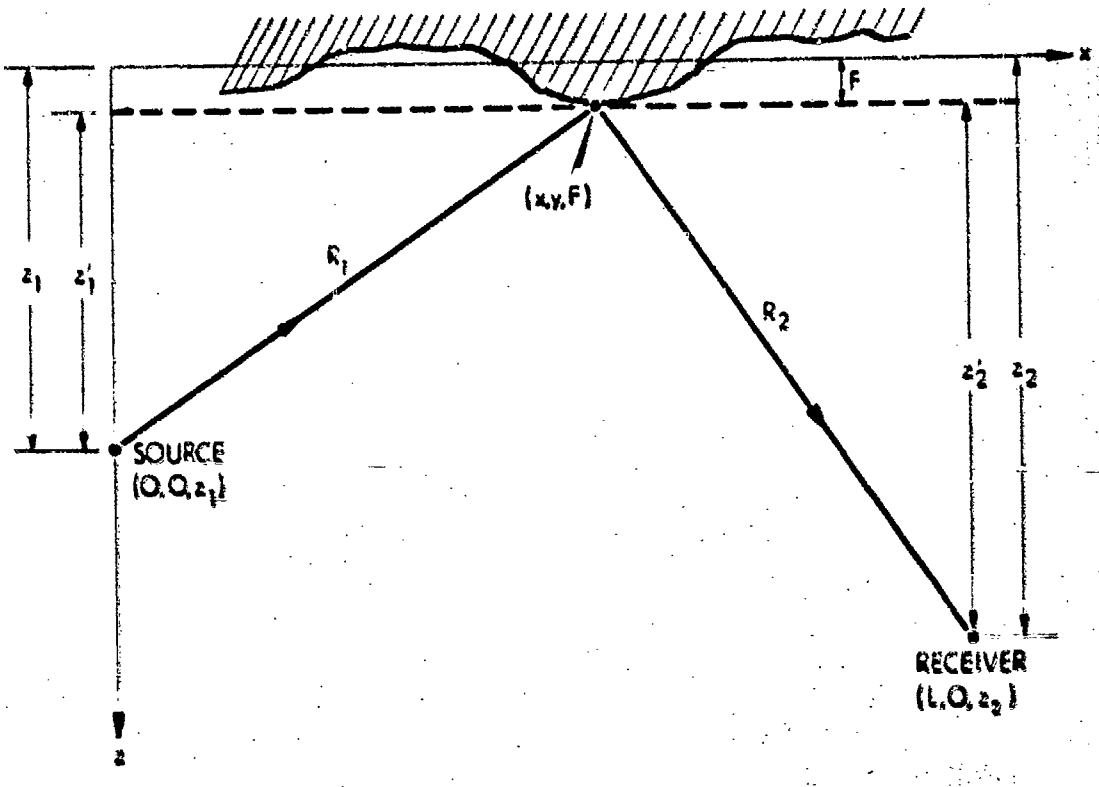


FIGURE 4
RANDOM QUANTITIES $z_1', z_2', F$

Defining (see Fig. 3)

$$R_1' = \left(x^2 + y^2 + z_1^2\right)^{1/2} \quad , \tag{10}$$

one can write $R_1$ as

$$R_1 \approx R_1' - \frac{z_1 F}{R_1'} \quad . \tag{11}$$

Similarly

$$R_2 = \left[(L - x)^2 + y^2 + (z_2 - F)^2\right]^{1/2} \quad ,$$

and $R_2$ can be written as

$$R_2 = \left[(L - x)^2 + y^2 + z_2^2\right]^{1/2}\left[1 - \frac{Fz_2}{(L - x)^2 + y^2 + z_2^2}\right] \quad .$$

Defining

$$R_2' = \left[(L - x)^2 + y^2 + z_2^2\right]^{1/2} \quad , \tag{12}$$

one can write $R_2$ as

$$R_2 \approx R_2' - \frac{z_2 F}{R_2'} \quad . \tag{13}$$

The approximations given by Eqs. (11) and (13) reduce Eq. (9) to

$$P \approx \frac{ik}{4\pi} \iint \frac{e^{ik(R_1' + R_2')}}{R_1' R_2'} \left[\left(\frac{z_1}{R_1'} + \frac{z_2}{R_2'}\right) - F\left(\frac{1}{R_1'} + \frac{1}{R_2'}\right)\right]$$

$$\times e^{-ikF\left(\frac{z_1}{R_1'} + \frac{z_2}{R_2'}\right)} dxdy \quad .$$

Since $F \ll z_1$ and $F \ll z_2$, the second term in the square brackets can be neglected. The pressure becomes

$$p = \frac{ik}{4\pi} \iint \frac{e^{ik(R_1'+R_2')}}{R_1'R_2'} \cdot \left(\frac{z_1}{R_1'} + \frac{z_2}{R_2'}\right) e^{-ikF\left(\frac{z_1}{R_1'} + \frac{z_2}{R_2'}\right)} dxdy \quad . \quad (14)$$

If the acoustic wavelength, $\lambda$, is greater than the surface relief, $F(x,y)$, or if the grazing angle is small, so that the following condition holds

$$\left| kF\left(\frac{z_1}{R_1'} + \frac{z_2}{R_2'}\right) \right| < 1 \quad , \quad (15)$$

then

$$e^{-ikF\left(\frac{z_1}{R_2'} + \frac{z_2}{R_2'}\right)} \approx 1 - ikF\left(\frac{z_1}{R_1'} + \frac{z_2}{R_1'}\right) \quad . \quad (16)$$

This approximation separates Eq. (14) into a nonfluctuating component

$$p_o = \frac{ik}{4\pi} \iint \frac{1}{R_1'R_2'} \left(\frac{z_1}{R_1'} + \frac{z_2}{R_2'}\right) e^{ik(R_1'+R_2')} dxdy \quad , \quad (17)$$

and a scattered, fluctuating component

$$p_1 = \frac{k^2}{4\pi} \iint \frac{1}{R_1'R_2'} \left(\frac{z_1}{R_1'} + \frac{z_2}{R_2'}\right)^2 e^{ik(R_1'+R_2')} F(x,y) dxdy \quad . \quad (18)$$

The pressure $p_o$ reflected from a plane "pressure release" surface is evaluated for the specular direction in Appendix C.

B. Amplitude and Phase Fluctuations in the Fraunhofer Approximation

The transition from the expressions for the sound field to expressions for the amplitude and phase fluctuations can be carried out by using a method utilized by Chernov (1960). The total pressure given by Eqs. (17) and (18)

$$p = p_o + p_1$$

can be written as

$$Ae^{i\Phi} = A_o e^{i\Phi_o} + A_1 e^{i\Phi_1} \quad , \text{ or}$$

$$\frac{A}{A_o} e^{i(\Phi-\Phi_o)} = 1 + \frac{A_1}{A_o} e^{i(\Phi_1-\Phi_o)} \quad . \tag{19}$$

Assuming that

$$A_1 \ll A_o \quad ,$$

one can set

$$A = A_o + \delta A \quad , \text{ and}$$

$$\Phi = \Phi_o + \delta\Phi \quad .$$

These approximations, with the use of the logarithm and $\ln(1+\epsilon) \approx \epsilon$ when $|\epsilon| \ll 1$, reduce Eq. (19) to

$$\frac{\delta A}{A_o} + i\delta\Phi \approx \frac{A_1}{A_o} e^{i(\Phi_1-\Phi_o)} \quad .$$

Since the right side of this equality is Eq. (18) divided by $A_o e^{i\Phi_o}$, one has for the variation in the amplitude

$$\frac{\delta A}{A_o} = \frac{k^2}{4\pi A_o} \iint \frac{1}{R_1' R_2'} \left(\frac{z_1}{R_1'} + \frac{z_2}{R_2'}\right)^2 \cos\left[k(R_1' + R_2') - \Phi_o\right] F(x,y)\,dx\,dy \quad , \tag{20}$$

and for the variation in phase

$$\delta\Phi = \frac{k^2}{4\pi A_o} \iint \frac{1}{R_1' R_2'} \left( \frac{z_1}{R_1'} + \frac{z_2}{R_2'} \right)^2 \sin\left[ k(R_1' + R_2') - \Phi_o \right] F(x,y)\,dx\,dy \quad . \quad (21)$$

In the Fraunhofer approximation (Appendix A, Eq. (A-20) for the specular direction

$$R_1' + R_2' \approx R_{10} + R_{20} \quad ,$$

so that the variation in amplitude is

$$\frac{\delta A}{A_o} = \frac{k^2 \sin^2 \psi \cos\left[ k(R_{10} + R_{20}) - \Phi_o \right]}{\pi A_o R_{10} R_{20}} \iint F(x_1,y)\,dx_1\,dy \quad . \quad (22)$$

where (Appendix A, Eq. (A-1)

$$x_1 = x - \frac{L z_1}{z_1 + z_2} \quad .$$

The variation in phase is

$$\delta\Phi = \frac{k^2 \sin^2 \psi \sin\left[ k(R_{10} + R_{20}) - \Phi_o \right]}{\pi A_o R_{10} R_{20}} \iint F(x_1,y)\,dx_1\,dy \quad . \quad (23)$$

$A_o$ and $\Phi_o$ are given by Eqs. (C-3) and (C-4) in Appendix C. These values reduce Eqs. (22) and (23) to

$$\frac{\delta A}{A_o} = 0 \quad , \text{ and} \quad (24)$$

$$\delta\Phi = \frac{k \sin \psi}{l(\Delta_1 + \Delta_2)} \int_{-\Delta_1}^{\Delta_2} \int_{-l}^{l} F(x_1,y)\,dx_1\,dy \quad , \quad (25)$$

where $\Delta_1$, $\Delta_2$, and $\ell$ are the dimensions of the active scattering area defined in Appendix B. $\delta\Phi$ is zero only if the integration extends over a significant area of the surface. If the active scattering region is small compared to the correlation distance, $\delta\Phi$ is likely to differ from zero for each single measurement.

Since $F(x_1,y)$ is a random variable, the quantities of interest are the ensemble averages. It is assumed that the surface relief is distributed so that

$$\left\langle \delta\Phi \right\rangle = 0 \quad . \tag{26}$$

Since the variation in amplitude is identically zero, one can write

$$\left\langle \frac{\delta A}{A_o} \right\rangle = 0 \quad , \tag{27}$$

without reference to the distribution of the surface relief.

The variance of a random variable v is defined as the average square of the deviation from the mean value

$$D(v) = \left\langle (v - \langle v \rangle)^2 \right\rangle = \left\langle v^2 \right\rangle - \left\langle v \right\rangle^2 \quad . \tag{28}$$

The square root of the variance,

$$\sigma = \sqrt{D(v)} \quad , \tag{29}$$

is called the standard deviation. Thus, utilizing Eq. (27), one can write for the relative standard deviation of the amplitude the expression

$$\sigma_A = \frac{1}{A_o} \sqrt{\left\langle (\delta A)^2 \right\rangle} \quad , \tag{30}$$

which hereafter will be called the amplitude fluctuations. In the same way

$$\sigma_\Phi = \sqrt{\left\langle (\delta\Phi)^2 \right\rangle} \quad , \tag{31}$$

will represent the phase fluctuations.

Eq. (24) indicates that the amplitude fluctuations in the specular direction are zero in the Fraunhofer field zone. To determine the phase fluctuations in the specular direction in the Fraunhofer approximation Eq. (25) is squared and averaged to give

$$\left\langle (\Im)^2 \right\rangle = \frac{k^2 \sin^2 \psi}{\ell^2(\Delta_1 + \Delta_2)^2} \times \int_{-\Delta_1}^{\Delta_2} \int_{-\ell}^{\ell} \int_{-\Delta_1}^{\Delta_2} \int_{-\ell}^{\ell} \left\langle F(x_1,y)F(x_1',y') \right\rangle dx_1 dy dx_1' dy' \quad , \tag{32}$$

where $\left\langle F(x_1,y)F(x_1',y') \right\rangle$ is defined as the spatial covariance function of the surface displacements. A complete solution of the problem will be delayed until Chapter III where by Eq. (56) an exponential convariance function is specified.

C. Amplitude and Phase Fluctuations in the Fresnel Approximation

The Fresnel approximation for the expansion of $R_1' + R_2'$ in the specular direction is given by Eq. (A-19) in Appendix A,

$$R_1' + R_2' = R_{10} + R_{20} + \frac{1}{R}(x_1^2 \sin^2 \psi + y^2) \quad , \tag{33}$$

where

$$R = \frac{2R_{10}R_{20}}{R_{10} + R_{20}} \quad . \tag{34}$$

Substitution of Eq. (33) into Eq. (20) gives for the variation in amplitude

$$\frac{\delta A}{A_0} = \frac{k^2 \sin^2 \psi}{\pi R_{10} R_{20} A_0} \iint \cos\left[\frac{kx_1^2 \sin^2 \psi}{R} + \frac{ky^2}{R} - \phi_0'\right] F(x_1,y)dx_1 dy \quad , \tag{35}$$

where

$$\phi_0' = \phi_0 - k(R_{10} + R_{20}) \quad . \tag{36}$$

$A_o$ and $\Phi_o$ are given by Eqs. (C-10) and (C-11) in Appendix C. Eqs. (33) and (21) give for the variation in phase

$$\delta\Phi = \frac{k^2 \sin^2 \psi}{\pi R_{10} R_{20} A_o} \iint \sin\left[\frac{kx_1^2 \sin^2 \psi}{R} + \frac{ky^2}{R} - \Phi_o'\right] F(x_1,y)\,dx_1\,dy \quad . \tag{37}$$

Assuming that the surface relief is distributed such that $\left\langle F(x_1,y)\right\rangle = 0$, the ensemble average of Eqs. (35) and (37) gives

$$\left\langle \frac{\delta A}{A_o} \right\rangle = 0 \quad , \text{ and} \tag{38}$$

$$\left\langle \delta\Phi \right\rangle = 0 \quad . \tag{39}$$

It is of interest to point out that in the Fraunhofer approximation $\delta A/A_o$ is identically zero, whereas in the Fresnel case it is only the average value $\left\langle \delta A/A_o \right\rangle$ that vanishes.

Squaring and averaging Eq. (35) and utilizing Eq. (38) one obtains for the square of the amplitude fluctuations

$$\frac{\left\langle (\delta A)^2 \right\rangle}{A_o^2} = \frac{k^4 \sin^4 \psi}{\pi^2 R_{10}^2 R_{20}^2 A_o^2} \iiiint \cos\left[\frac{kx_1^2 \sin^2 \psi}{R} + \frac{ky^2}{R} - \Phi_o'\right]$$

$$\times \cos\left[\frac{kx_1'^2 \sin^2 \psi}{R} + \frac{ky'^2}{R} - \Phi_o'\right] \tag{40}$$

$$\times \left\langle F(x_1,y)F(x_1',y')\right\rangle dx_1\,dy\,dx_1'\,dy' \quad .$$

Eqs. (37) and (39) give for the square of the phase fluctuations

$$\left\langle (\delta\Phi)^2 \right\rangle = \frac{k^4 \sin^4 \psi}{\pi^2 R_{10}^2 R_{20}^2 A_o^2} \int\int\int\int \sin\left[\frac{kx_1^2 \sin^2 \psi}{R} + \frac{ky^2}{R} - \Phi_o'\right]$$

$$\times \sin\left[\frac{kx_1'^2 \sin^2 \psi}{R} + \frac{ky'^2}{R} - \Phi_o'\right] \tag{41}$$

$$\times \left\langle F(x_1, y) F(x_1', y') \right\rangle dx_1 dy dx_1' dy' \quad .$$

The development of Eqs. (40) and (41) will be continued in Eqs. (67) and (73) of Chapter III, respectively.

D. Scattering Coefficient in the Fraunhofer Approximation

The Fraunhofer approximation in the specular direction is the substitution from Eq. (A-20) in Appendix A of

$$R_1' + R_2' = R_{10} + R_{20}$$

into the exponential of Eq. (14). With $z_1 = R_{10} \sin \psi$ and $z_2 = R_{20} \sin \psi$ Eq. (14) becomes

$$p = \frac{ik (\sin \psi) e^{ik(R_{10}+R_{20})}}{2\pi R_{10} R_{20}} \int\int e^{-2ikR \sin\psi} dx_1 dy \quad . \tag{42}$$

The intensity of the scattered wave is defined as

$$I = \frac{(pp^*)}{2\rho v} \quad ,$$

where

$\rho$ is the density,

$v$ is the velocity of the medium through which the wave is propagating,

$p^*$ is the complex conjugate of the pressure $p$.

The product $\rho v$ is called the specific acoustic impedance of the medium. Forming the product $pp^*$ from Eq. (42) and taking the ensemble average, one obtains

$$\left\langle pp^* \right\rangle = \frac{k^2 \sin^2 \psi}{4\pi^2 R_{10}^2 R_{20}^2} \times \iiiint \left\langle e^{-2ik(\sin\psi)[F(x_1,y)-F(x_1',y')]} \right\rangle dx_1 dy dx_1' dy' \quad . \tag{43}$$

It is assumed that the surface relief of the rough surface is characterized by a bivariate Gaussian distribution function, Eckart (1953) and Horton and Muir (1967), defined by

$$W_2(x_1,y,F,x_1',y',F') = \frac{1}{2\pi\sqrt{\left\langle F_o^2 \right\rangle^2 - C^2}} \times e^{-\frac{\left\langle F_o^2 \right\rangle F^2 - 2FF'C + \left\langle F_o^2 \right\rangle F'^2}{2\left(\left\langle F_o^2 \right\rangle^2 - C^2\right)}} \quad , \tag{44}$$

where

$$C = \left\langle F(x_1,y)F(x_1',y') \right\rangle \quad , \tag{45}$$

is the spatial covariance function of the surface displacements, and $\left\langle F_o^2 \right\rangle$ is the mean-square amplitude of the surface irregularities. It can be shown that with this function one obtains

$$\left\langle e^{-2ik(\sin\psi)(F-F')} \right\rangle = e^{-4k^2 \left\langle F_o^2 \right\rangle (\sin^2\psi)\left(1 - \frac{C}{\left\langle F_o^2 \right\rangle}\right)} \quad . \tag{46}$$

Eq. (46) reduces Eq. (43) to

$$\left\langle pp^* \right\rangle = \frac{k^2 \sin^2 \psi}{4\pi^2 R_{10}^2 R_{20}^2} e^{-4k^2 \left\langle F_o^2 \right\rangle \sin^2 \psi} \times \int\int\int\int e^{4k^2 C \sin^2 \psi} dx_1 dy dx_1' dy' \quad . \tag{47}$$

The scattering coefficient $\sigma_s$ is defined as the ratio of the intensity scattered from a rough surface to the intensity reflected from a plane surface,

$$\sigma_s = \frac{\langle I \rangle}{I_o} = \frac{\langle pp^* \rangle}{(p_o p_o^*)} \quad . \tag{48}$$

The term $p_o p_o^*$, which is proportional to the intensity reflected from a plane surface, is given in Appendix C by Eq. (C-5),

$$p_o p_o^* = \frac{k^2 \ell^2 (\Delta_1 + \Delta_2)^2 \sin^2 \psi}{\pi^2 R_{10}^2 R_{20}^2} \quad ,$$

where $\Delta_1$, $\Delta_2$, and $\ell$ are the dimensions of the active scattering region discussed in Appendix B. Thus, the scattering coefficient in the Fraunhofer approximation in the specular direction is given by

$$\sigma_s = \frac{1}{4\ell^2 (\Delta_1 + \Delta_2)^2} e^{-4k^2 \left\langle F_o^2 \right\rangle \sin^2 \psi} \times \int_{-\Delta_1}^{\Delta_2} \int_{-\ell}^{\ell} \int_{-\Delta_1}^{\Delta_2} \int_{-\ell}^{\ell} e^{4k^2 C \sin^2 \psi} dx_1 dy dx_1' dy' \quad . \tag{49}$$

The investigation of $\sigma_s$ will be continued with Eq. (75) in Chapter III.

E. Scattering Coefficient in the Fresnel Approximation

The Fresnel approximation in the specular direction is the substitution of Eq. (A-19) of Appendix A

$$R_1' + R_2' = R_{10} + R_{20} + \frac{1}{R}\left(x_1^2 \sin^2\psi + y^2\right)$$

into the exponential of Eq. (14). Putting $z_1 = R_{10}\sin\psi$ and $z_2 = R_{20}\sin\psi$, one obtains

$$p = \frac{ik\,(\sin\psi)e^{ik(R_{10}+R_{20})}}{2\pi R_{10}R_{20}} \iint e^{\frac{ik}{R}\left(x_1^2\sin^2\psi+y^2\right)-2ikF\sin\psi}\,dx_1dy \quad . \quad (50)$$

Forming the product $pp^*$, taking the ensemble average, one obtains

$$\left\langle pp^* \right\rangle = \frac{k^2\sin^2\psi}{4\pi^2 R_{10}^2 R_{20}^2} \times \iiint\!\!\int e^{i\left[\frac{k}{R}\left(x_1^2 - x_1'^2\right)\sin^2\psi + \frac{k}{R}\left(y^2 - y'^2\right)\right]} \quad (51)$$

$$\times \left\langle e^{-2ik(\sin\psi)\left[F(x_1,y)-F(x_1',y')\right]} \right\rangle dx_1dydx_1'dy' \quad .$$

With the aid of Eq. (46), Eq. (51) can be written as

$$\left\langle pp^* \right\rangle = \frac{k^2 \sin^2 \psi}{4\pi^2 R_{10}^2 R_{20}^2} e^{-4k^2 \left\langle F_o^2 \right\rangle \sin^2 \psi}$$

$$\times \int\int\int\int e^{i \left[\frac{k}{R}\left(x_1^2 - x_1'^2\right) \sin^2 \psi + \frac{k}{R}\left(y^2 - y'^2\right)\right]} \qquad (52)$$

$$\times e^{4k^2 C \sin^2 \psi} dx_1 dy dx_1' dy' \quad .$$

The intensity reflected from a plane surface in the Fresnel approximation is proportional to the expression given by Eq. (C-12) in Appendix C,

$$p_o p_o^* = \frac{K}{(R_{10} + R_{20})^2} \quad , \qquad (53)$$

where

$$K = \left[C_\ell \left(C_{\Delta_1} + C_{\Delta_2}\right) - S_\ell \left(S_{\Delta_1} + S_{\Delta_2}\right)\right]^2 + \left[S_\ell \left(C_{\Delta_1} + C_{\Delta_2}\right) + C_\ell \left(S_{\Delta_1} + S_{\Delta_2}\right)\right]^2 \quad . \qquad (54)$$

The Fresnel integrals, S and C, are defined by Eq. (C-9) in Appendix C.

The scattering coefficient is the ratio of Eqs. (52) and (53),

$$\sigma_s = \frac{k^2(R_{10} + R_{20})^2 \sin^2\psi}{4\pi^2 R_{10}^2 R_{20}^2 K} e^{-4k^2\left\langle F_o^2\right\rangle \sin^2\psi}$$

$$\times \int_{-\Delta_1}^{\Delta_2} \int_{-\ell}^{\ell} \int_{-\Delta_1}^{\Delta_2} \int_{-\ell}^{\ell} e^{i\left[\frac{k}{R}\left(x_1^2 - x_1'^2\right)\sin^2\psi + \frac{k}{R}\left(y^2 - y'^2\right)\right]} \qquad (55)$$

$$\times e^{4k^2 C \sin^2\psi} dx_1 dy dx_1' dy' \quad .$$

Eq. (55) will be carried forward in Eq. (80) of Chapter III.

## CHAPTER III

## THEORY USING AN EXPONENTIAL COVARIANCE FUNCTION

The statistical properties of the model surfaces, which shall be discussed in Chapter IV, suggest that an exponential function best describes the spatial covariance of the rough surfaces employed in the experimental study. The exponential spatial covariance function of the surface displacements is given by

$$C = \left\langle F(x_1,y)F(x_1',y')\right\rangle = \left\langle F_o^2\right\rangle e^{-\frac{1}{a}\left[(x_1-x_1')^2+(y-y')^2\right]^{1/2}} , \quad (56)$$

where $a$ is the spatial correlation interval of the surface displacements and $\left\langle F_o^2\right\rangle$ is the mean-square amplitude of the surface irregularities. The distance $a$, for which C will drop to the value $e^{-1}$, has the physical significance that it is a measurement of the relative distance between the hills and valleys on the randomly rough surface. The square root of $\left\langle F_o^2\right\rangle$ has the physical meaning that it represents the average heights of the hills and the average depth of the valleys.

### A. Amplitude and Phase Fluctuations in the Fraunhofer Approximation

The amplitude fluctuations in the Fraunhofer approximation are zero irrespective of the form of the spatial covariance function as shown by Eq. (24) in Chapter II.

The phase fluctuations in the Fraunhofer approximation are determined by the substitution of Eq. (56) into Eq. (32) to give

$$\left\langle (\delta\phi)^2\right\rangle = \frac{k^2\left\langle F_o^2\right\rangle \sin^2\psi}{z^2(\Delta_1+\Delta_2)^2} \times \int_{-\Delta_1}^{\Delta_2}\int_{-\ell}^{\ell}\int_{-\Delta_1}^{\Delta_2}\int_{-\ell}^{\ell} e^{-\frac{1}{a}\left[(x_1-x_1')^2+(y-y')^2\right]^{1/2}} dx_1\,dy\,dx_1'\,dy' \quad . \quad (57)$$

## CHAPTER III

## THEORY USING AN EXPONENTIAL COVARIANCE FUNCTION

The statistical properties of the model surfaces, which shall be discussed in Chapter IV, suggest that an exponential function best describes the spatial covariance of the rough surfaces employed in the experimental study. The exponential spatial covariance function of the surface displacements is given by

$$C = \left\langle F(x_1,y)F(x_1',y')\right\rangle = \left\langle F_o^2\right\rangle e^{-\frac{1}{a}\left[(x_1-x_1')^2+(y-y')^2\right]^{1/2}} , \quad (56)$$

where $a$ is the spatial correlation interval of the surface displacements and $\left\langle F_o^2\right\rangle$ is the mean-square amplitude of the surface irregularities. The distance $a$, for which C will drop to the value $e^{-1}$, has the physical significance that it is a measurement of the relative distance between the hills and valleys on the randomly rough surface. The square root of $\left\langle F_o^2\right\rangle$ has the physical meaning that it represents the average heights of the hills and the average depth of the valleys.

### A. Amplitude and Phase Fluctuations in the Fraunhofer Approximation

The amplitude fluctuations in the Fraunhofer approximation are zero irrespective of the form of the spatial covariance function as shown by Eq. (24) in Chapter II.

The phase fluctuations in the Fraunhofer approximation are determined by the substitution of Eq. (56) into Eq. (32) to give

$$\left\langle (\delta\phi)^2\right\rangle = \frac{k^2\left\langle F_o^2\right\rangle \sin^2\psi}{\ell^2(\Delta_1+\Delta_2)^2} \times \int_{-\Delta_1}^{\Delta_2}\int_{-\ell}^{\ell}\int_{-\Delta_1}^{\Delta_2}\int_{-\ell}^{\ell} e^{-\frac{1}{a}\left[(x_1-x_1')^2+(y-y')^2\right]^{1/2}} dx_1\,dy\,dx_1'\,dy' \quad . \quad (57)$$

Since $\Delta_1$ and $\Delta_2$ are not equal, it is convenient to make the preliminary change of variables (see Fig. 5)

$$u = x_1 - \frac{\Delta_2 - \Delta_1}{2} \quad , \qquad (58)$$

$$u' = x_1' - \frac{\Delta_2 - \Delta_1}{2} \quad ,$$

and introduce

$$\Delta = \frac{\Delta_1 + \Delta_2}{2} \quad . \qquad (59)$$

With these changes Eq. (57) becomes

$$\left\langle (\delta\phi)^2 \right\rangle = \frac{k^2 \left\langle F_o^2 \right\rangle \sin^2 \psi}{\ell^2 (\Delta_1 + \Delta_2)^2}$$

$$\times \int_{-\Delta}^{\Delta} \int_{-\ell}^{\ell} \int_{-\Delta}^{\Delta} \int_{-\ell}^{\ell} e^{-\frac{1}{a}\left[(u-u')^2 + (y-y')^2\right]^{1/2}} \, dudydu'dy' \quad . \qquad (60)$$

The approximate size of the active scattering region is $2\Delta$ by $2\ell$ as defined in Appendix B.

If one introduces relative coordinates as shown in Fig. 5 and defined by

$$\xi = u - u' \qquad (61)$$

$$\eta = y - y' \quad ,$$

and center of gravity coordinates defined by

$$x_o = \tfrac{1}{2}(u + u') \qquad (62)$$

$$y_o = \tfrac{1}{2}(y + y') \quad ,$$

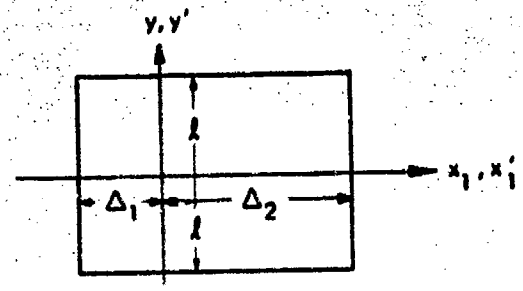


(a) ACTIVE SCATTERING REGION

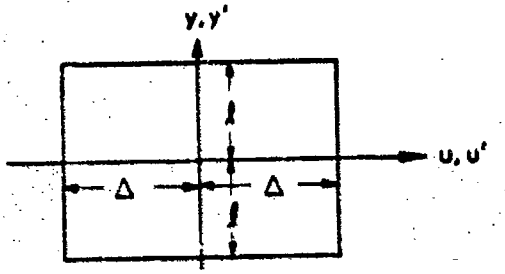


(b) TRANSFORMED REGION TO SYMMETRIC COORDINATES

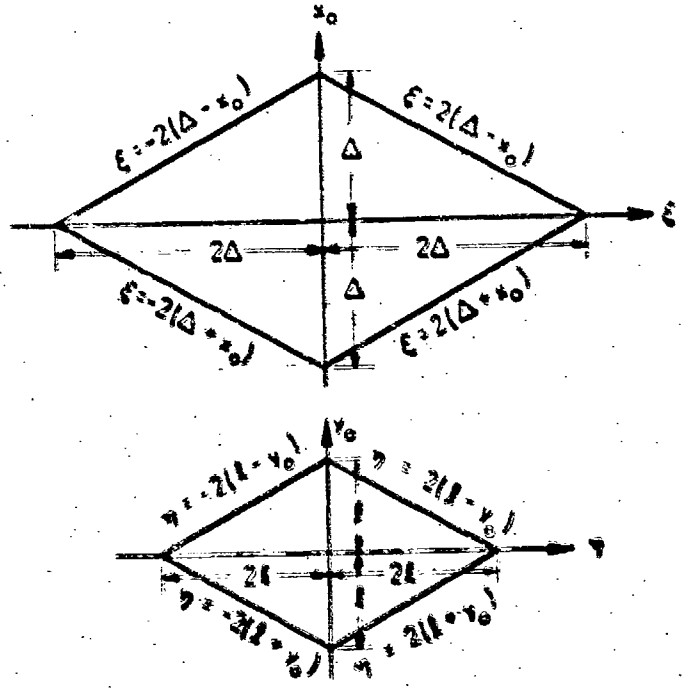


(c) TRANSFORMED REGION TO RELATIVE AND CENTER OF GRAVITY COORDINATES

FIGURE 5
TRANSFORMATION OF INTEGRATION VARIABLES

Eq. (60) becomes

$$\left\langle (\delta\Phi)^2 \right\rangle = \frac{4k^2 \left\langle F_o^2 \right\rangle \sin^2 \psi}{\ell^2 (\Delta_1 + \Delta_2)^2} \times \int_0^{\Delta} \int_0^{\ell} \int_{-2(\Delta - x_o)}^{2(\Delta - x_o)} \int_{-2(\ell - y_o)}^{2(\ell - y_o)} e^{-\frac{1}{a}(\xi^2 + \eta^2)^{1/2}} \, dx_o \, dy_o \, d\xi \, d\eta \quad . \tag{63}$$

The integrals in Eq. (63) can not be computed in open form. Further discussion shall be restricted to the case when the dimensions of the region essential to integration over $\xi$ and $\eta$ are considerably less than those of the irradiated part of the surface. That is, it is assumed that

$$a \ll 2\Delta, \, 2\ell \quad . \tag{64}$$

In keeping with this approximation one may extend the range of integration over $\xi$ and $\eta$ to infinity, so that Eq. (63) becomes

$$\left\langle (\delta\Phi)^2 \right\rangle = \frac{4k^2 \left\langle F_o^2 \right\rangle \sin^2 \psi}{\ell^2 (\Delta_1 + \Delta_2)^2} \times \int_0^{\Delta} \int_0^{\ell} \int_{-\infty}^{+\infty} \int_{-\infty}^{+\infty} e^{-\frac{1}{a}(\xi^2 + \eta^2)^{1/2}} \, dx_o \, dy_o \, d\xi \, d\eta \quad . \tag{65}$$

The integration may be performed readily by changing to polar coordinates, and one finds for Eq. (65)

$$\sigma_\Phi = \sqrt{\left\langle (\delta\Phi)^2 \right\rangle} = \left| 2k \sqrt{\left\langle F_o^2 \right\rangle} \sin \psi \right| a \sqrt{\frac{\pi}{\ell (\Delta_1 + \Delta_2)}} \quad . \tag{66}$$

This equation shows that the phase fluctuations in the Fraunhofer approximation are proportional to the Rayleigh parameter, $2k \sqrt{\left\langle F_o^2 \right\rangle} \sin \psi$ (for Rayleigh parameters much less than one), and to the spatial correlation interval, a. The fluctuations are inversely proportional to the square root of the approximate insonified area, $2\ell \, (\Delta_1 + \Delta_2)$.

B. Amplitude and Phase Fluctuations in the Fresnel Approximation

Substituting Eq. (56) into Eq. (40) of Chapter II, one finds for the square of the amplitude fluctuations

$$\frac{\langle (\delta A)^2 \rangle}{A_o^2} = J_1 + J_2 \quad , \tag{67}$$

where

$$J_1 = \frac{k^4 \langle F_o^2 \rangle \sin^4 \psi}{2\pi^2 R_{10}^2 R_{20}^2 A_o^2} \int_{-\Delta_1}^{\Delta_2} \int_{-\ell}^{\ell} \int_{-\Delta_1}^{\Delta_2} \int_{-\ell}^{\ell} e^{-\frac{1}{a}\left[(x_1 - x_1')^2 + (y-y')^2\right]^{1/2}} \tag{68}$$

$$\times \cos\left[\frac{k}{R} \sin^2 \psi \left(x_1^2 - x_1'^2\right) + \frac{k}{R}\left(y^2 - y'^2\right)\right] dx_1 dy dx_1' dy' \quad , \text{ and}$$

$$J_2 = \frac{k^4 \langle F_o^2 \rangle \sin^4 \psi}{2\pi^2 R_{10}^2 R_{20}^2 A_o^2} \int_{-\Delta_1}^{\Delta_2} \int_{-\ell}^{\ell} \int_{-\Delta_1}^{\Delta_2} \int_{-\ell}^{\ell} e^{-\frac{1}{a}\left[(x_1 - x_1')^2 + (y-y')^2\right]^{1/2}} \tag{69}$$

$$\times \cos\left[\frac{k}{R} \sin^2 \psi \left(x_1^2 + x_1'^2\right) + \frac{k}{R}\left(y^2 + y'^2\right) - 2\Phi_o'\right] dx_1 dy dx_1' dy' \quad .$$

The details in the integration of $J_1$ are given in Appendix D. The result is

$$J_1(a) = \frac{2k^2 \langle F_o^2 \rangle \sin^2 \psi}{\pi \left\{ \left[ C_\ell \left( C_{\Delta_1} + C_{\Delta_2} \right) - S_\ell \left( S_{\Delta_1} + S_{\Delta_2} \right) \right]^2 + \left[ C_\ell \left( S_{\Delta_1} + S_{\Delta_2} \right) + S_\ell \left( C_{\Delta_1} + C_{\Delta_2} \right) \right]^2 \right\}}$$

$$\times \left\{ \operatorname{arccot} \left[ \frac{R}{2ka\ell\Delta_1 \sin^2 \psi} \left( \ell^2 + \Delta_1^2 \sin^4 \psi + \frac{R^2}{4k^2 a^2} \right)^{1/2} \right] \right. \tag{70}$$

$$\left. + \operatorname{arccot} \left[ \frac{R}{2ka\ell\Delta_2 \sin^2 \psi} \left( \ell^2 + \Delta_2^2 \sin^4 \psi + \frac{R^2}{4k^2 a^2} \right)^{1/2} \right] \right\} \quad ,$$

where C and S are the Fresnel integrals defined by Eq. (C-9) in Appendix C.

A discussion of the $J_2$ term is given in Appendix E. The investigation shows that

$$J_2 \ll J_1 \tag{71}$$

so that the amplitude fluctuations as given by Eq. (67) can be approximated by

$$\frac{\sqrt{\langle (\delta A)^2 \rangle}}{A_o} \approx \sqrt{J_1} \quad . \tag{72}$$

Substituting Eq. (56) into Eq. (41) of Chapter II, one obtains for the phase fluctuations

$$\sqrt{\langle (\delta \Phi)^2 \rangle} = \sqrt{J_1 - J_2} \quad , \tag{73}$$

where $J_1$ and $J_2$ are given by Eqs. (68) and (69). Since $J_2 \ll J_1$, the amplitude and phase fluctuations are approximately equal for small Rayleigh parameters so that

$$\frac{\sqrt{\langle (\delta A)^2 \rangle}}{A_o} \approx \sqrt{\langle (\delta \Phi)^2 \rangle} \approx \sqrt{J_1} \quad . \tag{74}$$

Thus, the Fraunhofer approximation shows the phase fluctuations to be significantly larger than the amplitude fluctuations (which are zero) whereas the Fresnel approximation shows the amplitude and phase fluctuations to be approximatley of the same magnitude.

C. Scattering Coefficient in the Fraunhofer Approximation

Substituting Eq. (56) into Eq. (49) of Chapter II, one obtains

$$\sigma_s = \frac{e^{-4k^2 \langle F_o^2 \rangle \sin^2 \Psi}}{4\ell^2 (\Delta_1 + \Delta_2)^2} \times \int_{-\Delta_1}^{\Delta_2} \int_{-\ell}^{\ell} \int_{-\Delta_1}^{\Delta_2} \int_{-\ell}^{\ell} e^{4k^2 \langle F_o^2 \rangle (\sin^2 \Psi) e^{-\frac{1}{a}\left[(x_1 - x_1')^2 + (y-y')^2\right]^{1/2}}} dx_1 dy dx_1' dy' \quad . \tag{75}$$

Set

$$g = 4k^2\left\langle F_o^2\right\rangle \sin^2\psi \tag{76}$$

and refer to g as the Beckmann parameter (which in the specular direction is the square of the Rayleigh parameter).

The integrand can be written as

$$e^{ge^{-\frac{1}{a}\left[(x_1-x_1')^2+(y-y')^2\right]^{1/2}}} = \sum_{m=0}^{m=\infty}\left(\frac{g^m}{m!}e^{-\frac{m}{a}\left[(x_1-x_1')^2+(y-y')^2\right]^{1/2}}\right) . \tag{77}$$

Eq. (75) becomes

$$\sigma_s = e^{-g}\left[1 + \frac{1}{4\ell^2(\Delta_1+\Delta_2)^2}\sum_{m=1}^{m=\infty}\frac{g^m}{m!}\right.$$

$$\left. \times \int_{-\Delta_1}^{\Delta_2}\int_{-\ell}^{\ell}\int_{-\Delta_1}^{\Delta_2}\int_{-\ell}^{\ell} e^{-\frac{m}{a}\left[(x_1-x_1')^2+(y-y')^2\right]^{1/2}} dx_1\,dy\,dx_1'\,dy'\right] . \tag{78}$$

Since the integrals occurring in Eq. (78) are the same as those occurring in Eq. (57) for the phase fluctuations, one can write immediately from the square of Eq. (66),

$$\sigma_s = e^{-4k^2\left\langle F_o^2\right\rangle \sin^2\psi}\left[1 + \frac{a^2\pi}{\ell(\Delta_1+\Delta_2)}\sum_{m=1}^{m=\infty}\frac{1}{m!m^2}\left(4k\left\langle F_o^2\right\rangle \sin^2\psi\right)^m\right] . \tag{79}$$

for the scattering coefficient in the specular direction in the Fraunhofer approximation.

## D. Scattering Coefficient in the Fresnel Approximation

Substituting Eq. (56) into Eq. (55) of Chapter II, one obtains

$$\sigma_s = \frac{k^2(R_{10} + R_{20})^2 \sin^2 \psi}{4\pi^2 R_{10}^2 R_{20}^2 K} e^{-g}$$

$$\times \int_{-\Delta_1}^{\Delta_2} \int_{-\ell}^{\ell} \int_{-\Delta_1}^{\Delta_2} \int_{-\ell}^{\ell} e^{i\left[\frac{k}{R}\left(x_1^2 - x_1'^2\right)\sin^2 \psi + (y^2 - y'^2)\right]} \tag{80}$$

$$\times e^{ge^{-\frac{1}{a}\left[(x_1 - x_1')^2 + (y-y')^2\right]^{1/2}}} dx_1 dy dx_1' dy' \quad .$$

Using the infinite summation defined by Eq. (77), one obtains

$$\sigma_s = \frac{k^2(R_{10} + R_{20})^2 \sin^2 \psi}{4\pi^2 R_{10}^2 R_{20}^2 K} e^{-g} \left\{ \int_{-\Delta_1}^{\Delta_2} \int_{-\ell}^{\ell} \int_{-\Delta_1}^{\Delta_2} \int_{-\ell}^{\ell} e^{i\left[\frac{k}{R}(x_1^2 - x_1'^2)\sin^2 \psi \right.} \right.$$

$$\left. + \frac{k}{R}(y^2 - y'^2)\right] dx_1 dy dx_1' dy' + \sum_{m=1}^{m=\infty} \frac{g^m}{m!} \tag{81}$$

$$\times \int_{-\Delta_1}^{\Delta_2} \int_{-\ell}^{\ell} \int_{-\Delta_1}^{\Delta_2} \int_{-\ell}^{\ell} e^{i\left[\frac{k}{R}(x_1^2 - x_1'^2)\sin^2 \psi + \frac{k}{R}(y^2 - y'^2)\right]}$$

$$\left. \times e^{-\frac{m}{a}\left[(x_1 - x_1')^2 + (y-y')^2\right]^{1/2}} dx_1 dy dx_1' dy' \right\} \quad .$$

Integrating the first set of integrals as shown in Appendix C and separating the second set of integrals into their real and imaginary parts, one obtains

$$\sigma_s = e^{-g} + \frac{k^2(R_{10} + R_{20})^2 \sin^2 \psi}{4\pi^2 R_{10}^2 R_{20}^2 K} e^{-g} \sum_{m=1}^{m=\infty} \frac{g^m}{m!}$$

$$\times \left\{ \int_{-\Delta_1}^{\Delta_2} \int_{-l}^{l} \int_{-\Delta_1}^{\Delta_2} \int_{-l}^{l} \cos\left[\frac{k}{R}\left(x_1^2 - x_1'^2\right)\sin^2\psi + \frac{k}{R}\left(y^2 - y'^2\right)\right] \right.$$

$$\times e^{-\frac{m}{a}\left[(x_1 - x_1')^2 + (y-y')^2\right]^{1/2}} dx_1 dy dx_1' dy'$$

$$+ i \int_{-\Delta_1}^{\Delta_2} \int_{-l}^{l} \int_{-\Delta_1}^{\Delta_2} \int_{-l}^{l} \sin\left[\frac{k}{R}\left(x_1^2 - x_1'^2\right)\sin^2\psi + \frac{k}{R}\left(y^2 - y'^2\right)\right]$$

$$\left. \times e^{-\frac{m}{a}\left[(x_1 - x_1')^2 + (y-y')^2\right]^{1/2}} dx_1 dy dx_1' dy' \right\} .$$

The integration of the second group of integrals containing the sine function can be accomplished by following the procedure given for the integration of the $J_1$ term in Appendix D. The parallel development produces the integral (see Eq. (D-3) in Appendix D)

$$I_s = \int_{-\infty}^{+\infty}\int_{-\infty}^{+\infty} e^{-\frac{1}{a}(\xi^2+\eta^2)^{1/2}} \sin\left[\frac{2k}{R}\sin^2\psi\left(x_o + \frac{\Delta_2}{2} - \frac{\Delta_1}{2}\right)\xi + \frac{2k}{R}y_o\eta\right] d\xi d\eta$$

which can be reduced to

$$I_s = \int_0^{2\pi}\int_0^{\infty} e^{-\rho/a} \sin\left[\rho\sqrt{M^2+N^2}\cos\varphi\right]\rho d\rho d\varphi \quad .$$

From Gradshteyn and Ryzhik (integral 3.715-13, page 402), one obtains $I_s = 0$. Thus, the expression for the coefficient $\sigma_s$ becomes

$$\sigma_s = e^{-g}\left\{1 + \frac{k^2(R_{10}+R_{20})^2\sin^2\psi}{4\pi^2 R_{10}^2 R_{20}^2 K}\sum_{m=1}^{m=\infty}\frac{g^m}{m!}\right.$$
$$\times \int_{-\Delta_1}^{\Delta_2}\int_{-\ell}^{\ell}\int_{-\Delta_1}^{\Delta_2}\int_{-\ell}^{\ell} \cos\left[\frac{k}{R}(x_1^2 - x_1'^2)\sin^2\psi + \frac{k}{R}(y^2 - y'^2)\right] \qquad (82)$$
$$\left. \times e^{-\frac{m}{a}\left[(x_1-x_1')^2+(y-y')^2\right]^{1/2}} dx_1 dy dx_1' dy'\right\} \quad .$$

The integrals appearing in Eq. (82) are the same as the integrals appearing in in Eq. (68). Thus, the scattering coefficient calculated in the Fresnel approximation can be written as

$$\sigma_s = e^{-g}\left[1 + \frac{2\ell}{a}\sum_{m=1}^{m=\infty}\frac{g^m}{m!}J_1\left(\frac{a}{m}\right)\right] \qquad (83)$$

where $J_1\left(\frac{a}{m}\right)$ is given by Eq. (70).

## CHAPTER IV

## EXPERIMENTAL APPARATUS AND PROCEDURES

It is seen from the theory developed in Chapter II that one must know the statistical properties of the rough surface in order that the predictions of the theory can be compared with measurements on the rough surface. In particular, if $F(x_1,y)$ is the elevation of the reflecting surface, one must know the autocovariance $\left\langle F(x_1y)F(x_1',y')\right\rangle$ as shown by Eqs. (32), (40), (41), (49), and (55), and the bivariate distribution function as illustrated by Eq. (44).

The problem of selecting a topographic surface to be modeled has been discussed by Horton, Mitchell, and Barnard (1967). The model surface was generated from maps of aeromagnetic intensity over a portion of the Canadian Shield. Before these maps were used to construct the model, the two-dimensional autocovariance functions of these maps were studied by Horton, Hempkins, and Hoffman (1964). Details of the mathematical analysis used in the investigation of such maps are given by Horton, Hoffman, and Hempkins (1962).

A summary of the results obtained in these investigations will be given. The Canadian maps were contoured in gammas ($1\gamma = 10^{-5}$ Oe). The vertical relief of the model surface was obtained from this aeromagnetic dimension using the scale $10\gamma = 1/32$ in. The factor 1 mile = 1 in. was used to convert the area of the aeromagnetic maps into model surfaces of size 32 in. by 32 inches. The theory in Chapters II and III is based on the assumption that the reflecting surface is pressure release (see Eq. (5)), and the models were constructed from a material of small acoustic impedance compared with the acoustic impedance of the water in which the surfaces are submerged. The model was made of low-density expanded polystryrene by the Construction Service Company of Fort Worth, Texas. A square grid of sample points drawn 1/2 in. apart on the central one-fourth of the map surface was used to compute the autocovariance function. This square grid gave 1089 values of the elevation.

The autocovariance function was computed from a formula given by Horton, Hoffman, and Hempkins (1962)

$$C(s,t) = \frac{1}{(N - s)(M - t)} \sum_{i=1}^{N-s} \sum_{j=1}^{M-t} F(i,j)F(i + s, j + t) \quad , \qquad (84)$$

where

$N = M = 33$ is the number of samples along each 16 in. grid line,

$F$ is the surface relief,

$s$ and $t$ are units of shift along the grid, and

$C$ is the autocovariance function.

Profiles of the autocovariance function along the $s$ and $t$ directions are plotted in Fig. 6. The profiles show that the surface is possibly isotropic for values of $s$ and $t$ less than one inch. The mean-square surface relief, $\left\langle F_o^2 \right\rangle$, is 0.132 in.$^2$ A curve that will pass through the three points nearest the origin and approximately average the other anisotropic points for values of $s$ and $t$ greater than one inch is the exponential autocovariance function given by

$$C(r) = 0.132\, e^{-\frac{r}{2.55}} \quad , \qquad (85)$$

where 2.55 in. is the correlation length defined as the distance over which the covariance function is reduced by 1/e. Eq. (85) corresponds to Eq. (56) in Chapter III,

where

$$\left\langle F_o^2 \right\rangle = 0.132 \text{ in.}^2$$

$$a = 2.55 \text{ in.}$$

$$r = \left[(x_1 - x_1')^2 + (y - y')^2\right]^{1/2} \quad .$$

Although the properties of the model surface do not satisfy the assumption of isotropy on which the theory in Chapters' II and III is based, the agreement is close enough to justify a comparison between theory and experiment. Since no one has measured experimentally the bivariate

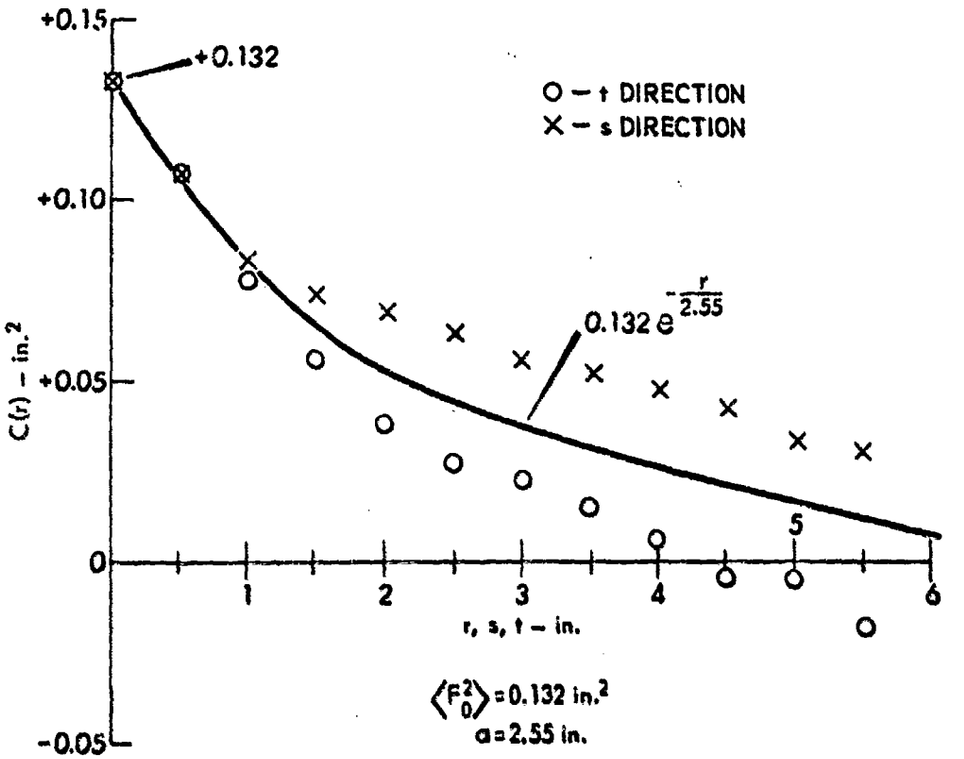


**FIGURE 6**
**PROFILE OF THE COVARIANCE FUNCTION**

probability density for a sample of topography, it is not possible to justify directly the choice given by Eq. (44) at the present time. However, Horton, Mitchell, and Barnard (1967) give convincing reasons why the bivariate Gaussian distribution may be used. The reader is referred to a thesis by Mitchell (1966) for further details concerning the model surface.

Three other model surfaces described statistically by the same exponential covariance function were constructed. The statistical properties of the four model surfaces are given in Table I. The ratio $\sqrt{\langle F_o^2 \rangle}\ /\lambda$ was calculated for a frequency of 95.800 kHz (wavelength $\lambda$ = 0.608 in.).

The experiments were performed with the model surface submerged in a water-filled tank with dimensions 15 ft wide, 60 ft long, and 12 ft deep. The surface was suspended vertically with its center approximately 46 in. below the waterline. An x,y,z mechanical positioning system mounted on the top of the tank was used to position the source and receiver in the experiment. Figure 7 shows the laboratory tank, positioning system, and electronic equipment used in the study. The source and receiver were mounted on two identical columns with the movement in the x,y,z directions read from a counter ($\pi$ milli-inches per smallest division or 318.310 divisions per inch on the counter). Also, the mechanism allows the projector and receiver to be rotated about the vertical axis in increments of 0.1 deg.

The source was a transducer that has an active face diameter of 12.5 cm and a resonance frequency of 94.0 kHz. The directivity pattern of the piston transducer is shown in Fig. 8. The beamwidth is approximately 9 deg measured between points where the radiated intensity falls to one-half the intensity along the forward axis (-3 dB points).

The receiver was a small cylinder of outside diameter 0.082 in., inside diameter 0.057 in., and length 0.125 inch. Its directivity pattern is approximately omnidirectional as shown by Fig. 9. The same side of the probe was directed along the slant-line distance to the model surfaces throughout the experiment.

TABLE I

STATISTICAL PROPERTIES OF THE MODEL SURFACES

| Model | rms Relief $\sqrt{\langle F_o^2 \rangle}$ in. | Correlation Length a in. | Relative Slope $\sqrt{\langle F_o^2 \rangle}/a$ | Ratio $\sqrt{\langle F_o^2 \rangle}/\lambda$ |
|---|---|---|---|---|
| I | 0.091 | 2.55 | 0.0357 | 0.150 |
| II | 0.182 | 2.55 | 0.0714 | 0.300 |
| III | 0.364 | 2.55 | 0.1428 | 0.600 |
| IV | 0.364 | 5.10 | 0.0714 | 0.600 |

TABLE I

STATISTICAL PROPERTIES OF THE MODEL SURFACES

| Model | rms Relief $\sqrt{\langle F_o^2 \rangle}$ in. | Correlation Length a in. | Relative Slope $\sqrt{\langle F_o^2 \rangle}/a$ | Ratio $\sqrt{\langle F_o^2 \rangle}/\lambda$ |
|---|---|---|---|---|
| I | 0.091 | 2.55 | 0.0357 | 0.150 |
| II | 0.182 | 2.55 | 0.0714 | 0.300 |
| III | 0.364 | 2.55 | 0.1428 | 0.600 |
| IV | 0.364 | 5.10 | 0.0714 | 0.600 |

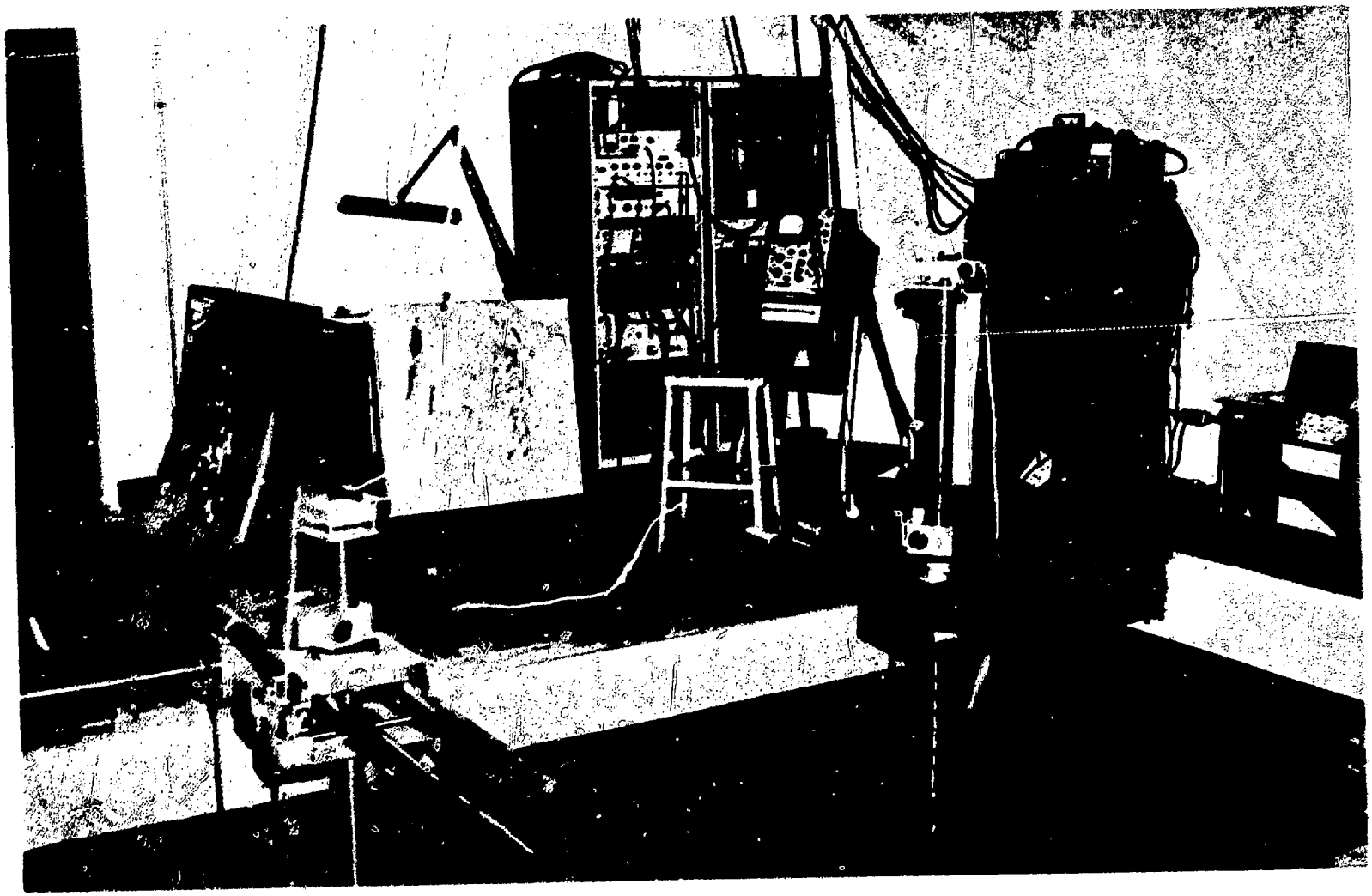

FIGURE 7
LABORATORY TANK AND INSTRUMENTATION
FOR REFLECTION AND SCATTERING STUDIES

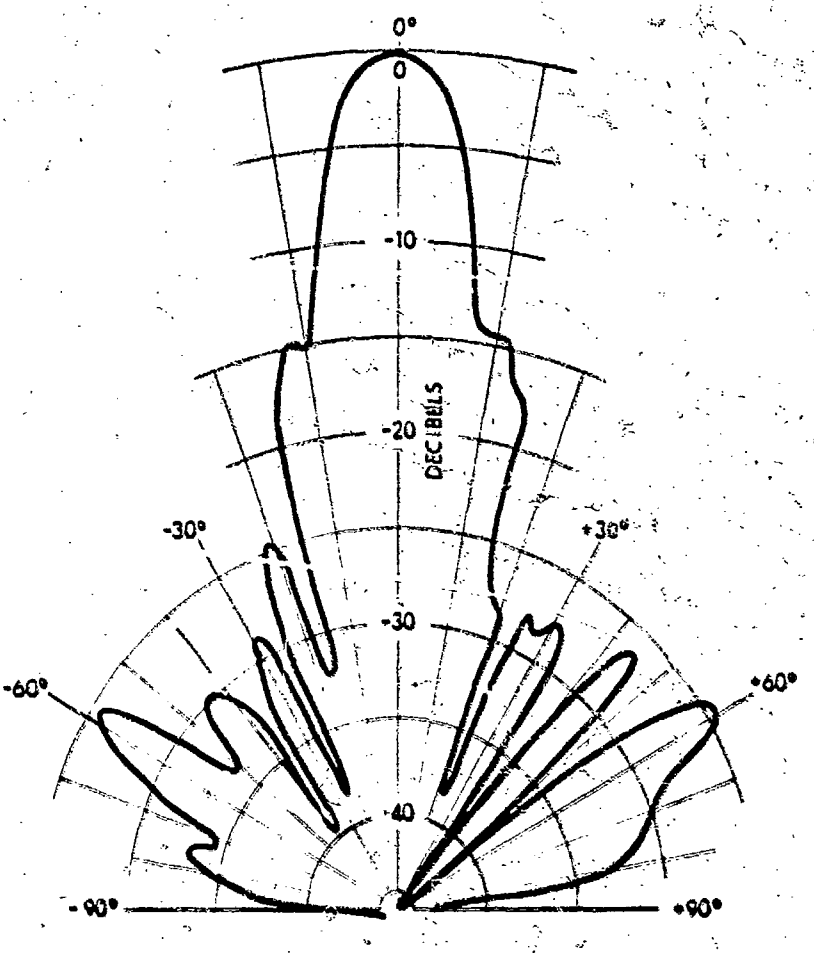


SOURCE AND RECEIVER SEPARATED BY 10 ft
INPUT VOLTAGE: 15 V
PULSEWIDTH: 640 μsec
RESONANCE FREQUENCY: 94.0 kHz

FIGURE 8
DIRECTIVITY PATTERN
TRANSDUCER DRL No. 116(1257)
FREQUENCY: 95.800 kHz

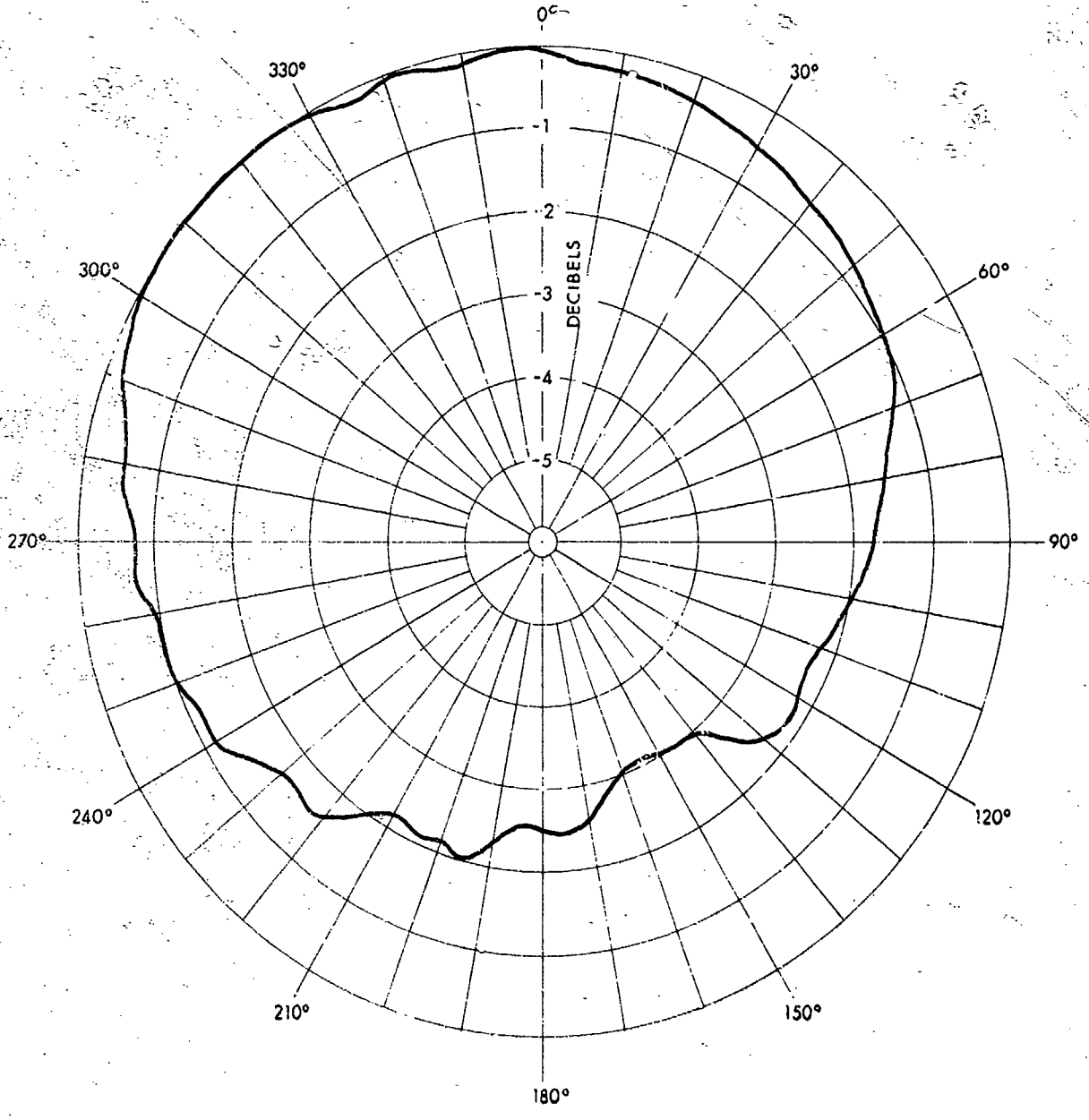


SOURCE AND RECEIVER SEPARATED BY 10 ft
INPUT VOLTAGE: 15 V
PULSEWIDTH: 640 μsec
RESONANCE FREQUENCY: 900 kHz

FIGURE 9
DIRECTIVITY PATTERN OF RECEIVER
FREQUENCY: 95.800 kHz

Figure 10 is a block diagram of the arrangement of the electronic and acoustic equipment. The continuous oscillator signal is gated into signals of 640 μsec duration at a rate of 28 times per second. These pulses are 95 cm ≈ 37 in. long in the water and contain 61 cycles at 95.809 kHz. The pulsed signals are used as the input of the power amplifier that drives the projecting transducer. The received signal scattered from the pressure release model surface is amplified and is displayed on the oscilloscope. The peak-to-peak voltage of the received signal is recorded. At the same instant the relative phase of the received signal is measured by recording the time delay of the scattered pulse relative to a continuous wave from the oscillator. The counter allows the experimenter to maintain the frequency to within one cycle throughout the data collecting.

All measurements were made with the projector and receiver in the specular direction. With the projector placed 60.0 in. from the origin on the rough surface and with the receiver placed 60.0 in. from the same origin (the origin lies on an imaginary plane that passes through the average height of the rough surface), the grazing angle was varied from 80 deg to 6 deg in increments of 2 deg. Figure 11 shows samples of the oscilloscope pictures for grazing angles of 50 and 80 deg.

The center of the received pulse is recorded since this represents a scattered pressure due to the total insonified area. The pulse to the left of the largest signal in Fig. 11a for a grazing angle of 80 deg is attributed to the side lobes of the projector.

If the source and the receiver are displaced as a rigid body parallel to the scattering surface, one would obtain different values for the amplitude and relative phase as the dominant scattered energy returns from different parts of the rough surface. Consequently, the sequence of values for the amplitude and relative phase constitute samples of a stochastic variable. Therefore, one is concerned not with specific values but rather with average values. In the process of collecting the data, ten different values of the amplitude and relative phase were obtained by insonifying ten different regions of the model surface. To insonify the different regions, the projector and receiver

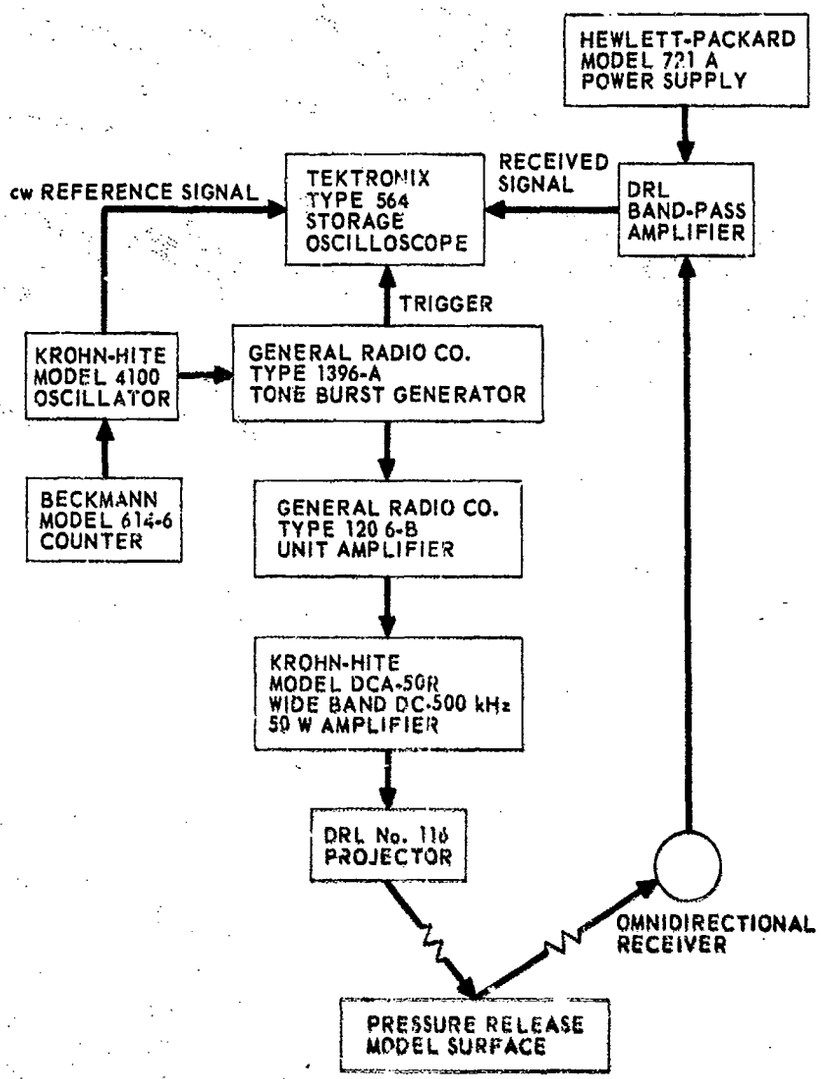


**FIGURE 10**
**EXPERIMENTAL EQUIPMENT**

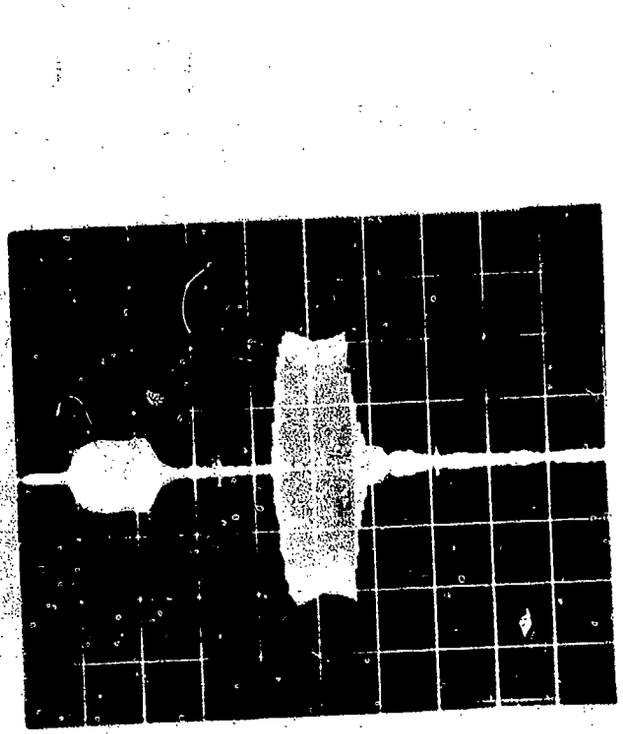

(a)
80 deg GRAZING ANGLE
SPEED: 500μsec/div
SCALE: 0.1 V/div

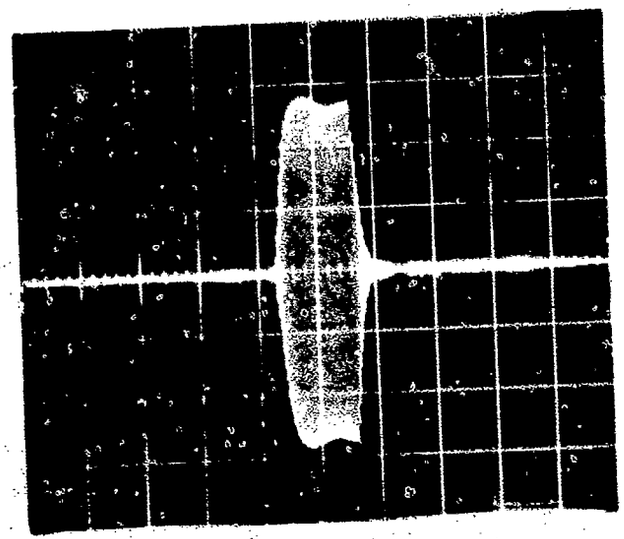

(b)
50 deg GRAZING ANGLE
SPEED: 500μsec/div
SCALE: 0.2 V/div

FIGURE 11
RECEIVED PULSE

were moved as a rigid body in the vertical direction to ten different positions in increments of one inch. Figure 12 shows three of the ten different positions of the area that the projector insonifies (numbering 1, 6, and 10). The ellipses indicate the approximate size of the insonified area (-3 dB) for a grazing angle of 40 deg. The active scattering area for each of the ten data runs is confined to a rectangular region 14.8 in. by 18.4 inches.

The amplitude fluctuations were measured for any one grazing angle with the receiver confined to the specular direction by recording the peak-to-peak voltage of the received signal for the ten different positions of the transmitter and receiver. The average amplitude

$$A_{av} = \frac{1}{10} \sum_{i=1}^{i=10} A_i \tag{86}$$

was used to calculate the variance

$$D(A) = \frac{1}{10} \sum_{i=1}^{i=10} (A_i - A_{av})^2 \quad , \tag{87}$$

from which the standard deviation

$$\sigma = \sqrt{D(A)} \tag{88}$$

was obtained. The relative standard deviation (the amplitude fluctuations) is the ratio of the standard deviation to the average amplitude

$$\sigma_A = \frac{1}{A_{av}} \sqrt{D(A)} \quad . \tag{89}$$

The phase fluctuations were measured by recording the time delay of the scattered pulse signal relative to a continuous wave that was displayed on the oscilloscope. The time for a wavelength of the cw signal was measured on the oscilloscope (10.2 μsec for 95.8 kHz); the ratio of these two times multiplied by 360 deg gives the relative phase $\delta$ in degrees. The average phase of the ten different measurements

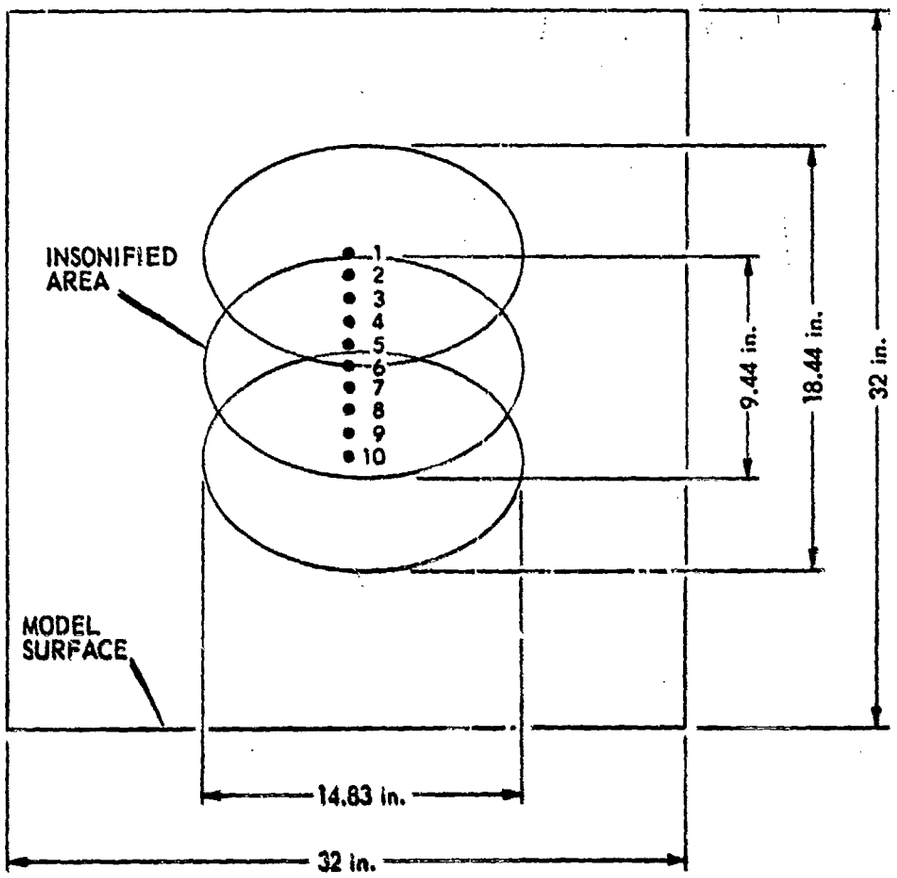


FIGURE 12
TEN POSITIONS OF INSONIFIED AREA

$$\Phi_{av} = \frac{1}{10} \sum_{i=1}^{i=10} \Phi_i \tag{90}$$

was used to calculate the variance

$$D(\Phi) = \frac{1}{10} \sum_{i=1}^{i=10} (\Phi_i - \Phi_{av})^2 \quad , \tag{91}$$

from which the standard deviation

$$\sigma_\Phi = \sqrt{D(\Phi)} \tag{92}$$

was obtained. In this case, the standard deviation represents the phase fluctuations.

The reference used to determine the scattering coefficient was obtained experimentally by measuring the peak-to-peak voltage of the pulsed signal reflected from a plane pressure release surface of the same dimensions, 32 in. by 32 in., as the rough surface. Assuming that the pressure of the underwater sound at the receiver is proportional to the voltage output of the receiving hydrophone, one defines the scattering coefficient for each individual measurement as the ratio of the scattered intensity from the rough surface to the reflected intensity from the plane surface. Thus, the experimental scattering coefficient can be written as

$$\sigma_e(\psi_i) = \left(\frac{V_s}{V_p}\right)^2 \quad . \tag{93}$$

where

$\psi_i$ is the grazing angle,

$V_s$ is the peak-to-peak voltage of the pulsed signal scattered from the rough surface, and

$V_p$ is the peak-to-peak voltage of the same pulsed signal reflected from the plane surface.

The average scattering coefficient, which is the correct coefficient to compare with the theory is

$$\sigma_e(j) = \frac{1}{10} \sum_{i=1}^{i=10} \left[ \frac{V_s(i,j)}{V_p(j)} \right]^2 \qquad (94)$$

where

$\underline{i}$ is the sample number ($i = 1,2,\ldots 10$), and

$\underline{j}$ is the grazing angle ($j = 2,4,\ldots 80$ deg).

The scattering coefficient expressed in decibels is

$$\sigma_e(\text{dB}) = 10 \log_{10} \sigma_e \quad . \qquad (95)$$

# CHAPTER V
# RESULTS

## A. Amplitude Fluctuations

The experimental results for the amplitude fluctuations in the specular direction for a frequency of 95.8 kHz are presented in Figs. 13 and 14. These results were obtained from averages of readings from ten different insonified regions of the rough surface by using Eqs. (86) through (89) of Chapter IV. The theoretical predictions of the amplitude fluctuations in the Fraunhofer approximation, given by Eq. (24), and in the Fresnel approximation, given by Eqs. (70) and (72) are illustrated in Fig. 13. A beamwidth of 9 deg measured at the half-power points (-3 dB) of the main lobe of the incident beam, as shown in Fig. 8 of Chapter IV, was used to calculate the dimensions of the insonified area.

The experimental data were used to construct the dependence of the amplitude fluctuations on the Rayleigh parameter, $2k\sqrt{\langle F_o^2 \rangle}\sin\psi$. Figure 13 pertains to measurements made on the model surface whose statistical properties were characterized by a root-mean-square relief, $\sqrt{\langle F_o^2 \rangle}$, of 0.091 inch. From the graph it is evident that, within 5% fluctuations, the experimental results correspond to the theoretical law in the Fresnel approximation for Rayleigh parameters less than 0.6. The theoretical law in the Fraunhofer approximation of zero amplitude fluctuations gives incorrect predictions for any value of the Rayleigh parameter. The experimental amplitude fluctuations for values of the Rayleigh parameter greater than one could not possibly be explained by means of the theoretical analysis, as the region of applicability of the analytical formulas is limited by the condition given by Eq. (15) that $2k\sqrt{\langle F_o^2 \rangle}\sin\psi < 1$.

When the projector and receiver were aimed at each other over a distance of 10 ft the amplitude fluctuations were measured to be less than one-half percent. Thus, changes in the properties of the water

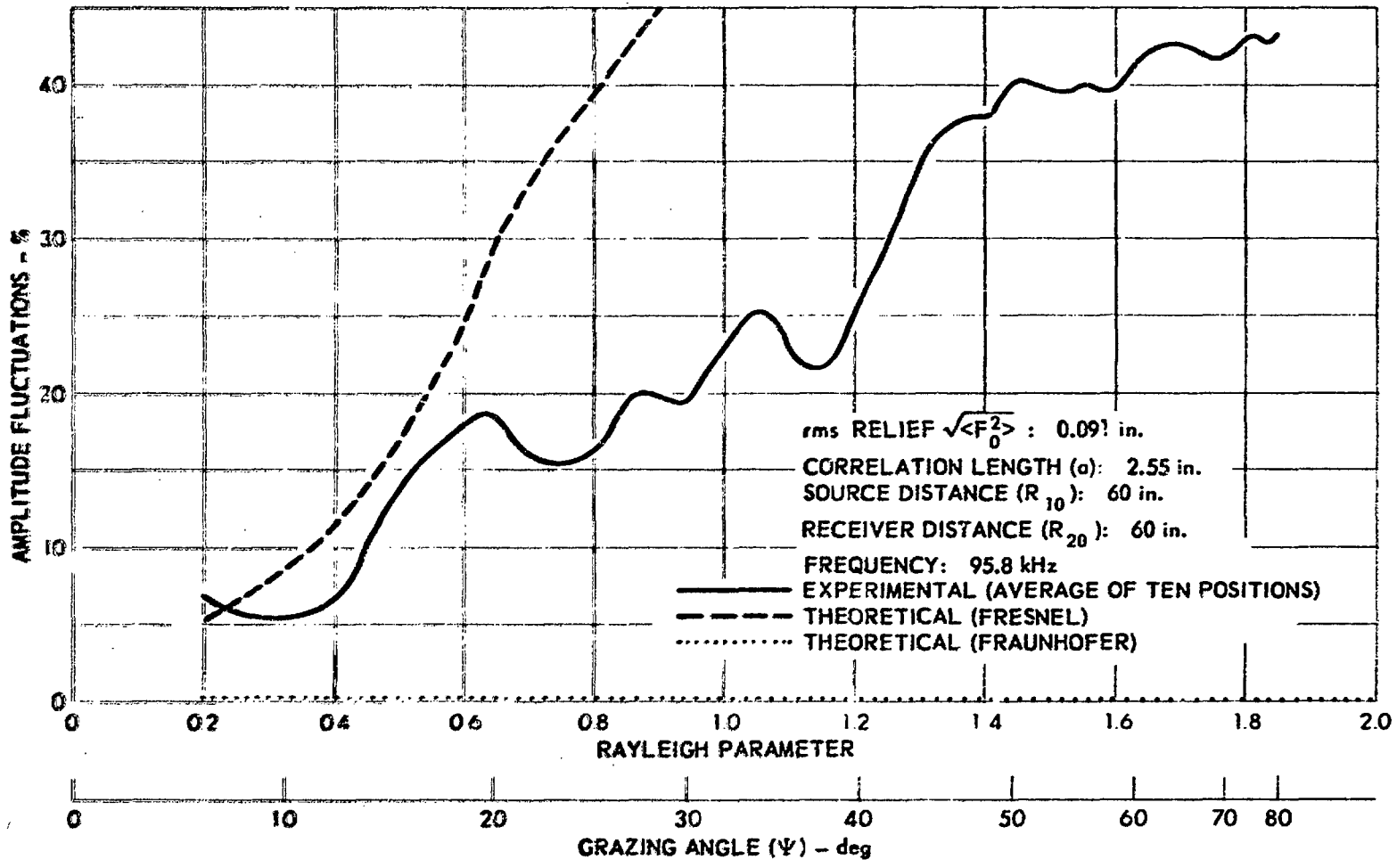


FIGURE 13
AMPLITUDE FLUCTUATIONS
IN THE SPECULAR DIRECTION
PRESSURE RELEASE RANDOM SURFACE

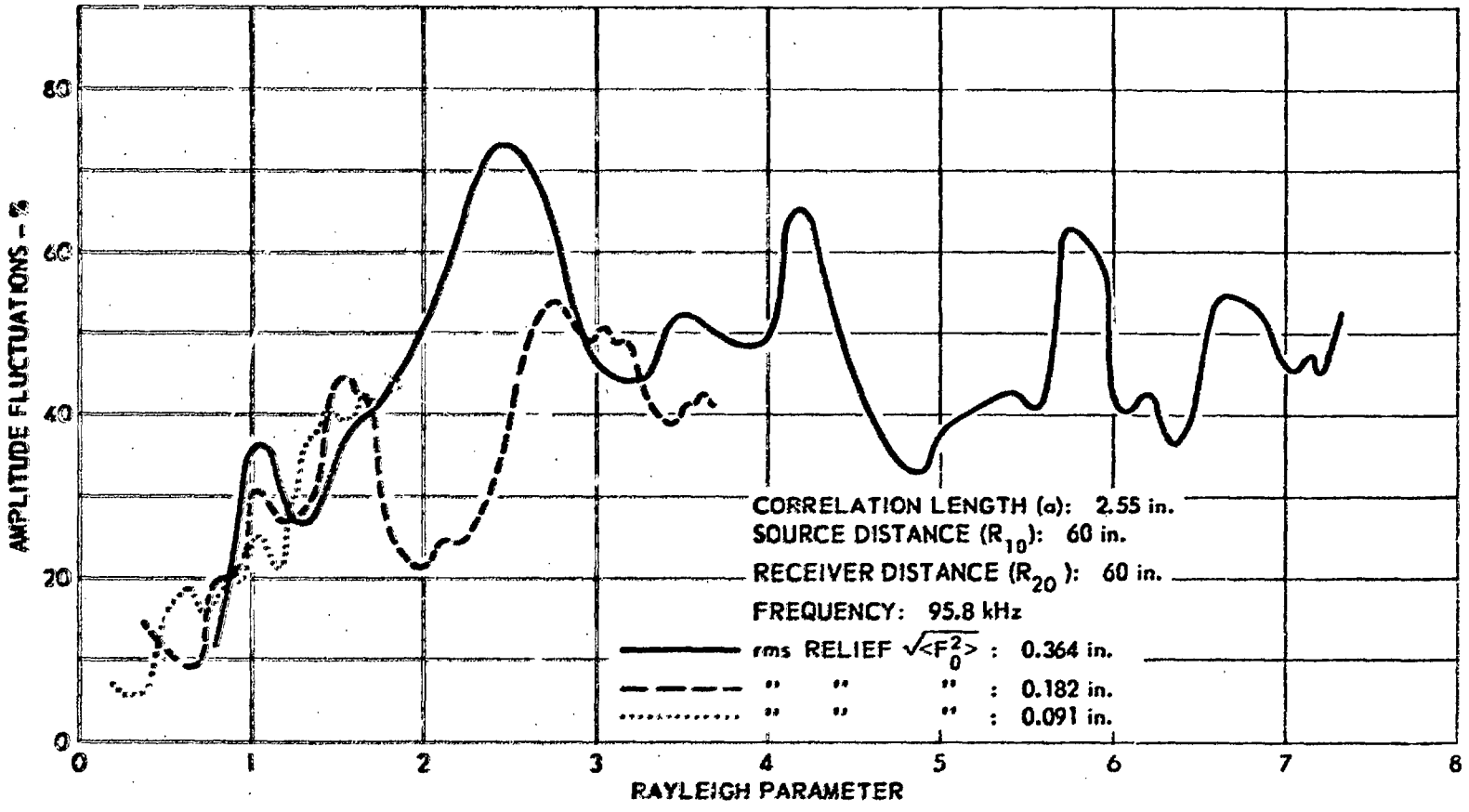


FIGURE 14
AMPLITUDE FLUCTUATIONS
IN THE SPECULAR DIRECTION
PRESSURE RELEASE RANDOM SURFACE

through which the transmitted and received pulsed wave propagated, and inaccuracies in positioning the projector and receiver contributed less than 0.5% to the amplitude fluctuations shown in Figs. 13 and 14.

The experimental data of the amplitude fluctuations depicted in Fig. 14 are the outcome of combining the results obtained from three different model surface, I, II, and III. For small values of the Rayleigh parameter up to 1.7 there is an apparent increase of the amplitude fluctuations from 10% to 40%, which is proportional to the value of this parameter. For values of the parameter greater than 2.5 the growth of the amplitude fluctuations ceases and it reaches its saturation point. For larger values of the parameter there is no further increase in the fluctuations, and the amplitude fluctuations disclose a spread of about 33 - 65% in the values. The graph shows a well-defined alternation of the amplitude fluctuations between maximum and minimum values. The fluctuation maxima are situated at $2k\sqrt{\langle F_o^2 \rangle}\sin\psi \approx 2.5$, 4.2. 5.8, and 6.7; the minima at $2k\sqrt{\langle F_o^2 \rangle}\sin\psi \approx 3.4$, 4.9, and 6.4.

The measurements illustrated in Fig. 14 verify the tentative results obtained by Gulin and Malyshev (1962) who scattered sound signals from the surface of the sea. Their results, which were stated in Chapter I, show that the amplitude fluctuations reach a saturation point when the Rayleigh parameter has the value 0.7 and for larger Rayleigh parameters the fluctuations experience an alternation between maximum and minimum values of 25 to 50%.

B. Phase Fluctuations

The experimental results for the phase fluctuations in the specular direction for a frequency of 15.8 kHz are presented in Figs. 15 and 16. These results were obtained from averages of readings from ten different insonified regions of the rough surface by using Eqs. (90) through (92) of Chapter IV. The theoretical predictions of the phase fluctuations in the Fraunhofer approximation, given by Eq. (66), and in the Fresnel approximation, given by Eqs. (70) and (74), are depicted in Fig. 15. A 9 deg beamwidth was used in the calculation for $\Delta_1$, $\Delta_2$, and $\ell$ appearing in the formulas.

through which the transmitted and received pulsed wave propagated, and inaccuracies in positioning the projector and receiver contributed less than 0.5% to the amplitude fluctuations shown in Figs. 13 and 14.

The experimental data of the amplitude fluctuations depicted in Fig. 14 are the outcome of combining the results obtained from three different model surface, I, II, and III. For small values of the Rayleigh parameter up to 1.7 there is an apparent increase of the amplitude fluctuations from 10% to 40%, which is proportional to the value of this parameter. For values of the parameter greater than 2.5 the growth of the amplitude fluctuations ceases and it reaches its saturation point. For larger values of the parameter there is no further increase in the fluctuations, and the amplitude fluctuations disclose a spread of about 33 - 65% in the values. The graph shows a well-defined alternation of the amplitude fluctuations between maximum and minimum values. The fluctuation maxima are situated at $2k\sqrt{\langle F_o^2 \rangle}\sin\psi \approx 2.5$, 4.2, 5.8, and 6.7; the minima at $2k\sqrt{\langle F_o^2 \rangle}\sin\psi \approx 3.4$, 4.9, and 6.4.

The measurements illustrated in Fig. 14 verify the tentative results obtained by Gulin and Malyshev (1962) who scattered sound signals from the surface of the sea. Their results, which were stated in Chapter I, show that the amplitude fluctuations reach a saturation point when the Rayleigh parameter has the value 0.7 and for larger Rayleigh parameters the fluctuations experience an alternation between maximum and minimum values of 25 to 50%.

B. Phase Fluctuations

The experimental results for the phase fluctuations in the specular direction for a frequency of 25.8 kHz are presented in Figs. 15 and 16. These results were obtained from averages of readings from ten different insonified regions of the rough surface by using Eqs. (90) through (92) of Chapter IV. The theoretical predictions of the phase fluctuations in the Fraunhofer approximation, given by Eq. (66), and in the Fresnel approximation, given by Eqs. (70) and (74), are depicted in Fig. 15. A 9 deg beamwidth was used in the calculation for $\Delta_1$, $\Delta_2$, and $\ell$ appearing in the formulas.

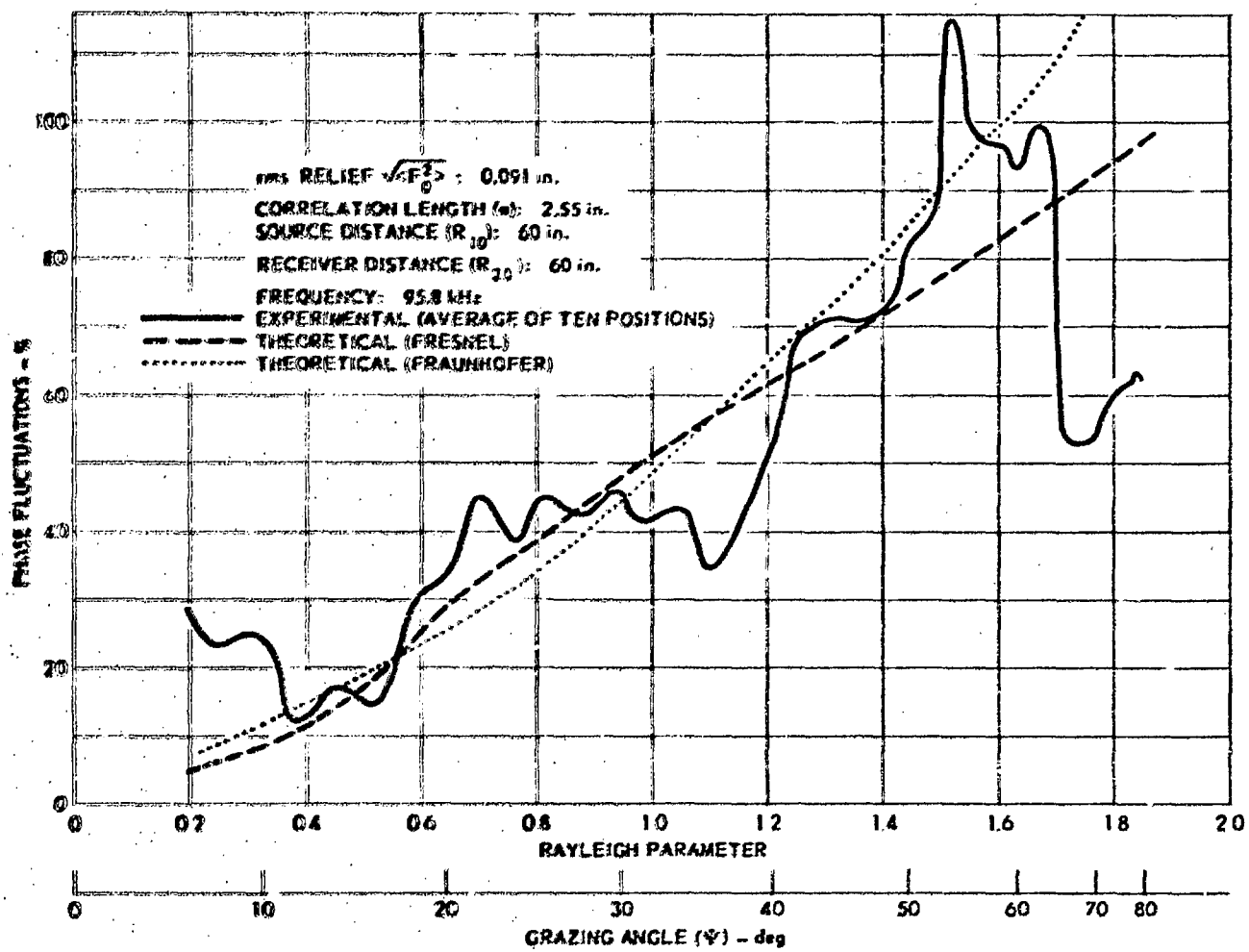


FIGURE 15
PHASE FLUCTUATIONS
IN THE SPECULAR DIRECTION
PRESSURE RELEASE RANDOM SURFACE

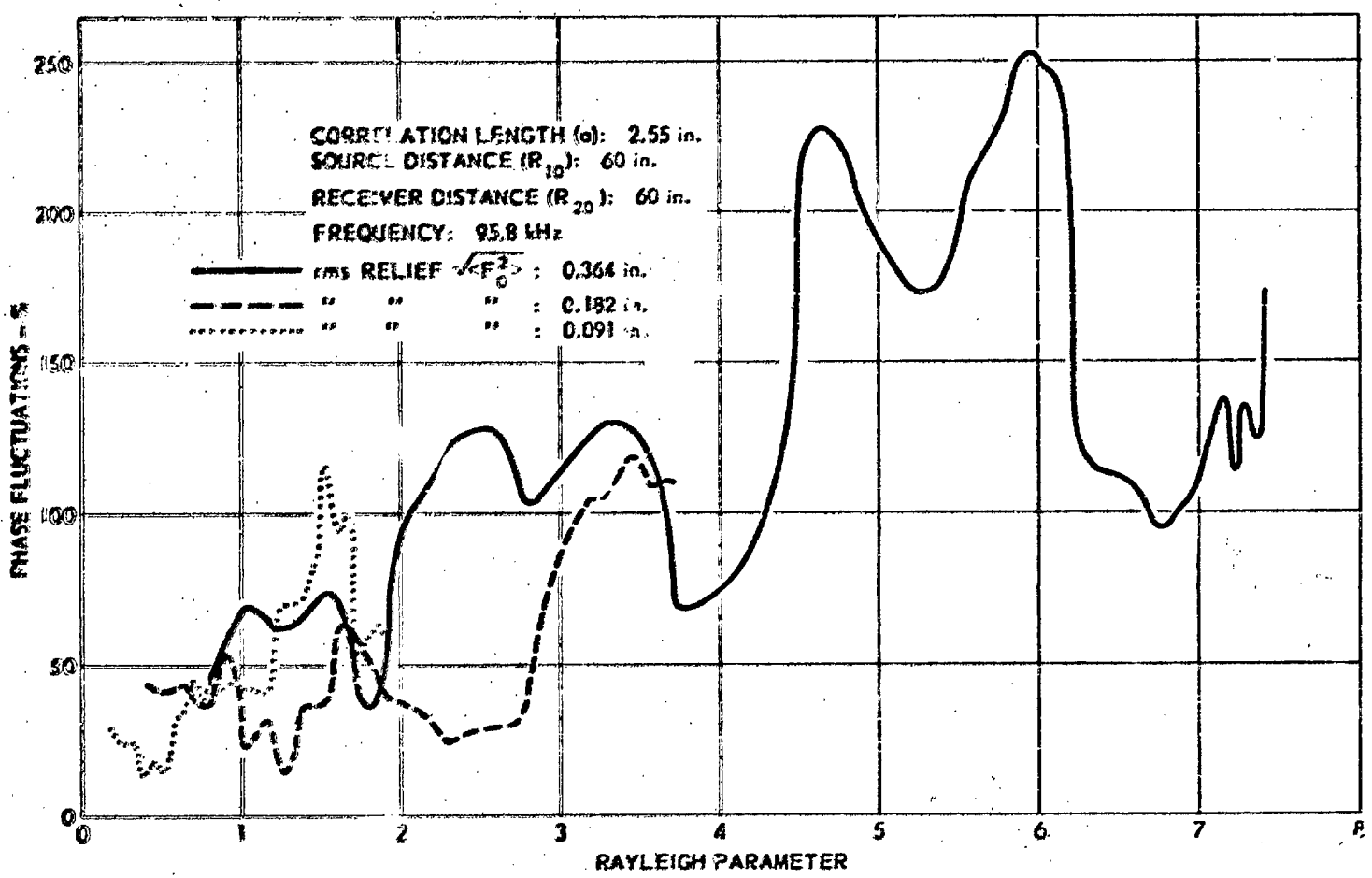


FIGURE 16
PHASE FLUCTUATIONS
IN THE SPECULAR DIRECTION
PRESSURE RELEASE RANDOM SURFACE

When the projector and receiver were aimed at each other over a distance of 10 ft the phase fluctuations were measured to be less than 5%. This small fluctuation in phase was caused by the inaccuracy in moving the source and receiver as a rigid body relative to the model surface, and also was brought about by local changes in the properties of the water through which the acoustic wave propagated.

The dependence of the phase fluctuations on the Rayleigh parameter for measurements made with the model surface that has a root-mean-square relief of 0.091 in. is shown in Fig. 15. The graph shows that the theoretical law in the Fraunhofer approximation gives predicted values within 4% of the values obtained using the Fresnel approximation for values of the Rayleigh parameter less than one. Over this range of Rayleigh parameters it is evident that, within 15% fluctuations, the experimental results which are expressed in percent relative to a radian, agree with both theoretical approaches. The phase fluctuations resulting from the irregularities on the model surface, for values of the Rayleigh parameter between 0.2 and 0.35 (theory predicts 7 to 14%) are concealed possibly by the fluctuations caused by the wave traveling directly from the source to the receiver and the wave scattered from the edge of the surface interfering with the wave scattered from the topograph of the rough surface (experimental results show about 25% relative to a radian). With this understanding one can assert that both theoretical procedures agree, within 6% fluctuation, with the experimental results for values of the Rayleigh parameter less than 0.6. The apparent good agreement between the experimental results and the theoretical predictions in the Fraunhofer approximation for values of the Rayleigh parameter between 1.225 and 1.67 is surprising but should be treated as purely coincidental since the theory is not valid for Rayleigh parameters greater than one.

The experimental phase fluctuations illustrated in Fig. 16 are the consequence of incorporating the measurements obtained from three model surfaces, I, II, and III. The dependence of the phase fluctuations on the Rayleigh parameter is not as well defined as the amplitude fluctuations on this parameter. Nevertheless, in general the phase fluctuations increase with the Rayleigh parameter from a low value of

12% to a high value of 250%. It is understood that the percentage for the experimental phase fluctuations is percent relative to a radian. The fluctuation maxima are situated at $2k\sqrt{\langle F_o^2 \rangle}\sin\psi \approx 1.5$, 3.3, 4.6, and 6.0; the minima at $2k\sqrt{\langle F_o^2 \rangle}\sin\psi \approx$ 1.8, 3.8, 5.3, and 6.8. Since the author is unaware of any other experimental investigation of the phase fluctuations of an underwater acoustic pulsed wave scattered from a randomly rough surface, no comparison can be made and these results should be considered tentative and in need of further verification.

When one attempts to compare the experimental phase fluctuations with the corresponding amplitude fluctuations, one is confronted with a problem. The issue is understood when it is realized that the experimental amplitude fluctuations given by Eq. (89) represent a relative standard deviation, whereas the experimental phase fluctuations given by Eq. (92) represent an absolute standard deviation. The experimental amplitude fluctuations in Fig. 13 are in percent relative to the average amplitude, whereas the phase fluctuations in Fig. 15 are in percent relative to a radian. The Fraunhofer and Fresnel theory for the amplitude and phase fluctuations, using the same convention for the ordinate scales, are presented in Figs. 13 and 15 in percent.

C. Scattering Coefficient

The experimental results for the scattering coefficient in the specular direction for a frequency of 95.8 kHz are presented in Figs. 17, 18, 19, and 20. These results were obtained from averages of readings from ten different insonified regions of the rough surface by employing Eqs. (93) through (95) of Chapter IV. The theoretical predictions of the scattering coefficient in the Fraunhofer approximation, given by Eq. (79), and in the Fresnel approximation, given by Eq. (85), are shown in the four graphs. The dimensions of the insonified area, $A_1$, $A_2$, and $\ell$ that appear in the formulas were calculated for a 9 deg beamwidth measured at the half-power points of the main lobe of the incident beam.

Figure 17 shows the dependence of the scattering coefficient on the Rayleigh parameter and the grazing angle, $\psi$, for the model surface that has an rms relief of 0.091 in. and a correlation length of 2.55 inches.

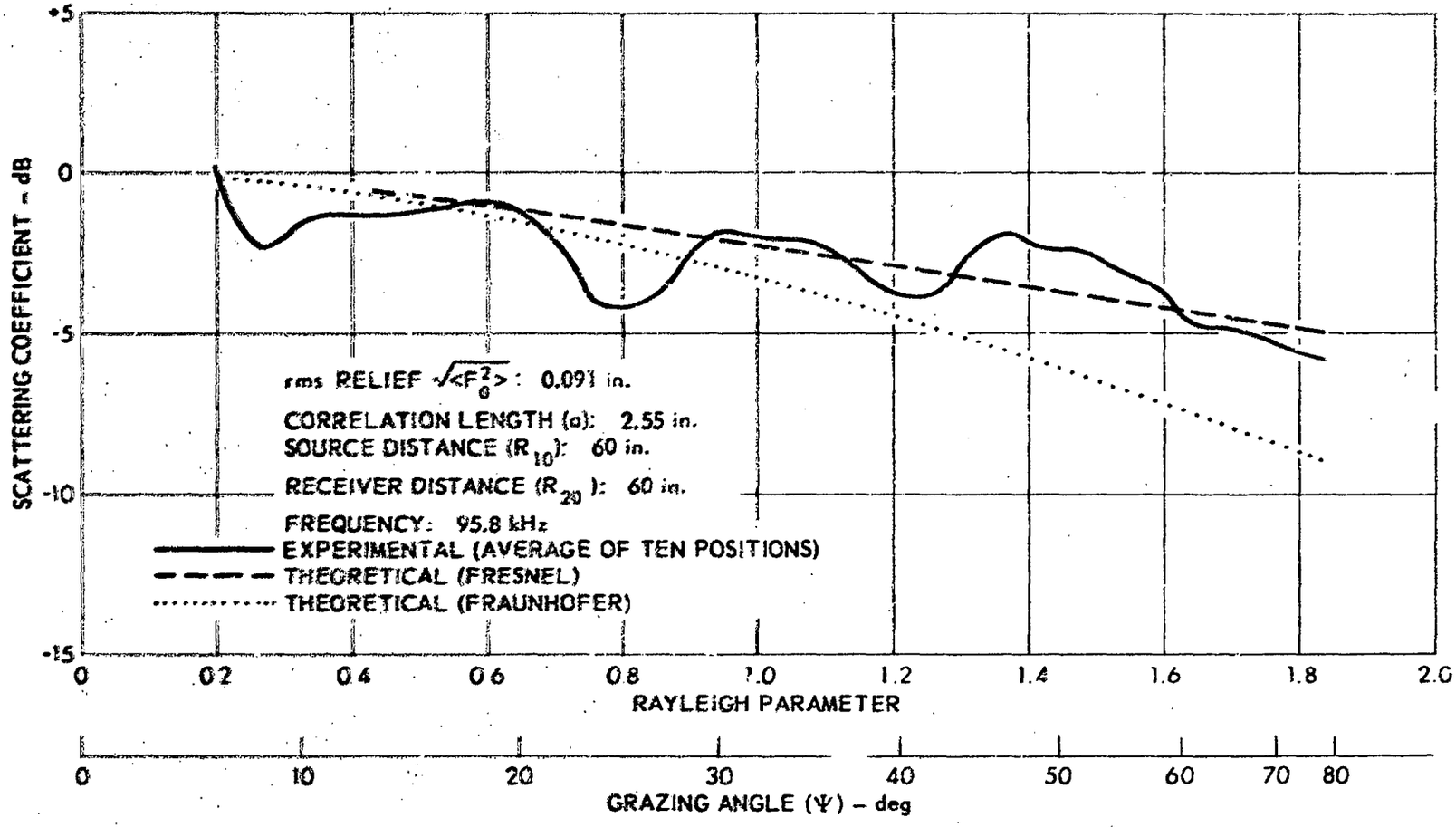


FIGURE 17
SCATTERING COEFFICIENT
IN THE SPECULAR DIRECTION
PRESSURE RELEASE RANDOM SURFACE

From the graph it is evident that, within 3 dB, the experimental results correspond to the theoretical law in the Fresnel approximation over the complete range of the Rayleigh parameters from values of 0.20 to 1.85. The theoretical law in the Fraunhofer approximation gives good agreement with the experimental results up to a value of 1.3 for the Rayleigh parameter. But for larger values of the parameter the Fraunhofer theory predicts lower values for the scattering coefficient than the experimental results show. At a Rayleigh parameter of 1.85 the Fraunhofer law gives values of the coefficient that are 4 dB smaller than the Fresnel predictions.

The scattering coefficient measured with the model surface that has an rms relief of 0.182 in. and a correlation length of 2.55 in. is illustrated in Fig. 18. Again, it is evident from the graph that the theory in the Fresnel approximation predicts the experimental values better than the Fraunhofer theory. The Fresnel theory predicts the experimental results to within 3 dB for Rayleigh parameters less than 2.35. For larger values of the Rayleigh parameter the Fresnel theory predicts values within 4.5 dB of the measured scattering coefficient. The Fraunhofer theory gives good agreement, within 3 dB, with the measured values of the scattering coefficient for values of the Rayleigh parameter less than 1.25. But for larger values of this parameter the theoretical law in the Fraunhofer approximation deviates notably from the measured coefficient, more than 16 dB for a Rayleigh parameter of 3.7.

Figure 19 describes the measurements and predicted values of the scattering coefficient for the model surface that has an rms relief of 0.364 in. and a correlation length of 2.55 inches. As in the two previous cases the theory derived using the Fresnel approximation agrees with the experimental results far better than does the Fraunhofer theory. The Fresnel theory is within 10 dB of the measured values of the scattering coefficient whereas the Fraunhofer theory is within 22 dB for the complete range of Rayleigh parameters shown in Fig. 19.

A comparison of Figs. 17, 18, and 19 shows that the theoretical law in the Fresnel approximation gives progressively worse agreement with the experimental results as the rms relief of the model surface increases. The reason for this disparity for the rougher surfaces is attributed to

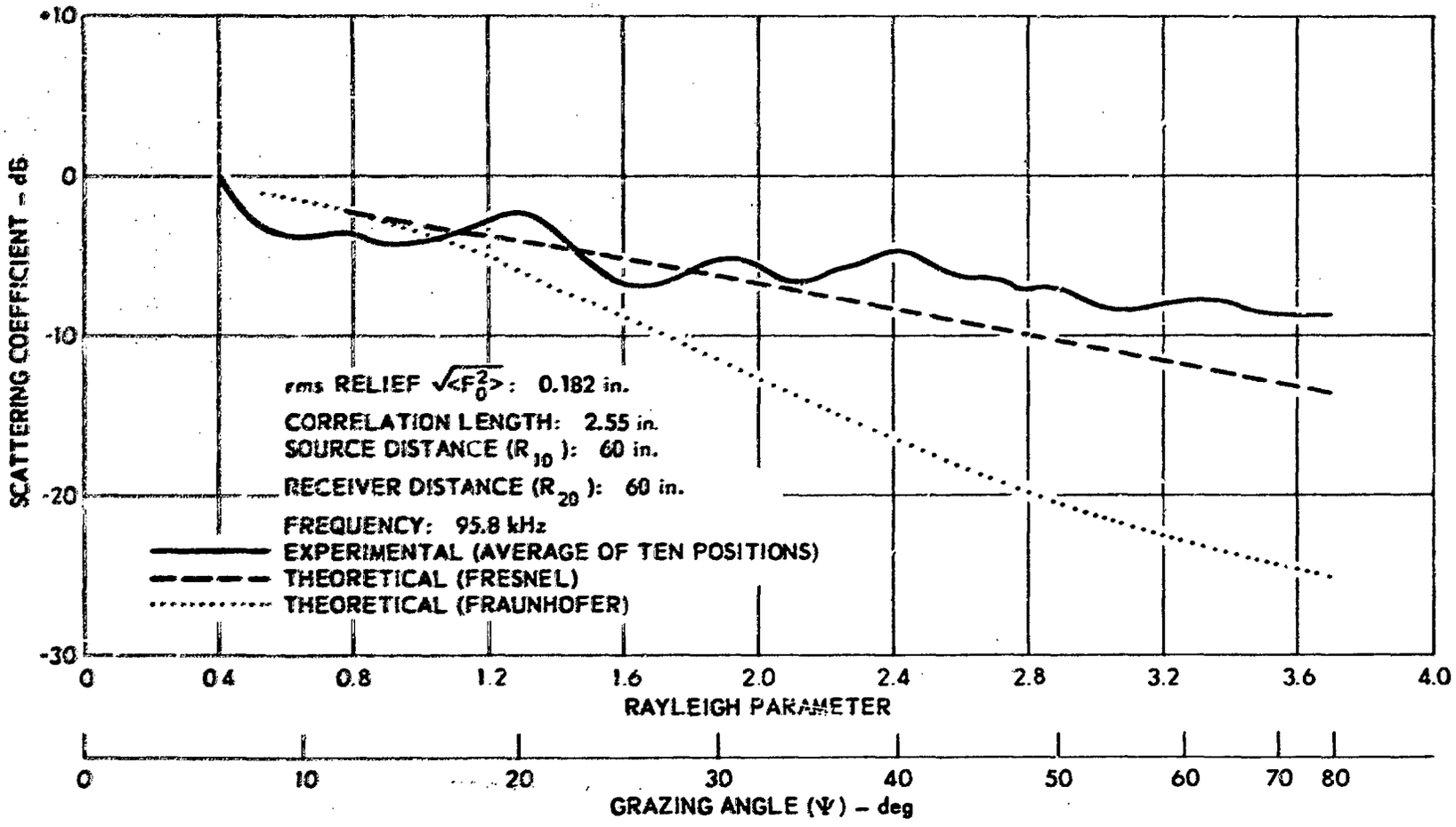


FIGURE 18
SCATTERING COEFFICIENT
IN THE SPECULAR DIRECTION
PRESSURE RELEASE RANDOM SURFACE

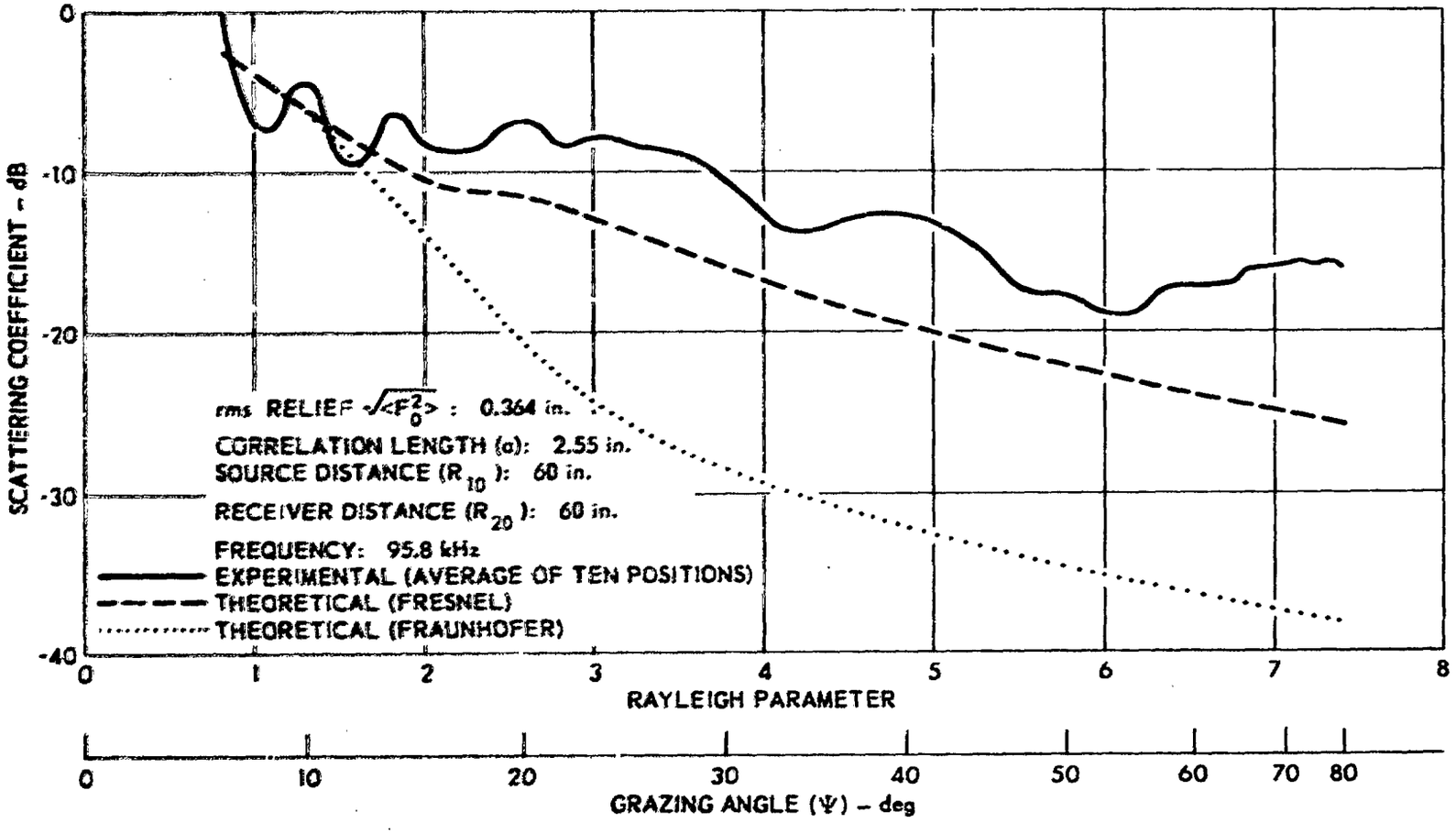


FIGURE 19
SCATTERING COEFFICIENT
IN THE SPECULAR DIRECTION
PRESSURE RELEASE RANDOM SURFACE

the breakdown of the approximation, $\frac{\partial}{\partial n} = \frac{-\partial}{\partial z}$ , used in deriving Eq. (8) from Eq. (7) in Chapter II. As shown in Table I of Chapter IV the slope of the irregularities on the surfaces increases at the same rate as the rms relief of the first three model surfaces. Apparently the slopes for model surface III, results depicted in Fig. 19, are too great to justify the replacement of differentiation along the normal with differentiation along the negative z-axis.

Figure 20 illustrates the experimental measurements and the theoretical predictions of the scattering coefficient for the model surface that has an rms relief of 0.364 in. and a correlation length of 5.10 inches. The irregularities on this model surface are characterized by the same slopes as the model surface studied in Fig. 18. The theory in the Fresnel approximation predicts values for the coefficient within 7 dB of the measured values whereas the Fraunhofer gives values within 19 dB.

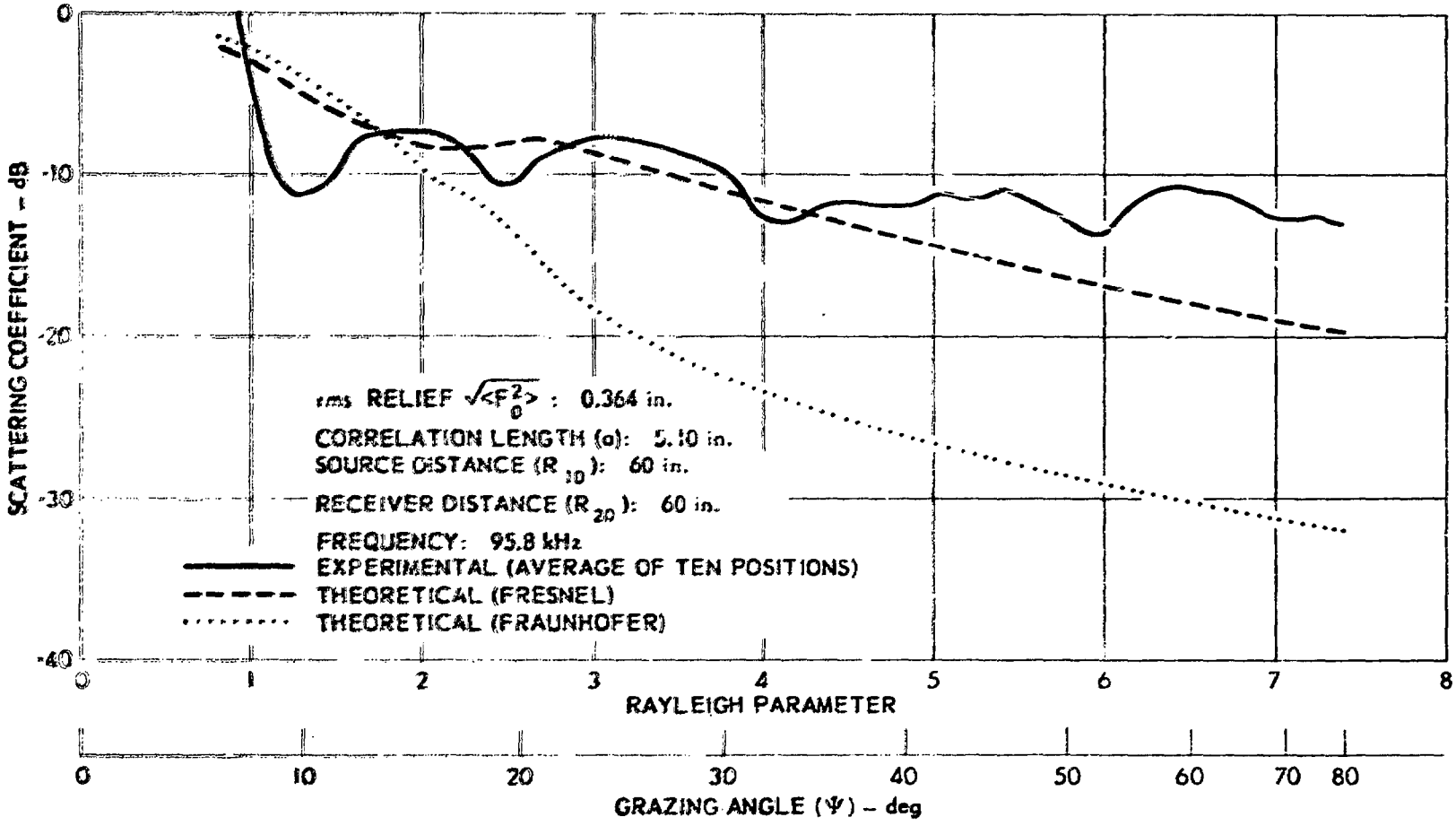


FIGURE 20
SCATTERING COEFFICIENT
IN THE SPECULAR DIRECTION
PRESSURE RELEASE RANDOM SURFACE

# CHAPTER VI
# GENERAL DISCUSSION

## A. Scattering Coefficient

In the previous chapter the dimensions of the insonified area, $\Delta_1$, $\Delta_2$, and $\ell$, which appear in the theoretical expressions, are calculated from Eqs. (B-1), (B-2), and (B-3), in Appendix C by using a 9 deg beamwidth for the incident radiation. Also, the mathematical analysis was simplified by approximating the elliptical scattering region with a rectangular scattering area as shown in Fig. 5a of Chapter III. The 9 deg beamwidth was chosen because

(1) it is the beamwidth measured at the half-power points (-3 dB) of the main lobe of the directivity pattern of the incident radiation illustrated in Fig. 8 of Chapter IV, and

(2) it gives the best agreement of the theoretical law in the Fresnel approximation with the experimental scattering coefficient measured from the "smoothest" model surface, rms relief of 0.091 in., as shown in Fig. 21.

Figure 21 illustrates the influence the value of the beamwidth, and hence the dimensions that the insonified area has on the theoretical predictions. At the Rayleigh parameter of 1.8 the 8 deg beamwidth results in predicted values 1.8 dB smaller than the observed scattering coefficient, the 9 deg beamwidth predicts 0.7 dB larger values, the 10 deg beamwidth predicts 4.6 dB larger values, and the 12 deg beamwidth gives values that are 3.2 dB larger than the measured values of the scattering coefficient.

The effect that a change in the beamwidth of the incident radiation has on the Fresnel theory for the roughest model surface, rms relief of 0.364 in., is illustrated in Fig. 22. With reference to a value of 7.2 for the Rayleigh parameter it is evident from the graph that a 6 deg beamwidth results in a theoretical value for the scattering coefficient that is 16 dB smaller than the measured coefficient, an 8 deg beamwidth predicts a 13.5 dB smaller value, a 9 deg beamwidth gives a 9 dB smaller value, 10 deg beamwidth gives a 4.5 dB lower value, and a 12 deg beamwidth results in a 5 dB lower value.

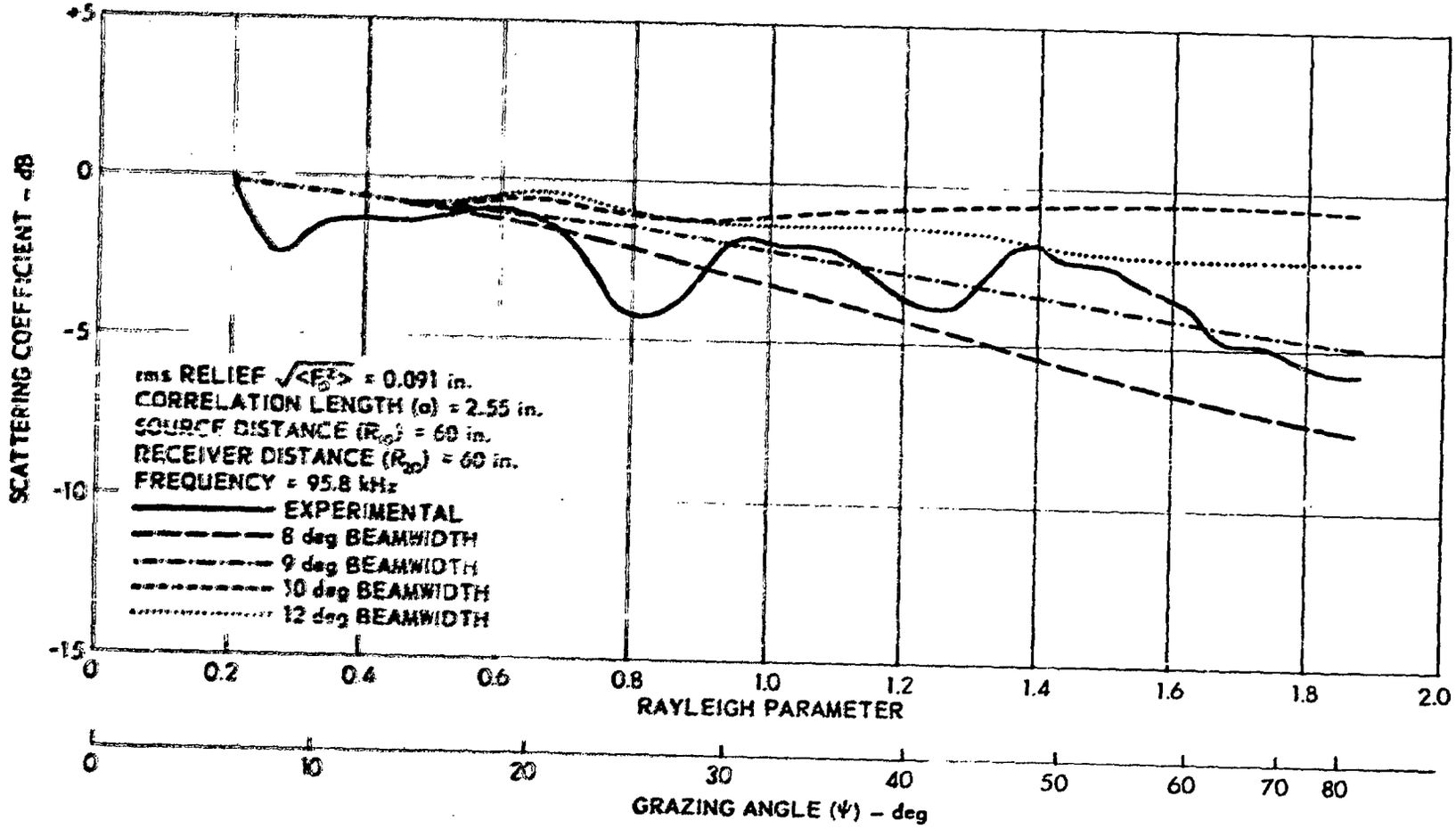


FIGURE 21
SCATTERING COEFFICIENT
FROM THE SMOOTHEST SURFACE
FOR VARIOUS BEAMWIDTHS

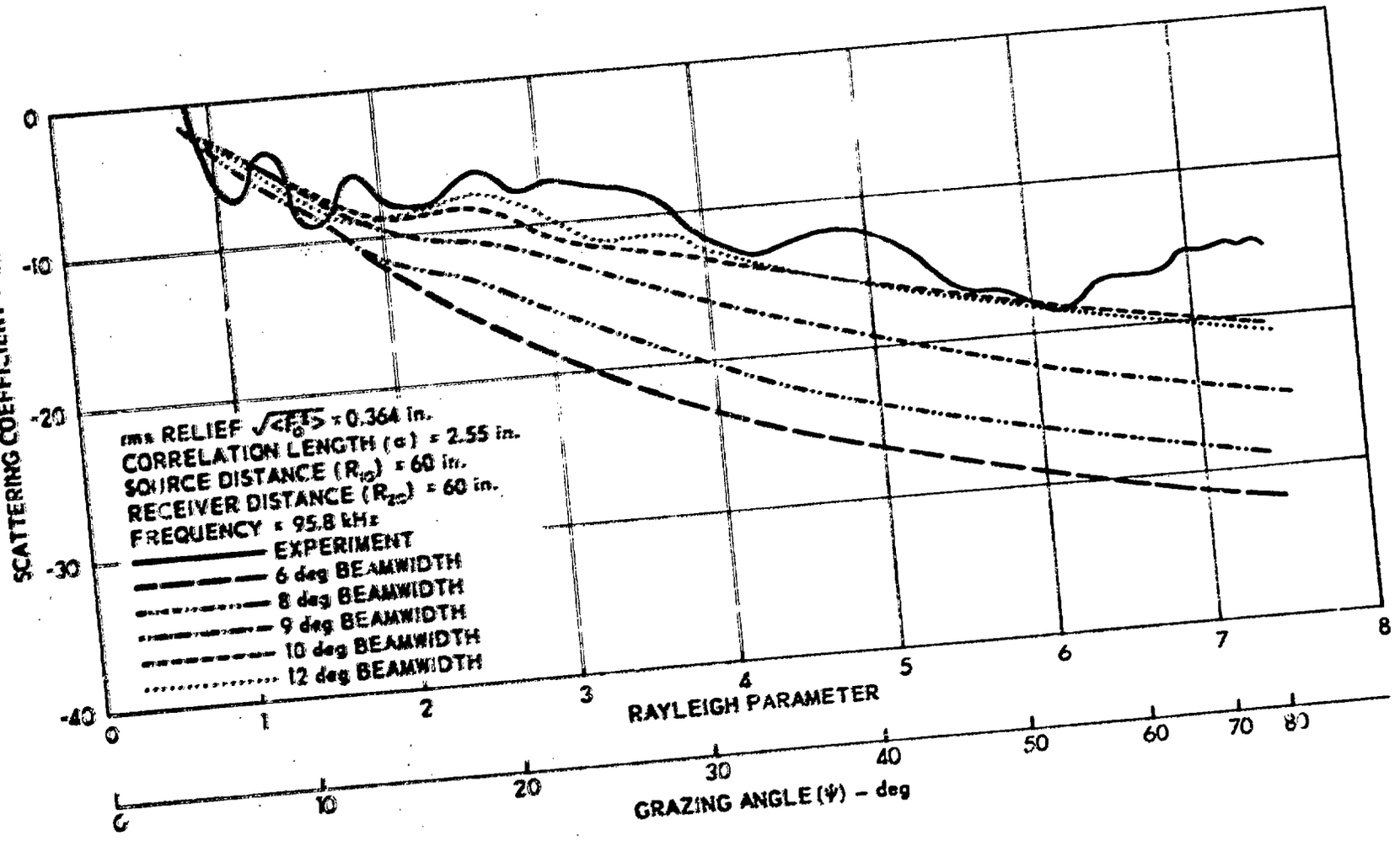


FIGURE 22
SCATTERING COEFFICIENT
FROM THE ROUGHEST SURFACE
FOR VARIOUS BEAMWIDTHS

Even though the 12 deg beam results in predicted values that give best agreement with the observed scattering coefficient for the roughest surface, a 9 deg beamwidth was chosen since this selection agrees best with the experimental results of the smoothest surface shown in Fig. 21. Table I in Chapter IV shows that the slopes of the irregularities of model surface III are four times as great as the slopes on model surface I, the smoothest surface. One would expect the theory, which is subject to the approximation $\partial/\partial n \approx -\partial/\partial z$, to give its best predictions for the experimental results obtained with the model surface that is characterized by the least slopes of the irregularities.

Figure 23 is a plot of Eqs. (53) and (54) of Chapter II,

$$p_o p_o^* = \frac{\left[C_\ell\left(C_{\Delta_1} + C_{\Delta_2}\right) - S_\ell\left(S_{\Delta_1} + S_{\Delta_2}\right)\right]^2 + \left[S_\ell\left(C_{\Delta_1} + C_{\Delta_2}\right) + C_\ell\left(S_{\Delta_1} + S_{\Delta_2}\right)\right]^2}{(R_{10} + R_{20})^2}$$

$$= \frac{K}{(R_{10} + R_{20})^2} \quad ,$$

which is proportional to the intensity in the Fresnel approximation of a wave scattered from a plane surface (the denominator of the scattering coefficient). The change in the intensity with change in the beamwidth is the result of the presence of the Fresnel integrals, C and S, in the expression for $p_o p_o^*$. This relation has been discussed thoroughly by Leizer (1966). A result of his study was that the term K tends to unity in a fluctuating manner as the number of Fresnel zones enclosed within the rectangular insonified area increases. Figure 23 exhibits this behavior very clearly for as the beamwidth of the incident radiation is increased without changing the source distance ($R_{10}$), receiver distance ($R_{20}$), and the frequency, the number of Fresnel zones enclosed in the insonified area increases. The graphs show that as the beamwidth increases from 6 deg to 12 deg the term $p_o p_o^*$ approaches $1/(R_{10} + R_{20})^2$, which is the straight line with the value $69.5 \times 10^{-6}$. Figure B-4 in Appendix B shows that a 9 deg beamwidth produces an insonified area that encloses only one Fresnel zone. A 6 deg beamwidth will insonify an area less than one Fresnel zone whereas a 12 deg beamwidth will insonify

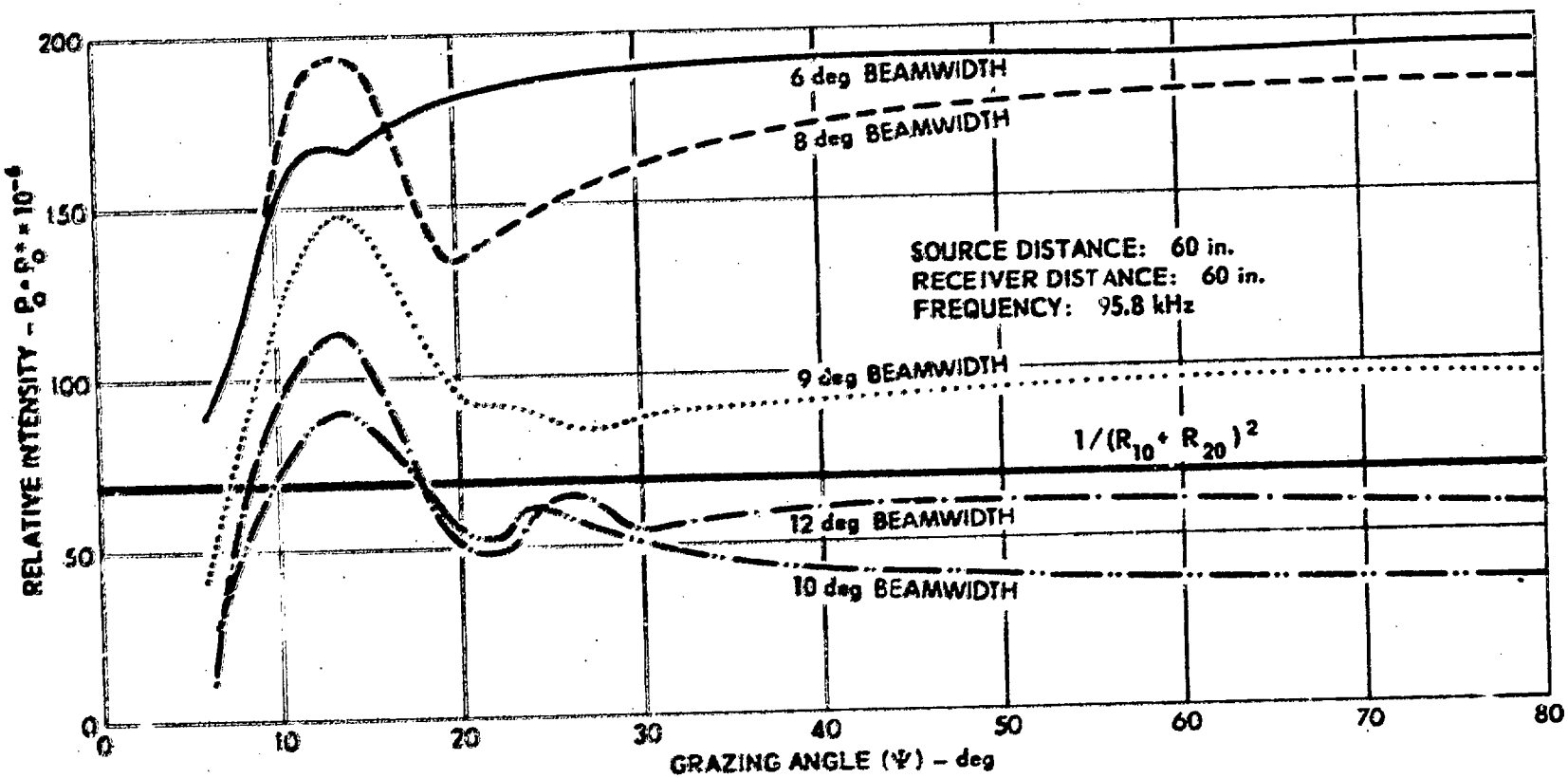


FIGURE 23
RELATIVE INTENSITY (FRESNEL)
REFLECTED IN THE SPECULAR DIRECTION
FROM A PLANE PRESSURE RELEASE SURFACE

approximately the first two Fresnel zones.. Thus, the solution for the intensity reflected from a plane surface calculated in the Fresnel approximation for an active scattering region that is rectangular will become steady as the value K = 1 is approached, and in turn the scattering coefficient will become stable.

Leizer (1965) has shown also that the stability of the intensity reflected from a plane surface is strongly governed by the shape of the insonified area used in the calculations in the Fresnel approximation. His study has shown that when an insonified area of elliptical shape is used in the calculation of $p_o p_o^*$ the term K will fluctuate between constant limits 0 and 4. The indicated minima (K = 0) and maxima (K = 4) are obtained when an even or odd number of Fresnel zones, respectively, exactly fit into the elliptical region. Thus, if an elliptical insonified area had been used in the derivation of the scattering coefficient in this paper, an infinite value for this coefficient would have resulted whenever a beamwidth was chosen that insonified an even number of Fresnel zones. The information of primary importance obtained from Leizer's study was that the solution for the reflected intensity would not stabilize as the number of Fresnel zones encompassed by the elliptical insonified area increased, whereas the solution would stabilize as the number of Fresnel zones enclosed by the rectangular insonified area increased.

This phenomenon does not occur experimentally because the insonified area is not well-defined as Fig. 8 shows. Consequently, the fluctuating behavior of the solution in the Fresnel approximation could be eliminated if better approximations of the transducer beam patterns could be inserted into the theory. Horton and Muir (1967) have used the expression

$$p_o' = \frac{e^{ikR_1}}{R_1} \times e^{-\left(\frac{x_1}{A}\right)^2 - \left(\frac{y}{B}\right)^2}$$

to describe the effect of the radiation pattern of the source on the scattered intensity. This relation describes a transducer pattern whose major lobe insonifies an area $\pi AB$ of elliptical shape on the surface, and that does not have any minor lobes. Their calculations were made in the Fraunhofer

approximation. It is conceivable that the theory presented in the current paper could be improved if the above approximation of the radiation pattern of the source could be inserted into the theoretical development in the Fresnel approximation. However, one may encounter insurmountable analytical difficulties.

The scattered intensity calculated by using the statistical parameters of model surface I and model surface III is plotted versus the grazing angle in Figs. 24 and 25, respectively. The term pp* is the numerator of the scattering coefficient and represents the intensity except for a factor of $1/2Z$ where Z is the specific acoustic impedance of the medium. The graphs show that there is only a small change in the intensity as the beamwidth varies from 8 deg to 12 deg compared with the fluctuating behavior of the formulas derived using the plane surface as depicted in Fig. 23. Thus, the variability of the scattering coefficient with beamwidth, as illustrated in Figs. 21 and 22, is attributed mainly to the fluctuating behavior of the theoretical expression for the intensity reflected from a plane surface, the denominator of the scattering coefficient.

B. Fraunhofer and Fresnel Approximations for the Intensity

The theoretical scattering coefficient in the Fraunhofer approximation gave progressively worse predictions for the observed scattering coefficient as the rms relief $\sqrt{\langle F_o^2 \rangle}$ and/or as the Rayleigh parameter of the rough surface increased. This deviation between the Fraunhofer theory and the experimental results was evident in Figs. 17, 18, and 19 of Chapter V. Thus, the Fraunhofer approximation predicts incorrect values for the scattering coefficient as defined by Eq. (48) of Chapter II, except possibly for the very "smoothest" surfaces.

This phenomenon is reversed when only the intensity of the wave is considered. From Eq. 48 the intensity is

$$\langle I \rangle = \frac{p_o p_o^*}{2\rho v} \sigma_s \quad . \tag{96}$$

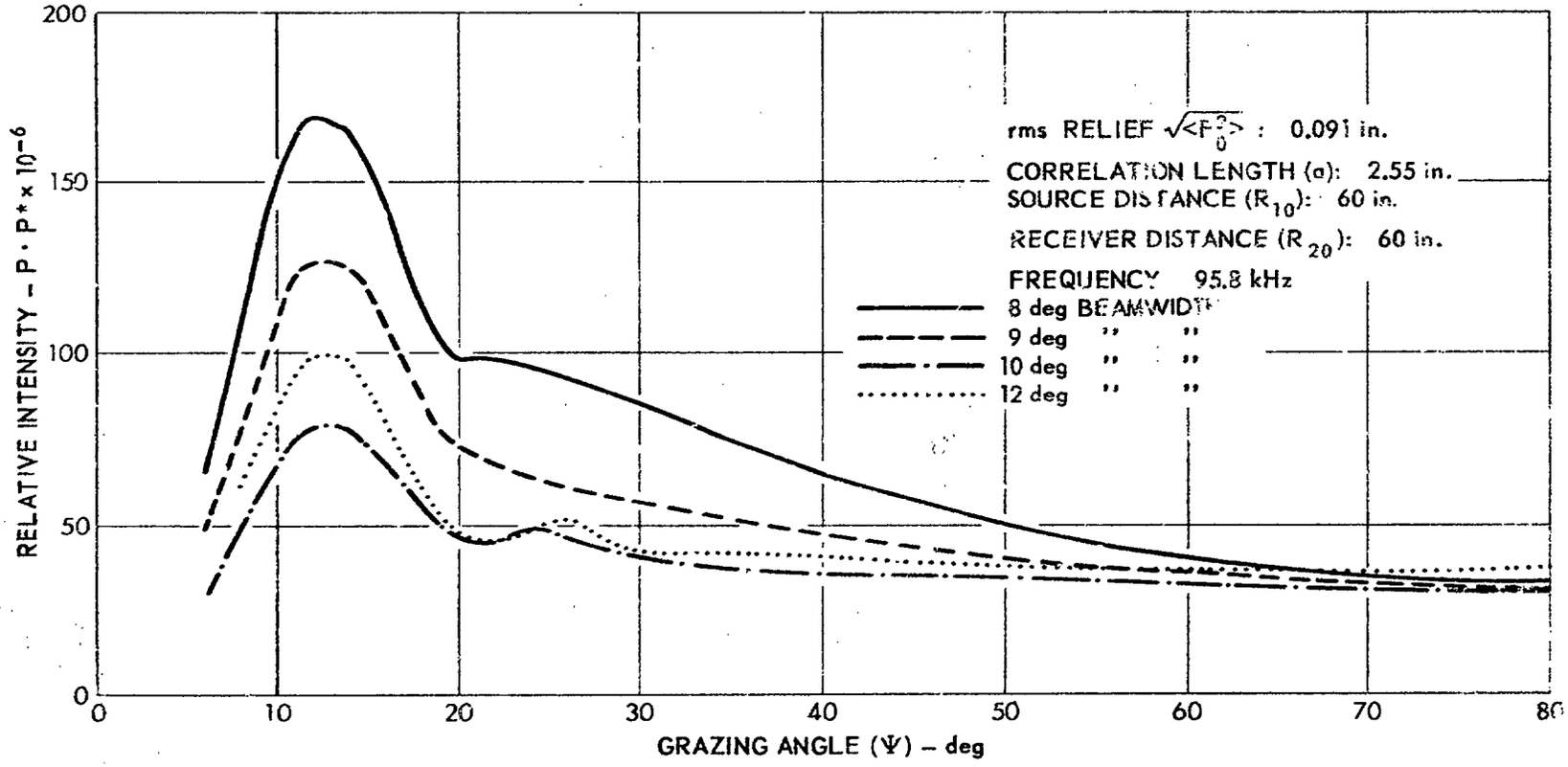


FIGURE 24
RELATIVE INTENSITY
IN THE SPECULAR DIRECTION
PRESSURE RELEASE RANDOM SURFACE

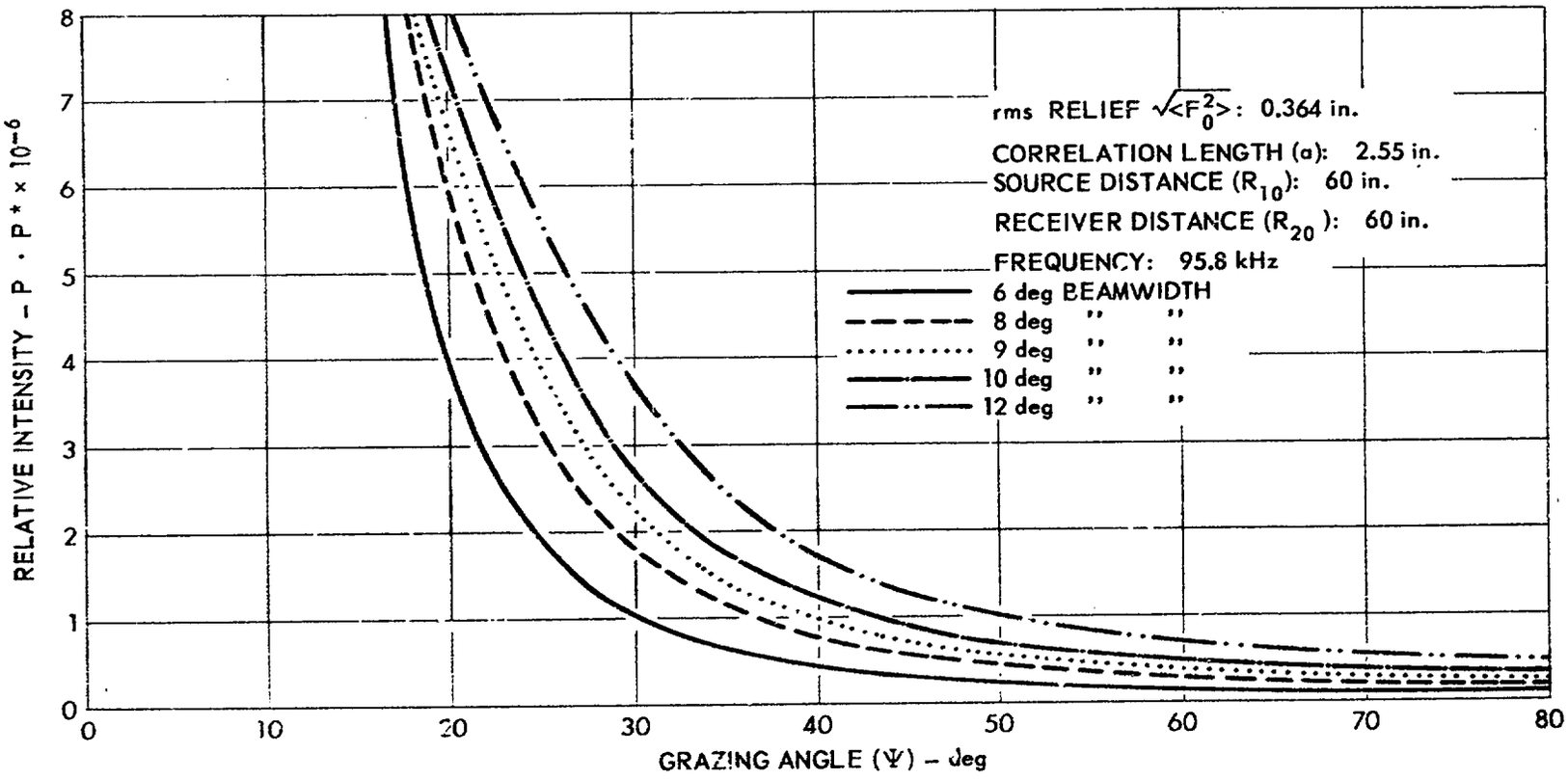


FIGURE 25
RELATIVE INTENSITY
IN THE SPECULAR DIRECTION
PRESSURE RELEASE RANDOM SURFACE

In the Fraunhofer approximation $p_o p_o^*$ is given by Eq. (C-5) in Appendix C, and $\sigma_s$ is given by Eq. (79) in Chapter III. These relations give for the Fraunhofer intensity

$$\langle I \rangle_{FR} = \frac{k^2 \ell^2 (\Delta_1 + \Delta_2)^2 \sin^2 \psi}{2\rho v \pi^2 R_{10}^2 R_{20}^2} e^{-g} \left[ 1 + \frac{a^2 \pi}{\ell(\Delta_1 + \Delta_2)} \sum_{m=1}^{m=\infty} \frac{g^m}{m! m^2} \right] . \quad (97)$$

In the Fresnel approximation $p_o p_o^*$ is given by Eq. (C-12) in Appendix C, and $\sigma_s$ by Eq. (83) in Chapter III. These expressions give for the Fresnel intensity

$$\langle I \rangle_{FL} = \frac{K}{2\rho v (R_{10} + R_{20})^2} e^{-g} \left[ 1 + \frac{2}{g} \sum_{m=1}^{m=\infty} \frac{g^m}{m!} J_1\left(\frac{a}{m}\right) \right] . \quad (98)$$

The ratio of the Fraunhofer to the Fresnel intensity is

$$\frac{\langle I \rangle_{FR}}{\langle I \rangle_{FL}} = \frac{k^2 \ell^2 (R_{10} + R_{20})^2 (\Delta_1 + \Delta_2)^2 \sin^2 \psi \left[ 1 + \frac{a^2 \pi}{\ell(\Delta_1 + \Delta_2)} \sum_{m=1}^{m=\infty} \frac{g^m}{m! m^2} \right]}{\pi^2 R_{10}^2 R_{20}^2 K \left[ 1 + \frac{2}{g} \sum_{m=1}^{m=\infty} \frac{g^m}{m!} J_1\left(\frac{a}{m}\right) \right]} . \quad (99)$$

Figure 26 is a plot of this ratio in decibels given by the relation

$$dB = 10 \log_{10} \left( \frac{\langle I \rangle_{FR}}{\langle I \rangle_{FL}} \right)$$

for the plane surface and the four model surfaces listed in Table I of Chapter IV. A 9 deg beamwidth was used in the calculations. At a grazing angle of 80 deg the ratio for the plane surface is 12 dB, for surface I the ratio is 8 dB, for surface II the ratio is 0.7 dB, and for surfaces III and IV the ratio is less than 0.2 dB. From the graph it is evident that for grazing angles greater than 30 deg the intensity calculated in the Fraunhofer approximation is within 1 dB of the intensity calculated in the

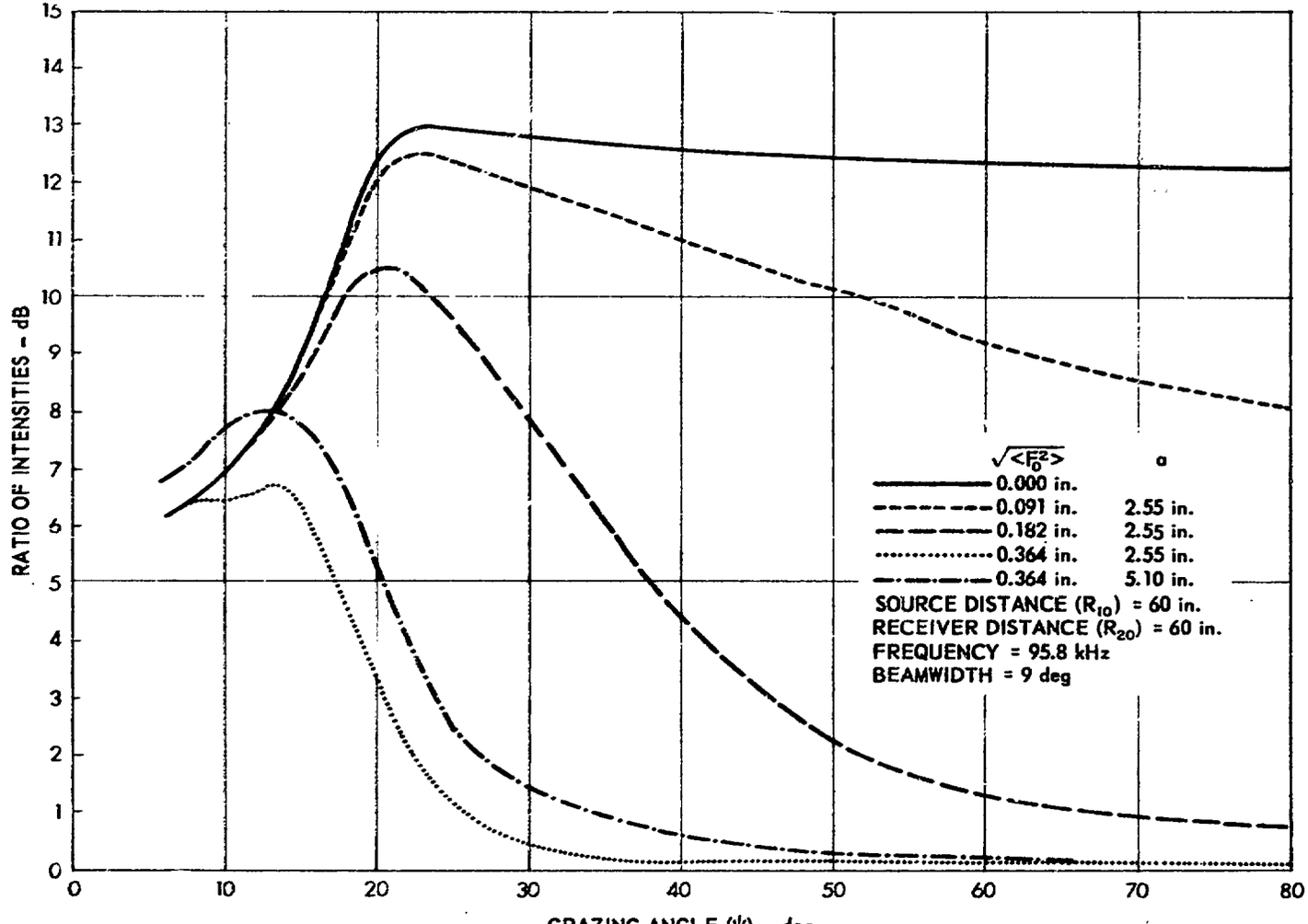


FIGURE 26
RATIO OF FRAUNHOFER TO FRESNEL INTENSITY

Fresnel approximation for the roughest model surface. But for the plane surface the two theories differ by as much as 13 dB for grazing angles greater than 30 deg. Also, the effect that the correlation length has on the approximations is revealed. As the correlation length of a rough surface decreases, the intensity derived using the Fraunhofer approximation approaches the values predicted by the Fresnel approximation. Therefore, the theoretical law for the intensity scattered from a rough surface calculated in the Fraunhofer approximation will give poor agreement with the observed intensity for the smoother surfaces and good agreement for the rougher surfaces.

Figure 27 is a plot of the same ratio vs the Rayleigh parameter for model surfaces I, II, and III. For Rayleigh parameters greater than 4 for the numerical example used throughout this paper, the Fraunhofer approximation will give values for the intensity that are within 1 dB of the values predicted by the theory using the Fresnel approximation. Thus, the choice to use either the Fraunhofer or Fresnel approximation to study the intensity scattered from a surface will depend upon the roughness. A study of the scattering coefficient will require the Fresnel approximation in every case except for a very smooth surface where the Rayleigh parameter is less than one.

C. Application of Model Studies to Ocean and Shallow Water Studies

The slant line distance from the source to the scattering surface in the model studies was 5 ft. A common distance from source to the sea bottom for ocean studies is 5000 ft, which requires a factor of 1000 to scale the model studies to an actual situation in the ocean. Shallow water studies are conducted in many instances at a depth of 100 ft. In this case a scale factor of 20 is needed. The type of source, diameter of source, and frequency of operation needed for these studies to be directly applicable are listed in Table II. Also, the rms relief and the correlation length of the model surfaces, listed in Table I of Chapter IV, should be scaled to conform with the shallow water and ocean studies.

TABLE II

SCALE OF EXPERIMENTAL MODEL STUDIES TO OCEAN AND SHALLOW WATER STUDIES

| Experimental Case | Scale Factor | Distance from Source to Surface ft | Diameter of Source ft | Frequency | Type of Source |
|---|---|---|---|---|---|
| Shallow Water | 20 | 100 | 8.20 | 4.79 kHz | Sonar Transducer Mounted on Ship |
| Ocean | 1000 | 5000 | 410 | 95.8 Hz | Array Mounted on Ocean Bottom |
| Model | 1 | 5 | 0.410 | 95.8 kHz | Transducer |

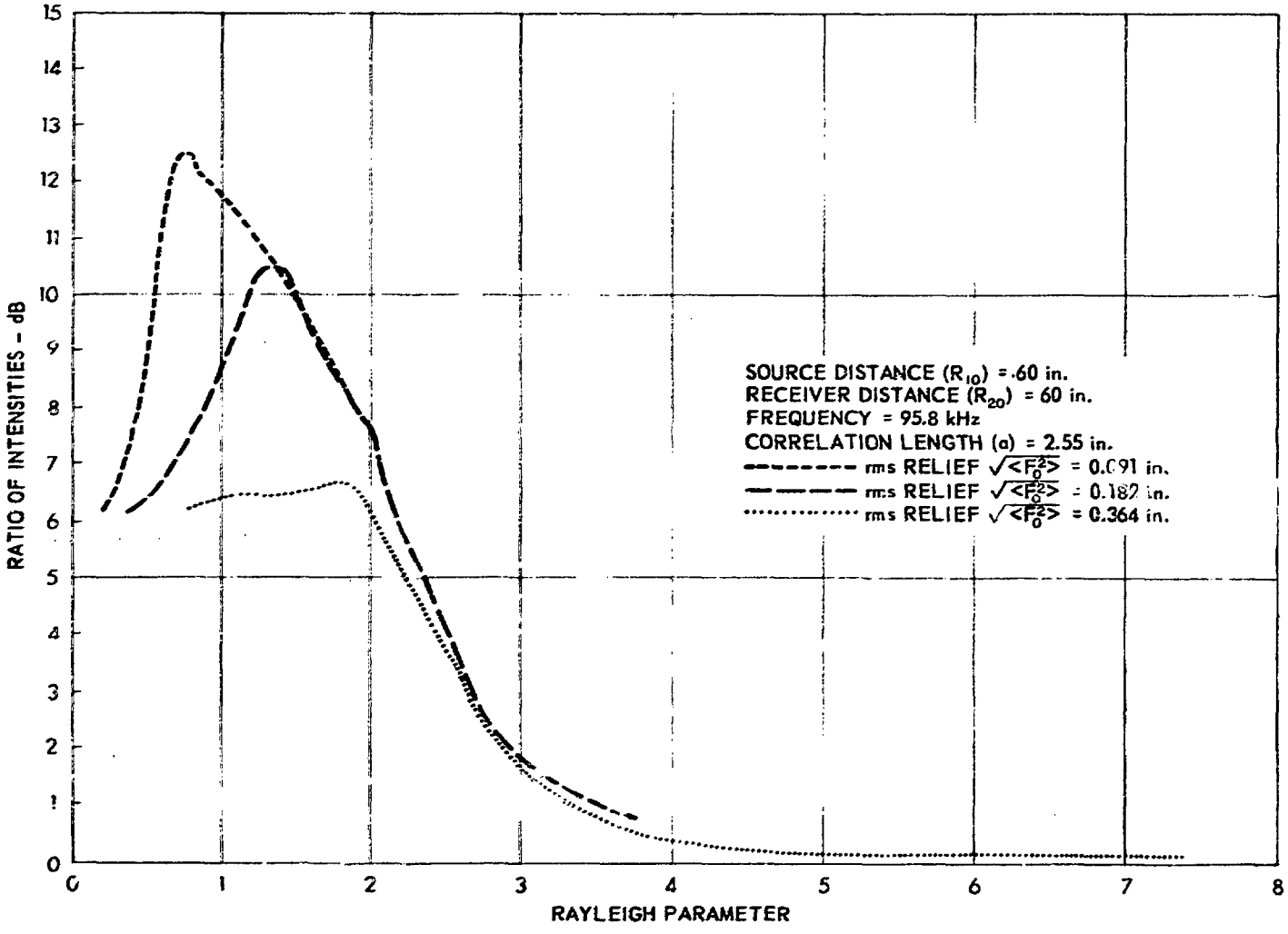


FIGURE 27
RATIO OF FRAUNHOFER TO FRESNEL INTENSITY
PRESSURE RELEASE RANDOM SURFACE

# CHAPTER VII
# CONCLUSIONS

The theoretical approach of Gulin (1962) has been used successfully to predict the observed amplitude and phase fluctuations of an acoustic wave scattered in the specular direction from a rough surface that is described statistically by an exponential covariance function. The theoretical expressions were limited to values of the Rayleigh parameter less than one. The comparison between experimental and theoretical results showed the necessity of the Fresnel theory to describe the amplitude fluctuations. Fraunhofer and Fresnel approximations gave equally good agreement with the experimental phase fluctuations.

The experimental amplitude and phase fluctuations were presented for values of the Rayleigh parameter less than 7.4. The observed amplitude fluctuations in the specular direction for the model studies showed the same behavior as the measurements made in the sea by Gulin and Malyshev (1962), who limited their study to values of the Rayleigh parameter less than 3.5. The author is unaware of any other measurements of the phase fluctuations of underwater acoustic waves scattered from a rough surface. Since accurate measurements of the phase fluctuations are difficult, further experimental studies are desirable.

The theoretical development had to be extended to the Fresnel approximation to obtain values for the scattering coefficient that were in good agreement with the measured values. Even though the theoretical model produced values, which fluctuated notably whenever only a few Fresnel zones were insonified, the theory in the Fresnel approximation gave significantly better agreement with the experimental scattering coefficient than the Fraunhofer approximation for the four randomly rough model surfaces used in this work.

The theory of rough surface scattering presented in this paper used the following assumptions or simplifying procedures:

1. It was assumed that all the radiation that impinged on the rough interface was either reflected or scattered.
2. Multiple scattering was neglected.

3. Shadowing effects were neglected.
4. The radius of curvature of the scattering elements was taken to be much greater than the wavelength of the incident radiation. This restriction along with assumptions 1, 2, and 3 allowed the field at each point of the surface to be represented as the sum of the incident wave and a wave reflected from the plane tangent to the surface at the given point. These statements constitute the Kirchhoff approximation.
5. The distances of the source and the receiver from the scattering surface were assumed to be much greater than a wavelength of the incident radiation.
6. The irregularities were assumed to have sufficiently small slopes so that differentiation along the normal to the surface can be approximately replaced by differentiation along the z-axis. Beckmann (1963) avoided making this assumption by inserting into his theory the complete "local" scattering geometry. However, the additional terms obtained by making this insertion reduced to unity whenever the problem was restricted to the special case of specular scattering.
7. Edge effects caused by the finite size of the model surfaces were neglected in the theory.
8. The amplitude of excitation of the incident radiation was assumed to be practically constant over the active scattering region.
9. The theory for the amplitude and phase fluctuations was restricted to values of the Rayleigh parameter less than one.
10. The probability-density function that governs the simultaneous occurrence of the elevations on the rough surface was assumed to be a bivariate Gaussian distribution.
11. The rough surface was assumed to be randomly rough, isotropic, and stationary in the wide sense.
12. All calculations were restricted to the specular direction.

13. The Fresnel approximation of neglecting cubic and higher ordered terms was employed.
14. The active scattering area was assumed to be large enough so that many surface irregularities were enclosed within this region.
15. In the application of the theoretical formulas to an actual situation it was assumed that the active scattering region was the insonified area irrespective of the number of Fresnel zones insonified.
16. The beam pattern of the energy radiated from the source was approximated by a cone that had a beamwidth measured at the half-power points (-3 dB) of the actual transducer radiation pattern.
17. The elliptical insonified area resulting from the intersection of the conical beam of incident radiation with the scattering surface was approximated by a rectangular active scattering region.

Although this list of assumptions is lengthy, they are utilized by nearly all workers in this field. The substantiated agreement between experiment and theory shows the assumptions are physically acceptable. The major innovation of the present study is assumption 13. Although the Fresnel assumption has been utilized in a few theoretical studies, nowhere has a systematic study been made of the importance of the Fresnel terms.

In future studies it may be possible to withdraw some of these assumptions at the cost of mathematical simplicity. For example, it may be possible to remove assumption 16 by using a better approximation for the radiation pattern of the source such as was discussed by Horton and Muir (1967). It is very likely that restriction 12 could be generalized somewhat to include the case of any receiving angle independent of the grazing angle in the plane of incidence.

# APPENDIX A

## THE FRAUNHOFER AND FRESNEL APPROXIMATIONS

Figure 3 depicts the coordinate system with the origin at O. The geometry of the scattering of acoustic waves from a randomly rough surface with the origin at O' is illustrated in Fig. A-1. As in Fig. 3 the source Q and the receiver A are confined to the x-z plane. This translation of the origin along the x-axis is expressed as

$$x = x_1 + R_{10} \cos \psi_1 \quad ,$$

and for the specular direction can be written as

$$x_1 = x - \frac{Lz_1}{z_1 + z_2} \quad . \tag{A-1}$$

With reference to Fig. A-1 the distance $R_1$ can be expanded in terms of $R_{10}$. With the angle between r and $R_{10}$ denoted as $\theta_1$, the law of cosines gives

$$R_1 = \left( R_{10}^2 + r^2 - 2R_{10} r \cos \theta_1 \right)^{1/2} \quad . \tag{A-2}$$

This equation can be expressed in terms of the directional angles, $\alpha_1$ and $\gamma_1$, of the unit vector, $\vec{n}_1$, directed from the origin O' toward the source Q,

$$\vec{n}_1 = \vec{e}_{x_1} \cos \alpha_1 + \vec{e}_z \cos \gamma_1 \quad ,$$

and writing r as

$$\vec{r} = x_1 \vec{e}_{x_1} + y \vec{e}_y + z \vec{e}_z \quad .$$

Thus, with

$$\vec{r} \cdot \vec{r} = r^2 = x_1^2 + y^2 + z^2 \quad , \text{ and}$$

$$\vec{r} \cdot \vec{n}_1 = |\vec{r}||n_1| \cos \theta_1 = r \cos \theta_1 = x_1 \cos \alpha_1 + z \cos \gamma_1 \quad ,$$

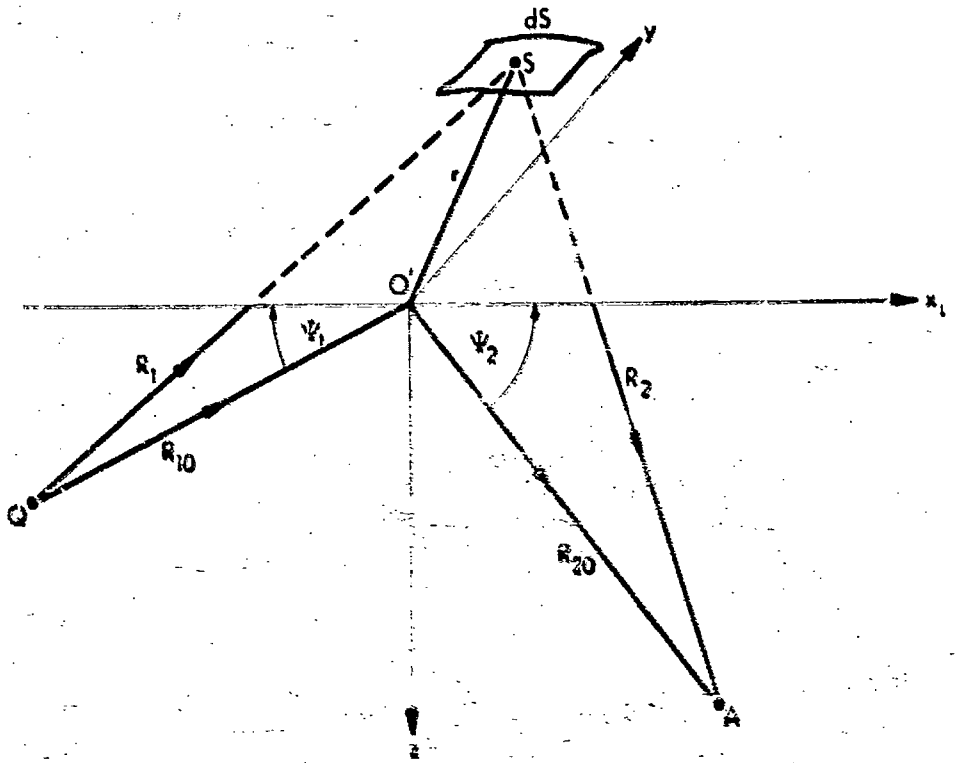


FIGURE A-1
COORDINATE SYSTEM
FOR THE EXPANSION OF $R_1$
AND $R_2$ IN TERMS OF $R_{10}$ AND $R_{20}$

$R_1$ becomes

$$R_1 = \left( R_{10}^2 - 2R_{10}x_1 \cos \alpha_1 - 2R_{10}z \cos \gamma_1 + x_1^2 + y^2 + z^2 \right)^{1/2} \quad . \quad \text{(A-3)}$$

$R_1$ can be expressed in terms of the grazing angle $\psi_1$,

$$\alpha_1 = 180 \text{ deg} - \psi_1$$

$$\cos \alpha_1 = - \cos \psi_1$$

$$\gamma_1 = 90 \text{ deg} - \psi_1$$

$$\cos \gamma_1 = \sin \psi_1 \quad ,$$

as

$$R_1 = R_{10} \left( 1 + \frac{2x_1 \cos \psi_1}{R_{10}} - \frac{2z \sin \psi_1}{R_{10}} + \frac{x_1^2 + y^2 + z^2}{R_{10}^2} \right)^{1/2} \quad . \quad \text{(A-4)}$$

Expanding Eq. (A-4), one obtains for $R_1$

$$\begin{aligned} R_1 = {} & (R_{10} + x_1 \cos \psi_1 - z \sin \psi_1) + \left( \frac{x_1^2 \sin^2 \psi_1}{2R_{10}} + \frac{y^2}{2R_{10}} \right. \\ & \left. + \frac{z^2 \cos^2 \psi_1}{2R_{10}} - \frac{x_1 z \sin \psi_1 \cos \psi_1}{R_{10}} \right) + \left( - \frac{x_1^3}{2R_{10}^2} \sin^2 \psi_1 \cos \psi_1 \right. \\ & + \frac{x_1 z^2}{2R_{10}^2} \sin \psi_1 \cos^2 \psi_1 + \frac{x_1^2 z}{2R_{10}^2} \sin^3 \psi_1 - \frac{x_1 z^2}{2R_{10}^2} \cos^3 \psi_1 \\ & \left. - \frac{x_1 y^2}{2R_{10}^2} \cos \psi_1 + \frac{z y^2 \sin \psi_1}{2R_{10}^2} \right) + \text{higher order terms} \quad . \end{aligned} \quad \text{(A-5)}$$

In a similar way $R_2$ can be written in terms of $R_{20}$ to give

$$R_2 = (R_{20} - x_1 \cos \psi_2 - z \sin \psi_2) + \left( \frac{x_1^2 \sin^2 \psi_2}{2R_{20}} + \frac{y^2}{2R_{20}} \right.$$

$$\left. + \frac{z^2 \cos \psi_2}{2R_{20}} + \frac{x_1 z \sin \psi_2 \cos \psi_2}{R_{20}} \right) + \left( \frac{x_1^3}{2R_{20}^2} \sin^2 \psi_2 \cos \psi_2 \right. \tag{A-6}$$

$$+ \frac{z^3}{2R_{20}^2} \sin \psi_2 \cos^2 \psi_2 + \frac{x_1^2 z}{2R_{20}^2} \sin^3 \psi_2 + \frac{x_1 z^2}{2R_{20}} \cos^3 \psi_2$$

$$\left. + \frac{x_1 y^2}{2R_{20}^2} \cos \psi_2 + \frac{zy^2}{2R_{20}^2} \sin \psi_2 \right) + \text{higher order terms} \quad .$$

Adding Eqs. (A-5) and (A-6), one obtains

$$R_1 + R_2 = \left[R_{10} + R_{20} + x_1(\cos\psi_1 - \cos\psi_2) - z(\sin\psi_1 + \sin\psi_2)\right]$$

$$+ \left[x_1^2\left(\frac{\sin^2\psi_1}{2R_{10}} + \frac{\sin^2\psi_2}{2R_{20}}\right) + y^2\left(\frac{1}{2R_{10}} + \frac{1}{2R_{20}}\right)\right.$$

$$\left. + z^2\left(\frac{\cos^2\psi_1}{2R_{10}} + \frac{\cos^2\psi_2}{2R_{20}}\right) + x_1 z\left(\frac{\sin\psi_2\cos\psi_2}{R_{20}} - \frac{\sin\psi_1\cos\psi_1}{R_{10}}\right)\right]$$

$$+ \left[x_1^3\left(\frac{\sin^2\psi_2\cos\psi_2}{2R_{20}^2} - \frac{\sin^2\psi_1\cos\psi_1}{2R_{10}^2}\right) + z^3\left(\frac{\sin\psi_1\cos^2\psi_1}{2R_{10}^2}\right.\right. \quad \text{(A-7)}$$

$$\left.\left. + \frac{\sin\psi_2\cos^2\psi_2}{2R_{20}^2}\right) + x_1^2 z\left(\frac{\sin^3\psi_1}{2R_{10}^2} + \frac{\sin^3\psi_2}{2R_{20}^2}\right)\right.$$

$$\left. + x_1 z^2\left(\frac{\cos^3\psi_2}{2R_{20}^2} - \frac{\cos^3\psi_1}{2R_{10}^2}\right) + x_1 y^2\left(\frac{\cos\psi_2}{2R_{20}^2} - \frac{\cos\psi_1}{2R_{10}^2}\right)\right.$$

$$\left. + zy^2\left(\frac{\sin\psi_1}{2R_{10}^2} + \frac{\sin\psi_2}{2R_{20}^2}\right)\right] + \text{higher order terms} \quad .$$

In the integrals appearing in Chapter II the z dependency is taken out of $R_1 + R_2$ as illustrated in Eqs. (11) and (13) so that one is interested in $R_1' + R_2'$. Thus, for $z = 0$, $R_1 = R_1'$ and $R_2 = R_2'$ and Eq. (A-7) reduces to

$$R_1' + R_2' = \left[R_{10} + R_{20} + x_1(\cos \psi_1 - \cos \psi_2)\right]$$

$$+ \left[x_1^2\left(\frac{\sin^2 \psi_1}{2R_{10}} + \frac{\sin^2 \psi_2}{2R_{20}}\right) + y^2\left(\frac{1}{2R_{10}} + \frac{1}{2R_{20}}\right)\right]$$

$$+ \left[x_1^3\left(\frac{\sin^2 \psi_2 \cos \psi_2}{2R_{20}^2} - \frac{\sin^2 \psi_1 \cos \psi_1}{2R_{10}^2}\right)\right. \tag{A-8}$$

$$\left. + x_1 y^2\left(\frac{\cos \psi_2}{2R_{20}^2} - \frac{\cos \psi_1}{2R_{10}^2}\right)\right] + \text{quartic and higher order terms} \quad .$$

The Fraunhofer approximation is the neglect of the quadratic and higher order terms in Eq. (A-8). The quadratic terms are insignificant whenever

$$k\left[\Delta_2^2\left(\frac{\sin^2 \psi_1}{2R_{10}} + \frac{\sin^2 \psi_2}{2R_{20}}\right) + \ell^2\left(\frac{1}{2R_{10}} + \frac{1}{2R_{20}}\right)\right] \ll 1 \quad , \tag{A-9}$$

where

$k$ is the wavenumber,

$\Delta_2$ is the maximum dimension of the active scattering region in the $+x_1$--direction, and

$\ell$ is the maximum dimension of the active scattering region in the $+y$--direction ($\Delta_2$ and $\ell$ are discussed in detail in Appendix B).

It is seen from solving Eq. (A-9) for $R_{20}$ that the receiver will be in the Fraunhofer zone (farfield) when

$$R_{20} \gg \frac{k\left(\Delta_2^2 \sin^2 \psi_2 + \ell^2\right)}{2 - \frac{k}{R_{10}}\left(\Delta_2^2 \sin^2 \psi_1 + \ell^2\right)} \quad . \tag{A-10}$$

The Fresnel approximation is the neglect of the cubic and higher order terms in Eq. (A-8). The receiver will be situated in the Fresnel zone when

$$k\left[\Delta_2^3\left(\frac{\sin^2\psi_2\cos\psi_2}{2R_{20}^2}-\frac{\sin^2\psi_1\cos\psi_1}{2R_{10}^2}\right)+\Delta_2\ell^2\left(\frac{\cos\psi_2}{2R_{20}^2}-\frac{\cos\psi_1}{2R_{10}^2}\right)\right]\ll 1 \quad . \quad \text{(A-11)}$$

Solving for $R_{20}$, one obtains

$$R_{20}\gg\left[\frac{k\cos\psi_2\left(\Delta_2^3\sin^2\psi_2+\Delta_2\ell^2\right)}{2+\frac{k\cos\psi_1}{R_{10}^2}\left(\Delta_2^3\sin^2\psi_1+\Delta_2\ell^2\right)}\right]^{1/2} \quad . \quad \text{(A-12)}$$

Thus, the receiver lies within the Fresnel zone when

$$\frac{k\left(\Delta_2^2\sin^2\psi_2+\ell^2\right)}{2-\frac{k}{R_{10}}\left(\Delta_2^2\sin^2\psi_1+\ell^2\right)}\gg R_{20}$$

$$\gg\left[\frac{k\cos\psi_2\left(\Delta_2^3\sin^2\psi_2+\Delta_2\ell^2\right)}{2+\frac{k\cos\psi_1}{R_{10}^2}\left(\Delta_2^3\sin^2\psi_1+\Delta_2\ell^2\right)}\right]^{1/2} \quad . \quad \text{(A-13)}$$

The Fraunhofer approximation to Eq. (A-8) can be written as

$$R_1'+R_2'=R_{10}+R_{20}+ex_1 \quad . \quad \text{(A-14)}$$

where

$$e=\cos\psi_1-\cos\psi_2 \quad . \quad \text{(A-15)}$$

The Fresnel approximation to Eq. (A-8) can be written as

$$R_1' + R_2' = R_{10} + R_{20} + cx_1 + \frac{1}{R_s} x_1^2 + \frac{1}{R} y^2 \quad , \tag{A-16}$$

where

$$R_s = \frac{2R_{10}R_{20}}{R_{10} \sin^2 \psi_2 + R_{20} \sin^2 \psi_1} \quad , \text{ and} \tag{A-17}$$

$$R = \frac{2R_{10}R_{20}}{R_{10} + R_{20}} \quad . \tag{A-18}$$

For the specular direction

$$\psi_1 = \psi_2 = \psi \quad ,$$

and Eq. (A-8) reduces to

$$R_1' + R_2' = R_{10} + R_{20} + \frac{1}{R} \left( x_1^2 \sin^2 \psi + y^2 \right) + \text{quartic and higher order terms} \quad . \tag{A-19}$$

Note that the linear and cubic terms have vanished so that the relation is exact through cubic terms for the Fresnel approximation in the specular direction. The Fraunhofer approximation in the specular direction is simply

$$R_1' + R_2' = R_{10} + R_{20} \quad . \tag{A-20}$$

When the Fraunhofer approximation, Eq. (A-20) or the Fresnel approximation, Eq. (A-19), is made in Eqs. (14), (17), (20), or (21) of Chapter II only the approximations

$$R_1'R_2' = R_{10}R_{20} \quad ,$$

$$R_1' = R_{10} \quad , \text{ and} \tag{A-21}$$

$$R_2' = R_{20} \quad ,$$

The Fresnel approximation to Eq. (A-8) can be written as

$$R_1' + R_2' = R_{10} + R_{20} + cx_1 + \frac{1}{R_s} x_1^2 + \frac{1}{R} y^2 \quad , \tag{A-16}$$

where

$$R_s = \frac{2R_{10}R_{20}}{R_{10} \sin^2 \psi_2 + R_{20} \sin^2 \psi_1} \quad , \text{ and} \tag{A-17}$$

$$R = \frac{2R_{10}R_{20}}{R_{10} + R_{20}} \quad . \tag{A-18}$$

For the specular direction

$$\psi_1 = \psi_2 = \psi \quad ,$$

and Eq. (A-8) reduces to

$$R_1' + R_2' = R_{10} + R_{20} + \frac{1}{R} \left( x_1^2 \sin^2 \psi + y^2 \right) + \text{quartic and higher order terms} \quad . \tag{A-19}$$

Note that the linear and cubic terms have vanished so that the relation is exact through cubic terms for the Fresnel approximation in the specular direction. The Fraunhofer approximation in the specular direction is simply

$$R_1' + R_2' = R_{10} + R_{20} \quad . \tag{A-20}$$

When the Fraunhofer approximation, Eq. (A-20) or the Fresnel approximation, Eq. (A-19), is made in Eqs. (14), (17), (20), or (21) of Chapter II only the approximations

$$R_1'R_2' = R_{10}R_{20} \quad ,$$

$$R_1' = R_{10} \quad , \text{ and} \tag{A-21}$$

$$R_2' = R_{20} \quad ,$$

are used in all the terms of the integrand except in the term $k(R_1' + R_2')$ that represents the phase. What is implied by these approximations is that at distances from the uneven surface, large compared to the dimensions of the active scattering region, the amplitude of the pressure wave produced by any particular surface element differs only slightly from that produced by any other element. On the other hand the relative phase of the pressures produced at the receiver by any two surface elements depends on the differences in the distance of the two elements from the receiver, and for distant points this difference is practically independent of $R_1'$ and $R_2'$. As a consequence, one must use the entire expressions given in Eqs. (A-19) and (A-20) in the term $k(R_1' + R_2')$ appearing in the integrands of Eqs. (14), (17), (20), and (21).

Consider a numerical calculation of the Fraunhofer and Fresnel distances, $R_{20}$, as given by Eqs. (A-10) and (A-12). The source is placed 60.0 in. ($R_{10}$) from the surface. With the source and receiver maintained in the specular direction, the grazing angle of the source is varied. It is desired to know where the receiver must be placed relative to the surface ($R_{20}$) so that the experimental data can be compared with theory that was developed using either the Fraunhofer or the Fresnel approximation. These positions of the receiver are referred to as the Fraunhofer field zone or the Fresnel field zone, whichever the case may be. The calculations are made for a frequency of 95.8 kHz and for a 9 deg beamwidth of the source. The active region of the surface is taken to be the insonified area whose dimensions are calculated from Eqs. (B-1), (B-2), and (B-3) in Appendix B. The results for this plane surface example are illustrated in Fig. A-2. The calculations show that it is physically impossible to place the receiver in the Fraunhofer field zone for specular reflection from a plane surface. The receiver must be placed at distances much greater than 44 in. ($R_{20}$) from the pressure release plane surface at 95.8 kHz in order that it remain in the Fresnel field zone at all receiving angles. The abrupt change in the boundary of the Fresnel field zone at 22 deg receiving angle is the result of the finite dimensions of the reflecting surface, that is, $\Delta_2$ is held constant = 16 in. for grazing angles less than 22 deg.

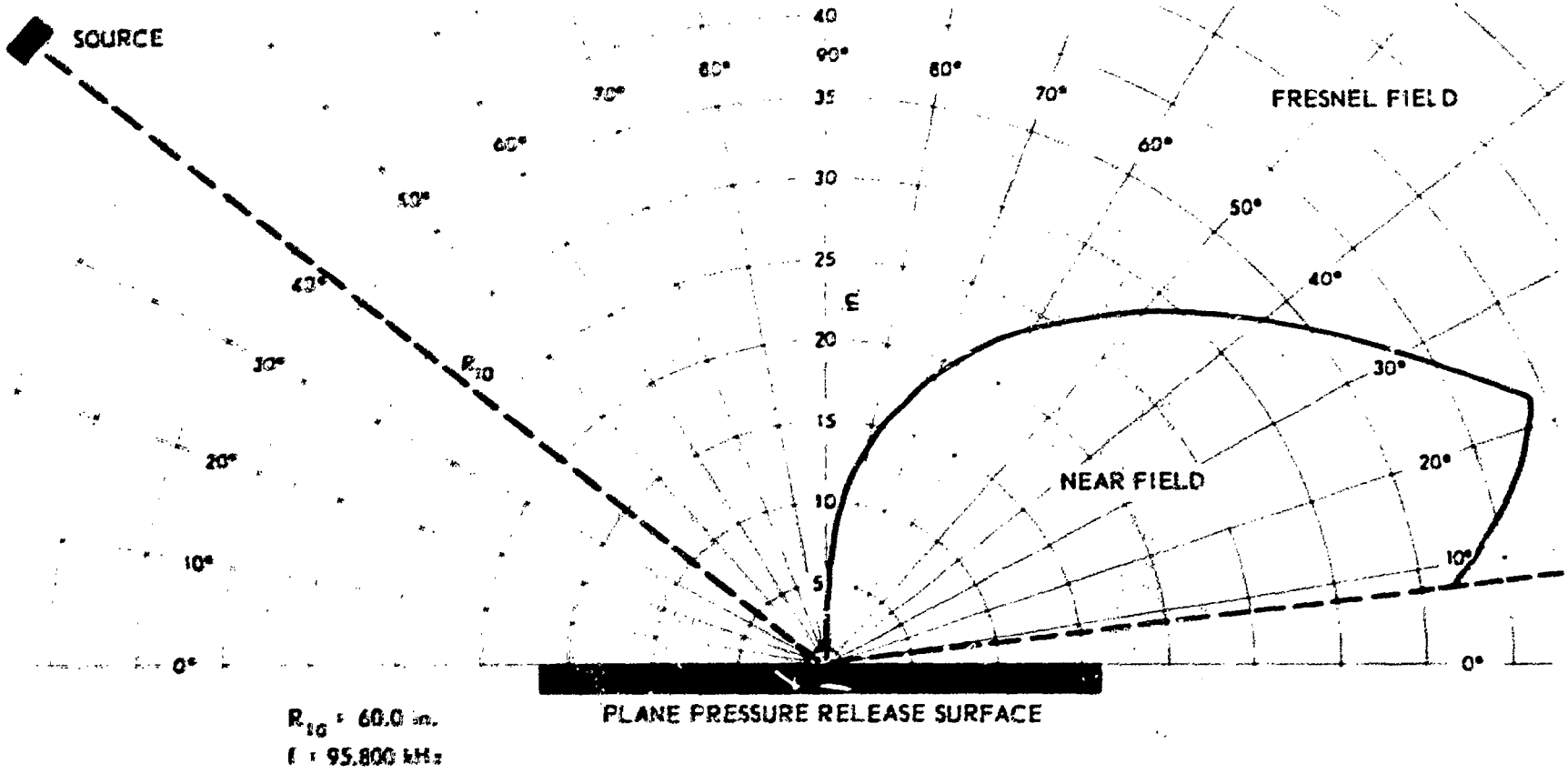


FIGURE A-2
NEAR AND FRESNEL FIELD
PLANE PRESSURE RELEASE SURFACE
SPECULAR DIRECTION

In Chapter VI it is shown (see Fig. 27) that as the roughness (the Rayleigh parameter which for a plane surface is zero) increases, the Fraunhofer field zone moves in from infinity to some finite distance from the rough surface. Figure 27 of Chapter VI shows for the numerical example cited that for values of the Rayleigh parameter greater than 4 the Fraunhofer approximation predicts quantities that are well within 1 dB of the values obtained using the Fresnel approximation. The interpretation of this behavior is that for very rough surfaces the irregularities on the surface act as individual scatterers. Thus, one should not insert into Eqs. (A-10) and (A-12) the dimensions of the active scattering region, $\Delta_2$ and $\ell$, but should substitute the dimensions of the surface irregularities. For example, if one took the correlation length $\underline{a}$ (2.55 in. for three of the model surfaces) for the maximum x and y dimensions, Eq. (A-10) would give for the previously cited example for a grazing angle of 40 deg

$$R_{20} \gg 15 \text{ in.} \quad ,$$

for the Fraunhofer field zone.

In summary, for Rayleigh parameters much less than one the dimensions of the active scattering region are used in Eqs. (A-10) and (A-12). When only a few Fresnel zones on the surface are insonified the dimensions of the active scattering region are taken to be the dimensions of the insonified area (see Appendix B). For Rayleigh parameters much greater than one the dimensions of the irregularities on the surface are used. A satisfactory approximation of the size of the irregularities is the correlation length, $\underline{a}$.

# APPENDIX B

## ACTIVE SCATTERING REGION

What regions of the scattering surface are the most important in contributing to the total field at a given receiving point when the surface is illuminated by a source at a given point? Beckmann (1963) has stated that the answer is "the first few Fresnel zones" located on the scattering surface. For an omnidirectional source one would use the dimensions of the first few Fresnel zones as the limits on the integrals appearing in Chapter II.

In the experimental work a directional source was used, which has a directivity pattern illustrated in Fig. B-1. Only a finite portion of the scattering surface is insonified. The insonified area will be defined as the intersection of the half-power points (-3 dB) of the main lobe of the directivity pattern with the scattering surface. It is of interest to determine both the dimensions of the first few Fresnel zones and the dimensions of the irradiated surface.

The length of the irradiated surface is determined by the angular width of the directivity characteristic of the transmitter, the slope of its axis, and the distance from the transmitter to the scattering surface. The dimensions of the insonified area can be derived in the following manner. From Fig. B-1

$$A = 180 \text{ deg} - \frac{\Phi}{2} - \Psi_1$$

where $\Psi_1$ is the grazing angle and $\Phi$ is the beamwidth measured at the half-power points of the major lobe. The relations

$$D = 180 \text{ deg} - A = \frac{\Phi}{2} + \Psi_1 \quad , \text{ and}$$

$$B = 180 \text{ deg} - \frac{\Phi}{2} - C = -\frac{\Phi}{2} + \Psi_1 \quad ,$$

give for the linear dimensions $\Delta_1$ and $\Delta_2$ in the $x_1$ direction

$$\Delta_1 = R_{10} \cos \Psi_1 - r_1 \cos(\Psi_1 + \tfrac{\Phi}{2}) \quad , \text{ and}$$

$$\Delta_2 = r_2 \cos(\Psi_1 - \tfrac{\Phi}{2}) - R_{10} \cos \Psi_1 \quad .$$

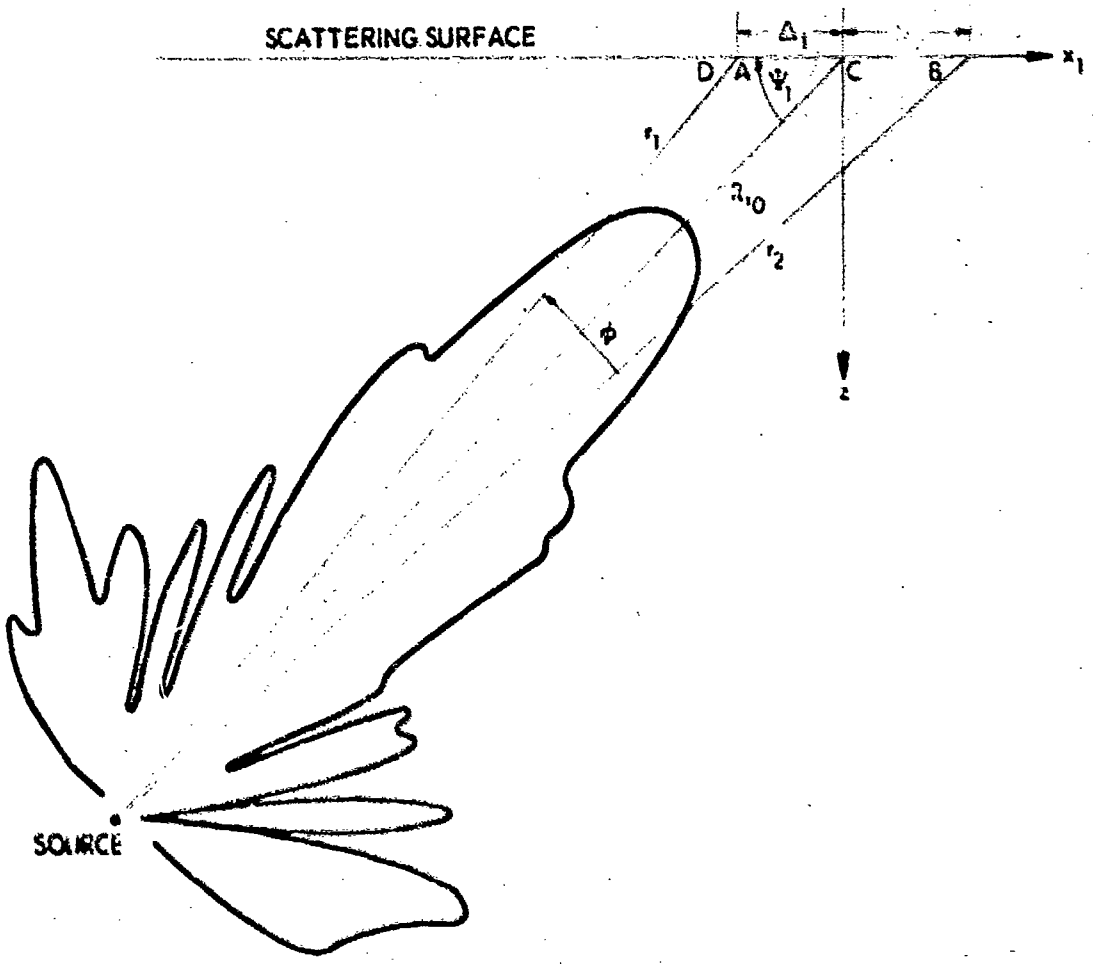


FIGURE B-1
SOURCE DIRECTIVITY PATTERN
AND INSONIFIED AREA

From the law of sines

$$r_1 = \frac{R_{10} \sin \psi_1}{\sin(\psi_1 + \frac{\varphi}{2})} \quad , \text{ and}$$

$$r_2 = \frac{R_{10} \sin \psi_1}{\sin(\psi_1 - \frac{\varphi}{2})}$$

give for $\Delta_1$ and $\Delta_2$,

$$\Delta_1 = R_{10}\left[\cos \psi_1 - \cot(\psi_1 + \tfrac{\varphi}{2})\sin \psi_1\right] \quad , \tag{B-1}$$

$$\Delta_2 = R_{10}\left[- \cos \psi_1 + \cot(\psi_1 - \tfrac{\varphi}{2})\sin \psi_1\right] \quad . \tag{B-2}$$

With the projector confined to the $x_1$-z plane the linear dimensions of the insonified area in the y direction is calculated easily from the right triangle in Fig. B-2a to give

$$\ell = R_{10} \tan \tfrac{\varphi}{2} \quad . \tag{B-3}$$

The insonified area, shown in Fig. B-2b, is an ellipse with a semimajor axis given by

$$a = \tfrac{1}{2}(\Delta_1 + \Delta_2) \quad , \tag{B-4}$$

and a semiminor axis given by

$$b = \frac{\ell(\Delta_1 + \Delta_2)}{\sqrt{10\Delta_1\Delta_2 - 3\left(\Delta_1^2 + \Delta_2^2\right)}} \tag{B-5}$$

The area of an ellipse is $\pi ab$, so that

$$\text{area} = \frac{\pi\ell(\Delta_1 + \Delta_2)^2}{2\sqrt{10\Delta_1\Delta_2 - 3\left(\Delta_1^2 + \Delta_2^2\right)}} \tag{B-6}$$

Kerr (1951) gives formulas for the calculation of the dimensions of the Fresnel zones. The geometrical arrangement of source and receiver for these calculations is shown in Fig. B-3. The origin lies on the

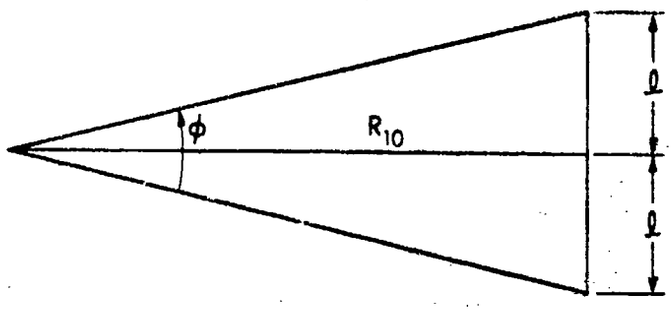


(a) DIMENSION OF THE INSONIFIED AREA IN THE y-DIRECTION

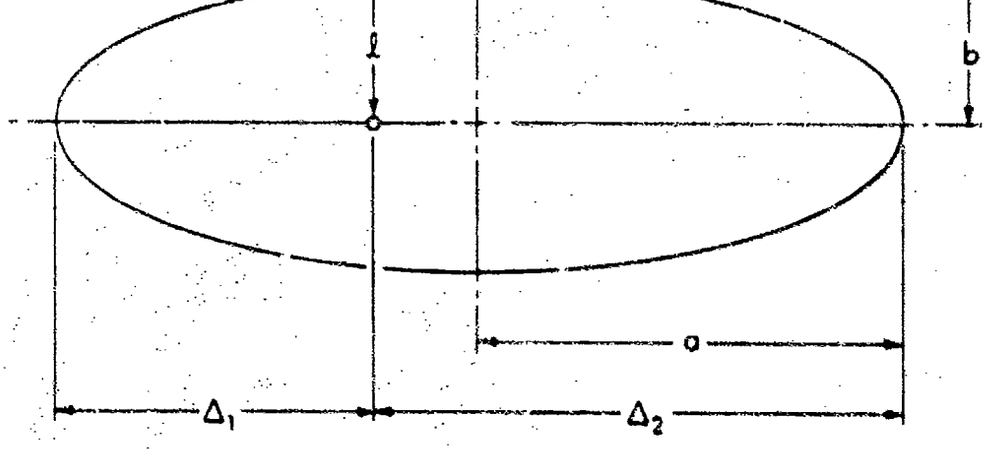


(b) THE ELLIPTICAL INSONIFIED AREA

FIGURE B-2
INSONIFIED AREA

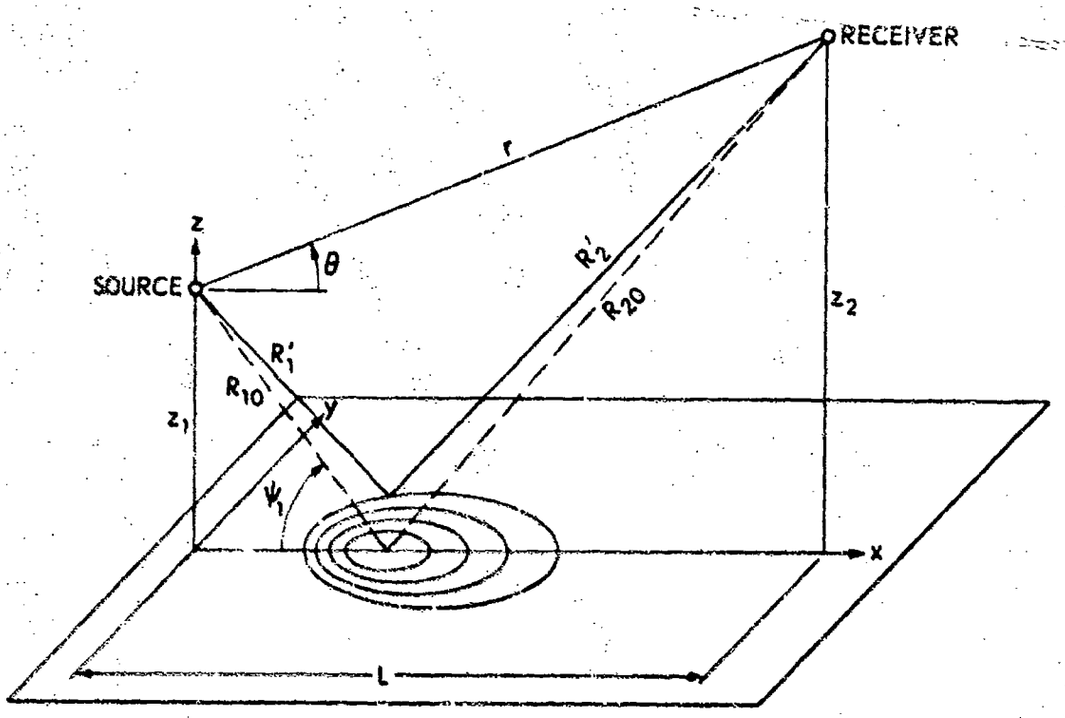


FIGURE B-3
THE FRESNEL ZONES ON A REFLECTING PLANE

reflecting plane directly below the source. The receiver is in the specular direction. The locus of all points in the x - y plane, from which the secondary radiation arrives at the receiver with a constant phase difference $\delta$ with respect to the direct radiation along r, is given by the relation

$$R_1' + R_2' - r = \delta \quad .$$

The path difference $\delta_o$ via the geometrical point of reflection is

$$R_{10} + R_{20} - r = \delta_o \quad .$$

The nth ellipse (Fresnel zone) is determined from

$$\delta_n - \delta_o = n \frac{\lambda}{2} \quad ,$$

or

$$\delta_n = R_{10} + R_{20} - r + n \frac{\lambda}{2} \tag{B-7}$$

where $\lambda$ is the wavelength of the incident radiation. Expressing the ellipses in terms of L, $\delta_n$, $z_1$, and $z_2$ one obtains for the x coordinate of the center of the ellipse

$$x_{on} = \frac{L}{2}\left\{1 - \frac{\left(\frac{z_2 - z_1}{L}\right)^2}{\left[\frac{\delta_n}{L} + \sqrt{1 + \left(\frac{z_2 - z_1}{L}\right)^2}\right]^2 - 1}\right\} - \frac{Lz_1}{z_1 + z_2} \quad , \tag{B-8}$$

where the origin depicted in Fig. B-3 has been transformed to the point of geometrical reflection by means of Eq. (A-1) in Appendix A. The semiminor axis is

$$b_n = \pm \frac{L}{2}\sqrt{\left(\frac{\delta_n}{L}\right)^2 + \frac{2\delta_n}{L}\sqrt{1 + \left(\frac{z_1 - z_2}{L}\right)^2}} \times \sqrt{1 - \frac{\left(\frac{z_1 + z_2}{L}\right)^2}{\left[\frac{\delta_n}{L} + \sqrt{1 + \left(\frac{z_2 - z_1}{L}\right)^2}\right]^2 - 1}} \tag{B-9}$$

and the semimajor axis is

$$a_n = b_n \sqrt{1 + \frac{1}{\left[\frac{\delta_n}{L} + \sqrt{1 + \left(\frac{z_2 - z_1}{L}\right)^2}\right]^2 - 1}} \quad . \tag{B-10}$$

The x intercepts relative to the geometrical point of reflection are

$$\Delta_{1n} = a_n - x_{on} \quad , \text{ and} \tag{B-11}$$

$$\Delta_{2n} = a_n + x_{on} \quad . \tag{B-12}$$

From Eq. (B-5) the y intercepts are

$$\ell_n = \pm \frac{b_n}{2a_n} \sqrt{10\Delta_1\Delta_2 - 3\Delta_1^2 + \Delta_2^2} \tag{B-13}$$

These three equations for the Fresnel zones correspond to Eqs. (B-1), (B-2), and (B-3) for the irradiated area.

Consider a numerical calculation of the dimensions of the insonified area and the dimensions of the first three Fresnel zones. The source is placed 60.0 in. ($R_{10}$) from the surface and the receiver is maintained in the specular direction at the distance of 60.0 in. ($R_{20}$) from the surface. The beamwidth of the projector (source) is 9 deg. The results are depicted in Fig. B-4 for a frequency of 95.8 kHz for grazing angles 30 and 60 deg. The calculations show that the dimensions of the insonified area are slightly larger than the dimensions of the first Fresnel zone. The scattering surface boundary shows the relative size of the model surfaces to the insonified area.

If the beamwidth of the source is varied from 6 deg to 12 deg for the situation just described, the insonified area will enclose slightly less than one Fresnel zone to almost two Fresnel zones.

It is difficult to ascertain with analytical precision the part of the scattering surface that should be taken as the active scattering region. However, since only a few Fresnel zones are insonified in the experimental study in this paper, the insonified area will be taken as the active

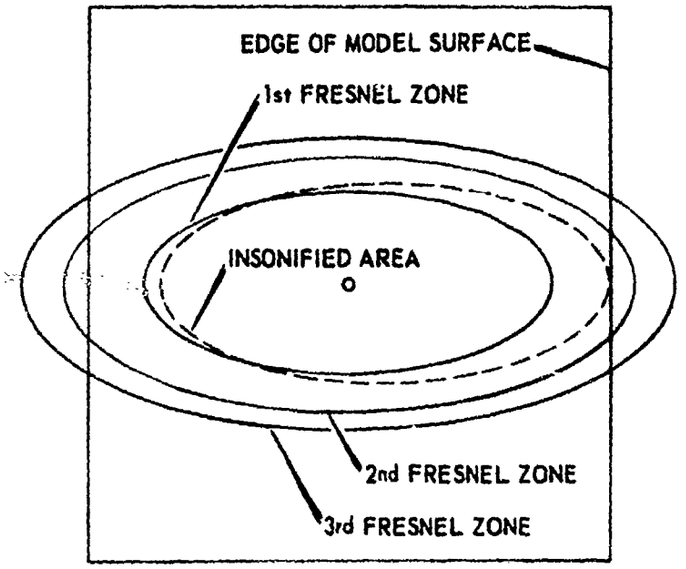


(a) GRAZING ANGLE = 20 deg

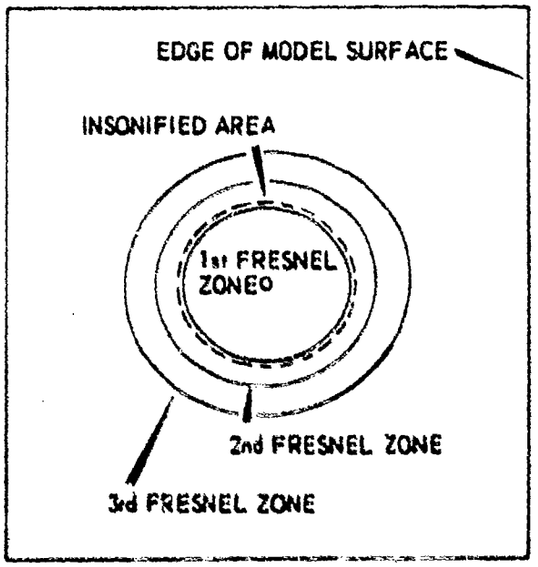


(b) GRAZING ANGLE = 60 deg

SOURCE ← → RECEIVER

FIGURE B-4
THE FIRST THREE FRESNEL ZONES AND THE INSONIFIED AREA
FOR A BEAMWIDTH OF 9 deg

scattering region. Thus, the limits of the integrals appearing in Chapter II and III will be taken as the values of $\Delta_1$, $\Delta_2$, and $\ell$ calculated from Eqs. (B-1), (B-2), and (B-3), respectively.

It is noted that the approximate dimensions of the insonified area $\Delta_1$, $\Delta_2$, and $\ell$ are used as the limits rather than the exact dimensions of the insonified areas a and b. This approximation is equivalent to integrating over a rectangular area, which approximates closely the elliptical area.

Table B-I lists the values for $\Delta_1$, $\Delta_2$, and $\ell$ for grazing angles from 6 deg to 80 deg for the previous cited numerical example for a 9 deg beamwidth of source. The dimensions $\Delta_1$, $\Delta_2$, and $\ell$ are calculated from Eqs. (B-1), (B-2), and (B-3), respectively. The irradiated surface area for grazing angles from 6 deg through 20 deg is calculated from the relation

$$2\ell(\Delta_1 + \Delta_2) \quad .$$

whereas the area for grazing angles from 22 deg degrees to 80 deg is calculated from Eq. (B-6).

TABLE B-1

DIMENSIONS OF INSONIFIED AREA FOR VARIOUS GRAZING ANGLES

| Grazing Angle | $\Delta_1$ | $\Delta_2$ | $\ell$ | Insonified Area |
|---|---|---|---|---|
| Degrees | Inches | Inches | Inches | Sq. Inches |
| 6 | 16.00 | 16.00 | 4.72 | 302.21 |
| 8 | 16.00 | 16.00 | 4.72 | 302.21 |
| 10 | 16.00 | 16.00 | 4.72 | 302.21 |
| 12 | 16.00 | 16.00 | 4.72 | 302.21 |
| 14 | 14.84 | 16.00 | 4.72 | 291.22 |
| 16 | 13.44 | 16.00 | 4.72 | 278.06 |
| 18 | 12.30 | 16.00 | 4.72 | 267.28 |
| 20 | 11.35 | 16.00 | 4.72 | 258.32 |
| 22 | 10.55 | 15.65 | 4.72 | 211.05 |
| 24 | 9.87 | 14.10 | 4.72 | 190.06 |
| 26 | 9.28 | 12.84 | 4.72 | 173.35 |
| 28 | 8.76 | 11.81 | 4.72 | 159.72 |
| 30 | 8.31 | 10.93 | 4.72 | 148.38 |
| 32 | 7.91 | 10.20 | 4.72 | 138.30 |
| 34 | 7.56 | 9.56 | 4.72 | 130.61 |
| 36 | 7.25 | 9.01 | 4.72 | 123.53 |
| 38 | 6.97 | 8.53 | 4.72 | 117.36 |
| 40 | 6.72 | 8.11 | 4.72 | 111.94 |
| 42 | 6.49 | 7.73 | 4.72 | 107.15 |
| 44 | 6.29 | 7.40 | 4.72 | 102.89 |
| 46 | 6.10 | 7.10 | 4.72 | 99.10 |
| 48 | 5.93 | 6.84 | 4.72 | 95.71 |
| 50 | 5.78 | 6.60 | 4.72 | 92.66 |
| 52 | 5.65 | 6.39 | 4.72 | 89.92 |
| 54 | 5.53 | 6.19 | 4.72 | 87.45 |
| 56 | 5.41 | 6.02 | 4.72 | 85.22 |
| 58 | 5.31 | 5.86 | 4.72 | 83.21 |
| 60 | 5.22 | 5.71 | 4.72 | 81.39 |
| 62 | 5.13 | 5.58 | 4.72 | 79.76 |
| 64 | 5.06 | 5.46 | 4.72 | 78.29 |
| 66 | 4.99 | 5.36 | 4.72 | 76.96 |
| 68 | 4.94 | 5.26 | 4.72 | 75.78 |
| 70 | 4.89 | 5.17 | 4.72 | 74.73 |
| 72 | 4.84 | 5.10 | 4.72 | 73.80 |
| 74 | 4.80 | 5.03 | 4.72 | 72.99 |
| 76 | 4.77 | 4.96 | 4.72 | 72.28 |
| 78 | 4.75 | 4.91 | 4.72 | 71.68 |
| 80 | 4.73 | 4.86 | 4.72 | 71.17 |

TABLE B-1

DIMENSIONS OF INSONIFIED AREA FOR VARIOUS GRAZING ANGLES

| Grazing Angle | $\Delta_1$ | $\Delta_2$ | $l$ | Insonified Area |
|---|---|---|---|---|
| Degrees | Inches | Inches | Inches | Sq. Inches |
| 6 | 16.00 | 16.00 | 4.72 | 302.21 |
| 8 | 16.00 | 16.00 | 4.72 | 302.21 |
| 10 | 16.00 | 16.00 | 4.72 | 302.21 |
| 12 | 16.00 | 16.00 | 4.72 | 302.21 |
| 14 | 14.84 | 16.00 | 4.72 | 291.22 |
| 16 | 13.44 | 16.00 | 4.72 | 278.06 |
| 18 | 12.30 | 16.00 | 4.72 | 267.28 |
| 20 | 11.35 | 16.00 | 4.72 | 258.32 |
| 22 | 10.55 | 15.65 | 4.72 | 211.05 |
| 24 | 9.87 | 14.10 | 4.72 | 190.06 |
| 26 | 9.28 | 12.84 | 4.72 | 173.35 |
| 28 | 8.76 | 11.81 | 4.72 | 159.72 |
| 30 | 8.31 | 10.93 | 4.72 | 148.38 |
| 32 | 7.91 | 10.20 | 4.72 | 138.30 |
| 34 | 7.56 | 9.56 | 4.72 | 130.61 |
| 36 | 7.25 | 9.01 | 4.72 | 123.53 |
| 38 | 6.97 | 8.53 | 4.72 | 117.36 |
| 40 | 6.72 | 8.11 | 4.72 | 111.94 |
| 42 | 6.49 | 7.73 | 4.72 | 107.15 |
| 44 | 6.29 | 7.40 | 4.72 | 102.89 |
| 46 | 6.10 | 7.10 | 4.72 | 99.10 |
| 48 | 5.94 | 6.84 | 4.72 | 95.71 |
| 50 | 5.78 | 6.60 | 4.72 | 92.66 |
| 52 | 5.65 | 6.39 | 4.72 | 89.92 |
| 54 | 5.52 | 6.19 | 4.72 | 87.45 |
| 56 | 5.41 | 6.02 | 4.72 | 85.22 |
| 58 | 5.31 | 5.86 | 4.72 | 83.21 |
| 60 | 5.22 | 5.71 | 4.72 | 81.39 |
| 62 | 5.13 | 5.59 | 4.72 | 79.76 |
| 64 | 5.06 | 5.46 | 4.72 | 78.29 |
| 66 | 4.99 | 5.36 | 4.72 | 76.96 |
| 68 | 4.94 | 5.26 | 4.72 | 75.78 |
| 70 | 4.89 | 5.17 | 4.72 | 74.73 |
| 72 | 4.84 | 5.10 | 4.72 | 73.80 |
| 74 | 4.80 | 5.03 | 4.72 | 72.99 |
| 76 | 4.77 | 4.96 | 4.72 | 72.28 |
| 78 | 4.73 | 4.91 | 4.72 | 71.68 |
| 80 | 4.73 | 4.86 | 4.72 | 71.17 |

# APPENDIX C

## EVALUATION OF THE PRESSURE REFLECTED FROM A PLANE SURFACE

In Chapter II, Eq. (17), we encountered the integral

$$p_o = \frac{ik}{4\pi} \int_{-\Delta_1}^{\Delta_2} \int_{-\ell}^{\ell} \frac{1}{R_1' R_2'} \left( \frac{z_1}{R_1'} + \frac{z_2}{R_2'} \right) e^{ik(R_1' + R_2')} dx_1 dy \quad , \qquad \text{(C-1)}$$

where the limits $\Delta_1$, $\Delta_2$, and $\ell$ are the dimensions of the active scattering region defined in Appendix B. Calculations shall be limited to the specular direction.

The Fraunhofer approximation is the neglect of the quadratic and higher order terms in the expansion of the term $R_1' + R_2'$ appearing in the exponential of Eq. (C-1). For the specular direction and for the Fraunhofer approximation Eq. (A-14) in Appendix A reduces to

$$R_1' + R_2' = R_{10} + R_{20} \quad .$$

Setting $z_1 = R_{10} \sin \psi$ , $z_2 = R_{20} \sin \psi$ and $R_1' = R_{10}$ , $R_2' = R_{20}$ in the denominator of Eq. (C-1), one obtains

$$p_o = \frac{ik\ell(\Delta_1 + \Delta_2) \sin \psi}{\pi R_{10} R_{20}} e^{i\left[\frac{\pi}{2} + k(R_{10} + R_{20})\right]} \quad , \text{ or} \qquad \text{(C-2)}$$

$$A_o = \frac{k\ell(\Delta_1 + \Delta_2) \sin \psi}{\pi R_{10} R_{20}} \quad , \qquad \text{(C-3)}$$

$$\phi_o = \frac{\pi}{2} + k(R_{10} + R_{20}) \quad . \qquad \text{(C-4)}$$

where

$A_o$ is the amplitude, and

$\phi_o$ is the phase.

The pressure squared $p_o p_o^*$, which is proportional to the intensity reflected from a plane surface, is

$$p_o p_o^* = \frac{k^2 \ell^2 (\Delta_1 + \Delta_2)^2 \sin^2 \psi}{\pi^2 R_{10}^2 R_{20}^2} \quad . \tag{C-5}$$

For the Fresnel approximation the quadratic terms are retained in the expansion of $R_1' + R_2'$. The desired expansion given by Eq. (A-19) in Appendix A

$$R_1' + R_2' \approx R_{10} + R_{20} + \frac{1}{R}(x_1^2 \sin^2 \psi + y^2) \quad ,$$

reduces Eq. (C-1) to

$$p_o = \frac{ik \sin \psi}{2\pi R_{10} R_{20}} e^{ik(R_{10}+R_{20})} \int_{-\Delta_1}^{\Delta_2} e^{ik\left(\frac{x_1^2 \sin^2 \psi}{R}\right)} dx_1 \int_{-\ell}^{\ell} e^{i\frac{k}{R}y^2} dy \quad . \tag{C-6}$$

The integrals can not be integrated in closed form but yield infinite series. They are called Fresnel integrals and are defined as

$$C(u) = \int_0^u \cos\left(\frac{\pi}{2} u^2\right) du \quad ,$$

$$S(u) = \int_0^u \sin\left(\frac{\pi}{2} u^2\right) du \quad . \tag{C-7}$$

Integration of Eq. (C-6) yields

$$p_o = \frac{\left\{\left[C_\ell\left(C_{\Delta_1} + C_{\Delta_2}\right) - S_\ell\left(S_{\Delta_1} + S_{\Delta_2}\right)\right]^2 + \left[S_\ell\left(C_{\Delta_1} + C_{\Delta_2}\right) + C_\ell\left(S_{\Delta_1} + S_{\Delta_2}\right)\right]^2\right\}^{1/2}}{(R_{10} + R_{20})}$$

$$\times e^{i\left\{\pi + k(R_{10}+R_{20}) - \arctan\left[\frac{C_\ell\left(C_{\Delta_1}+C_{\Delta_2}\right) - S_\ell\left(S_{\Delta_1}+S_{\Delta_2}\right)}{S_\ell\left(C_{\Delta_1}+C_{\Delta_2}\right) + C_\ell\left(S_{\Delta_1}+S_{\Delta_2}\right)}\right]\right\}} , \tag{C-8}$$

where

$$C_{\Delta_1} = C\left(\Delta_1\sqrt{\frac{2k}{\pi R}}\sin\psi\right) ,$$

$$C_{\Delta_2} = C\left(\Delta_2\sqrt{\frac{2k}{\pi R}}\sin\psi\right) ,$$

$$C_\ell = C\left(\ell\sqrt{\frac{2k}{\pi R}}\right) ,$$

$$S_{\Delta_1} = S\left(\Delta_1\sqrt{\frac{2k}{\pi R}}\sin\psi\right) , \tag{C-9}$$

$$S_{\Delta_2} = S\left(\Delta_2\sqrt{\frac{2k}{\pi R}}\sin\psi\right) ,$$

$$S_\ell = S\left(\ell\sqrt{\frac{2k}{\pi R}}\right) .$$

The amplitude is

$$A_o = \frac{\left\{\left[C_\ell\left(C_{\Delta_1} + C_{\Delta_2}\right) - S_\ell\left(S_{\Delta_1} + S_{\Delta_2}\right)\right]^2 + \left[S_\ell\left(C_{\Delta_1} + C_{\Delta_2}\right) + C_\ell\left(S_{\Delta_1} + S_{\Delta_2}\right)\right]^2\right\}^{1/2}}{(R_{10} + R_{20})} \quad , (C\text{-}10)$$

and the phase is

$$\Phi_o = \pi + k(R_{10} + R_{20}) - \arctan\left[\frac{C_\ell\left(C_{\Delta_1} + C_{\Delta_2}\right) - S_\ell\left(S_{\Delta_1} + S_{\Delta_2}\right)}{S_\ell\left(C_{\Delta_1} + C_{\Delta_2}\right) + C_\ell\left(S_{\Delta_1} + S_{\Delta_2}\right)}\right] \quad . \quad (C\text{-}11)$$

The pressure squared is

$$p_o p_o^* = \frac{\left[C_\ell\left(C_{\Delta_1} + C_{\Delta_2}\right) - S_\ell\left(S_{\Delta_1} + S_{\Delta_2}\right)\right]^2 + \left[S_\ell\left(C_{\Delta_1} + C_{\Delta_2}\right) + C_\ell\left(S_{\Delta_1} + S_{\Delta_2}\right)\right]^2}{(R_{10} + R_{20})^2} \quad . \quad (C\text{-}12)$$

The amplitude and phase obtained in the Fraunhofer approximation can be obtained from the amplitude and phase derived in the Fresnel approximation if it is assumed that the argument of the Fresnel integrals is very small so that

$$C(u) \approx u \quad , \text{ and}$$

$$S(u) \approx 0 \quad .$$

Physically, this approximation implies that both the source and receiver must be moved to infinity with the restriction that the source have a very narrow beam spread so that the dimensions of the insonified area, $\Delta_1$, $\Delta_2$, and $\ell$ are very small compared to the distance from the surface to the source.

These statements assert that it is theoretically impossible to predict the intensity reflected from a plane surface in the specular direction in the Fraunhofer approximation. A comparison of Eqs. (C-4) and (C-11) will substantiate the invalidity of the Fraunhofer approximation

in predicting the correct phase. One would expect a phase change at the receiver relative to the source of $\pi$ radians at the surface and $k(R_{10} + R_{20})$ radians as a result of the travel path. Figure C-1 depicts the phase in the Fraunhofer and Fresnel approximation for the case where

$f = 95.8$ kHz,

$k = 10.328$ in.$^{-1}$,

$R_{10} = R_{20} = 60.0$ in.

The values for $\Delta_1$, $\Delta_2$, and $\ell$ for a 9 deg beamwidth of source are given in Appendix B. The term $\pi + k(R_{10} + R_{20})$ is not included in the calculations. For this numerical example the Fresnel phase lies between 20 and 30 deg for grazing angles greater than 30 deg. The Fraunhofer phase is -90 deg for all grazing angles.

The amplitude in the Fraunhofer approximation, Eq. (C-5), and the amplitude in the Fresnel approximation, Eq. (C-10), are plotted for this numerical example on a relative scale for various grazing angles in Fig. C-2. Over a wide range of grazing angles (40 to 80 deg) the Fraunhofer amplitude is approximately 4.1 times the Fresnel amplitude.

The term $p_o p_o^*$ that is proportional to the intensity in the Fraunhofer approximation, Eq. (C-5), and the term $pp^*$ in the Fresnel approximation, Eq. (C-12) are plotted for this numerical example in Fig. C-3. The Fraunhofer intensity is over 16 times the intensity in the Fresnel approximation for grazing angles greater than 20 deg.

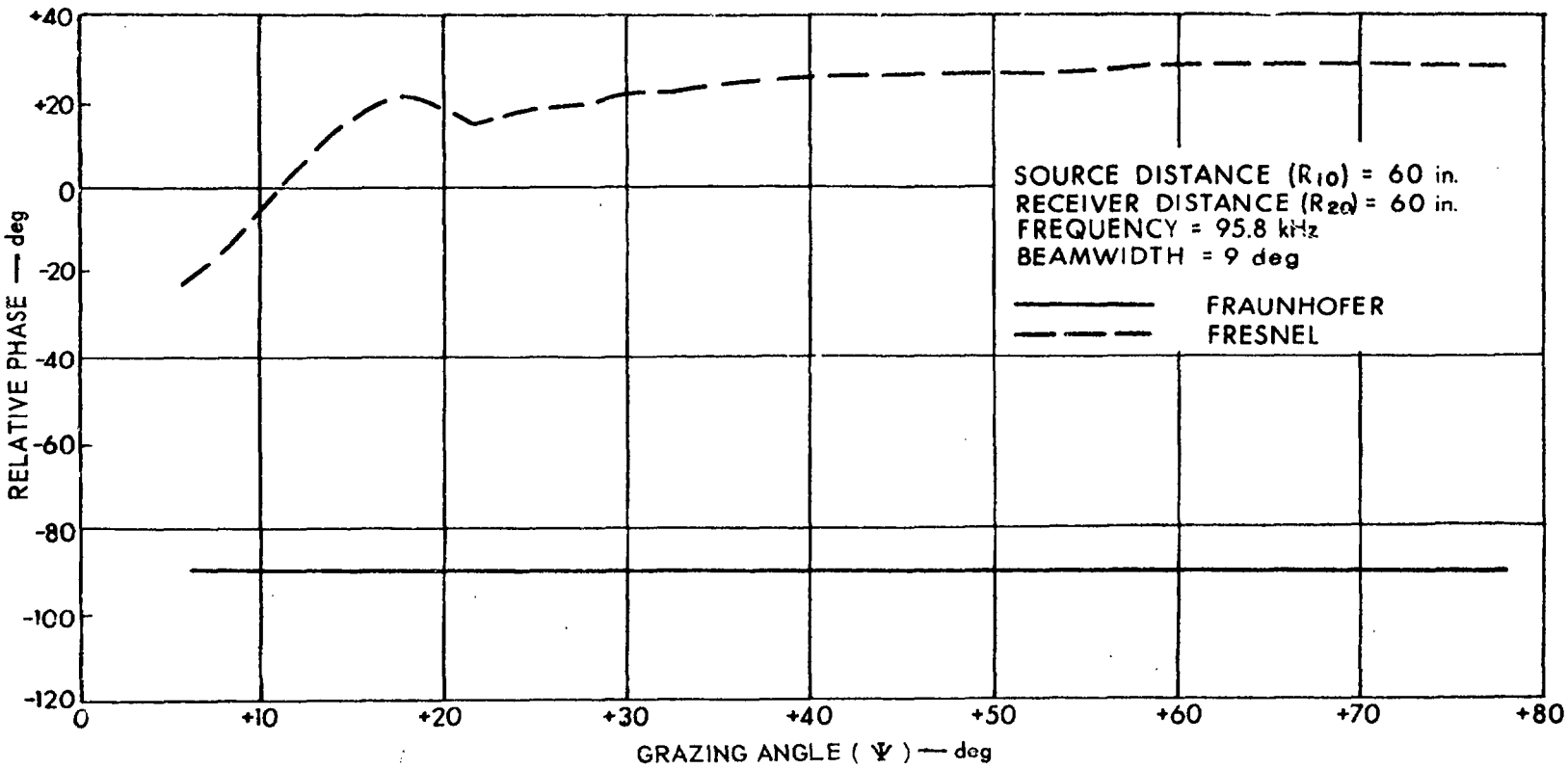


FIGURE C-1
RELATIVE PHASE IN THE SPECULAR DIRECTION
PLANE PRESSURE RELEASE SURFACE

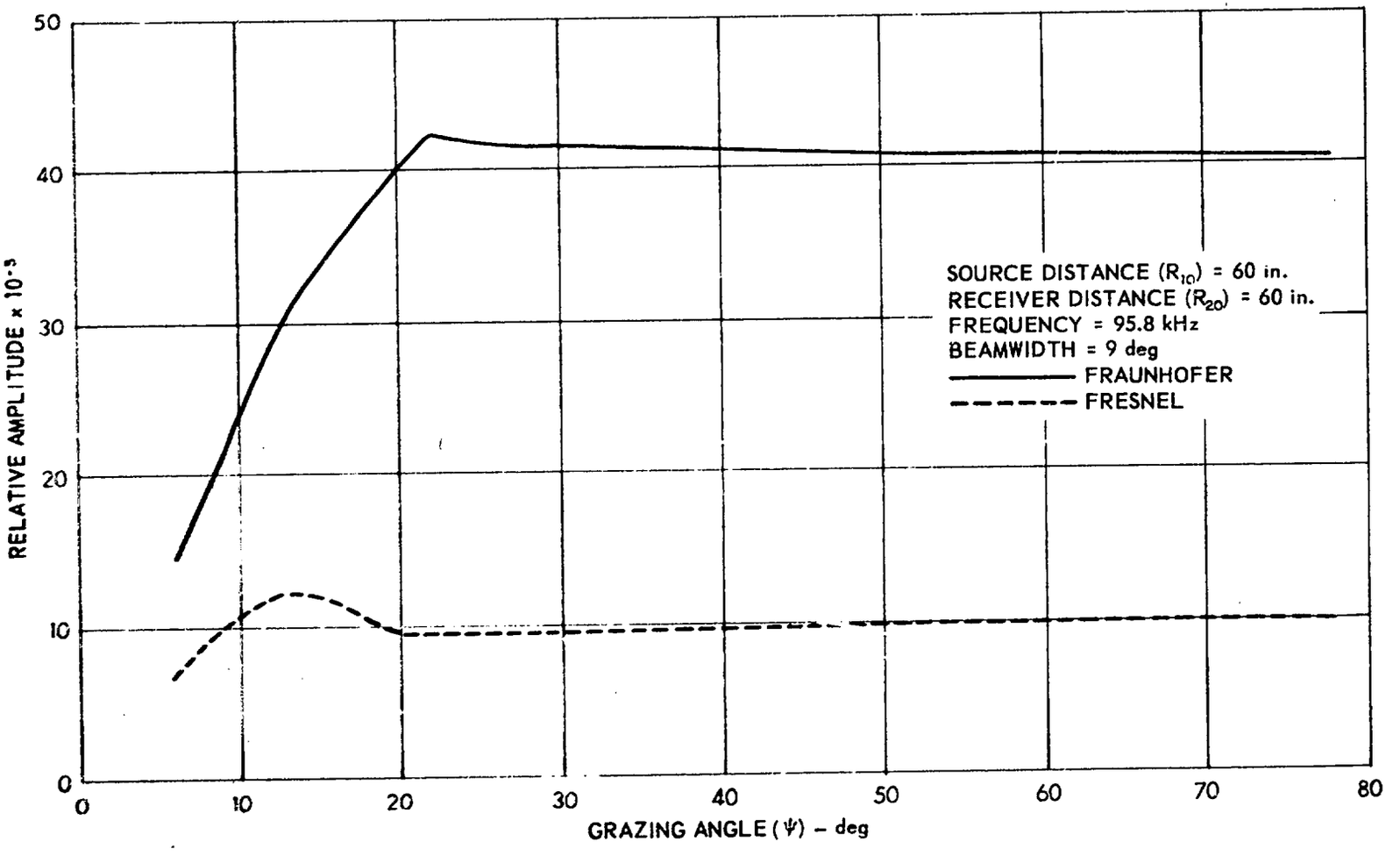


FIGURE C-2
RELATIVE AMPLITUDE
IN THE SPECULAR DIRECTION
PRESSURE RELEASE PLANE SURFACE

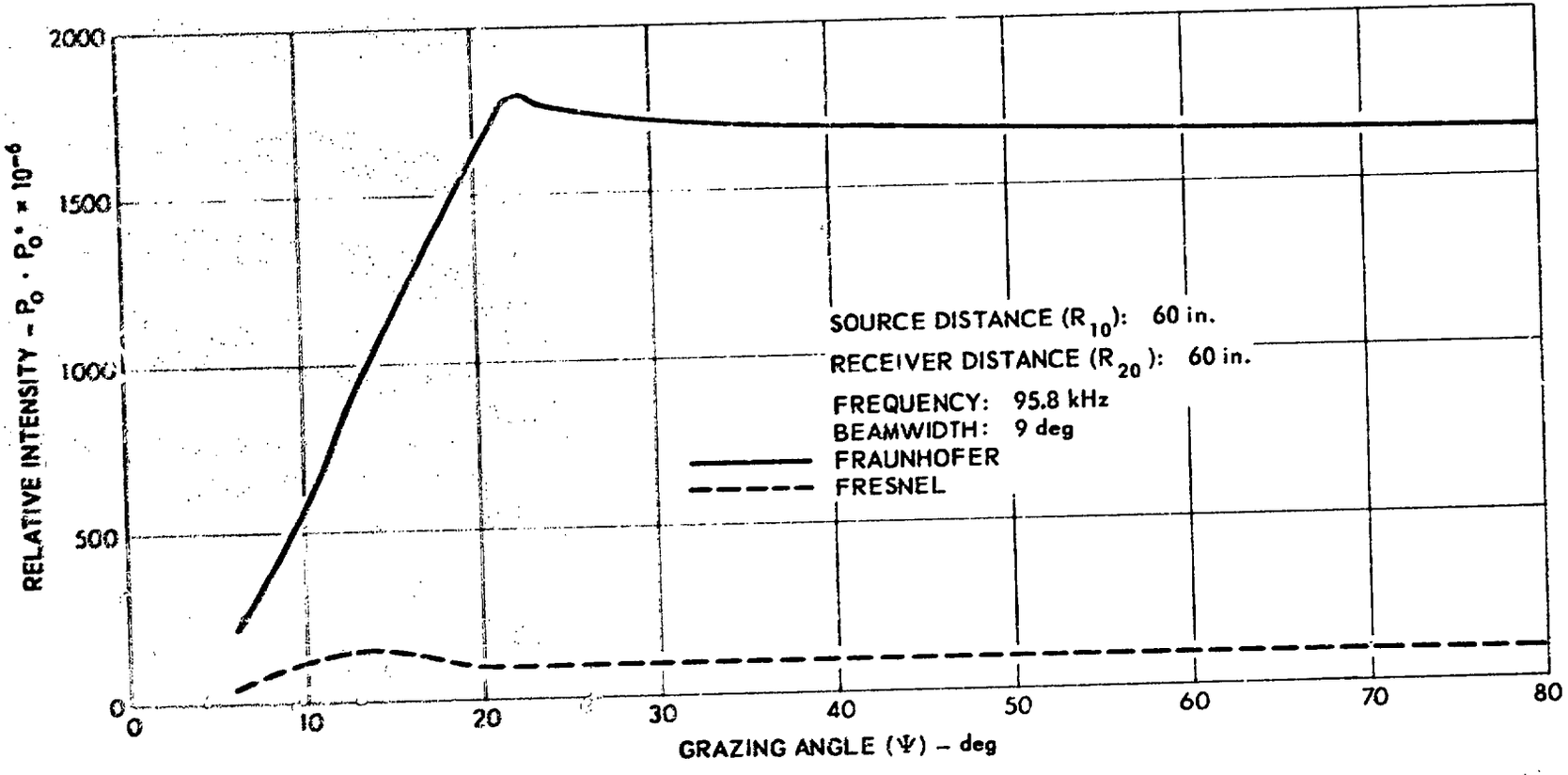


FIGURE C-3
RELATIVE INTENSITY
REFLECTED IN THE SPECULAR DIRECTION
FROM A PLANE PRESSURE RELEASE SURFACE

# APPENDIX D

## INTEGRATION OF $J_1$ TERM

In Chapter III, Eq. (68), we encountered the integral

$$J_1 = \frac{k^4 \langle F_o^2 \rangle \sin^4 \psi}{2\pi^2 R_{10}^2 R_{20}^2 A_o^2} \int_{-\Delta_1}^{\Delta_2} \int_{-\ell}^{\ell} \int_{-\Delta_1}^{\Delta_2} \int_{-\ell}^{\ell} e^{-\frac{1}{a}\left[(x_1-x_1')^2+(y-y')^2\right]^{1/2}}$$

$$\times \cos\left[\frac{k}{R} \sin^2 \psi \left(x_1^2 - x_1'^2\right) + \frac{k}{R} (y^2 - y'^2)\right] dx_1 dy dx_1' dy' \quad . \tag{D-1}$$

Making the change in variables defined by Eq. (58), one finds for $J_1$

$$J_1 = \frac{k^4 \langle F_o^2 \rangle \sin^4 \psi}{2\pi^2 R_{10}^2 R_{20}^2 A_o^2} \int_{-\Delta}^{\Delta} \int_{-\ell}^{\ell} \int_{-\Delta}^{\Delta} \int_{-\ell}^{\ell} e^{-\frac{1}{a}\left[(u-u')^2+(y-y')^2\right]^{1/2}}$$

$$\times \cos\left[\frac{k}{R} (u^2 - u'^2)\sin^2 \psi + \frac{k}{R} (\Delta_2 - \Delta_1)(u - u')\sin^2 \psi \right.$$

$$\left. + \frac{k}{R} (y^2 - y'^2)\right] du du' dy dy' \quad .$$

Introducing relative and center of gravity coordinates defined by Eqs. (61) and (62), one obtains

$$J_+ = \frac{k^4 \langle F_o^2 \rangle \sin^4 \psi}{\pi^2 R_{10}^2 R_{20}^2 A_o^2} \int_0^{\Delta} \int_0^{\ell} \int_{-2(\Delta-x_o)}^{2(\Delta-x_o)} \int_{-2(\ell-y_o)}^{2(\ell-y_o)} e^{-\frac{1}{a}(\xi^2+\eta^2)^{1/2}}$$

$$\times \cos\left[\frac{2k}{R}\sin^2 \psi \left(x_o + \frac{\Delta_2}{2} - \frac{\Delta_1}{2}\right)\xi + \frac{2k}{R} y_o \eta\right] dx_o dy_o d\xi d\eta \quad ,$$

where

$$J_1 = J_+(\Delta_1,\Delta_2) + J_+(\Delta_2,\Delta_1) \quad .$$

Making the assumption (see Eq. 64) that

$$a \ll 2\Delta, 2\ell$$

one can write for $J_+$

$$J_+ = \frac{k^4 \langle F_o^2 \rangle \sin^4 \psi}{\pi^2 R_{10}^2 R_{20}^2 A_o^2} \int_0^{\Delta}\int_0^{\ell}\int_{-\infty}^{+\infty}\int_{-\infty}^{+\infty} e^{-\frac{1}{a}(\xi^2+\eta^2)^{1/2}} \times \cos\left[\frac{2k}{R}\sin^2\psi\left(x_o + \frac{\Delta_2}{2} - \frac{\Delta_1}{2}\right)\xi + \frac{2k}{R} y_o \eta\right] dx_o dy_o d\xi d\eta \quad . \tag{D-2}$$

Consider the double integral

$$I = \int_{-\infty}^{+\infty}\int_{-\infty}^{+\infty} e^{-\frac{1}{a}(\xi^2+\eta^2)^{1/2}} \cos\left[\frac{2k}{R}\sin^2\psi\left(x_o + \frac{\Delta_2}{2} - \frac{\Delta_1}{2}\right)\xi + \frac{2k}{R} y_o \eta\right] d\xi d\eta \quad , \tag{D-3}$$

and set

$$\xi = \rho \cos\varphi$$
$$\eta = \rho \sin\varphi$$

to get

$$I = \int_0^{2\pi}\int_0^{\infty} e^{-\rho/a} \cos\left[\rho(M\cos\varphi + N\sin\varphi)\right] \rho d\rho d\varphi \quad ;$$

where

$$M = \frac{2k}{R}(\sin^2\psi)\left(x_o + \frac{\Delta_2}{2} - \frac{\Delta_1}{2}\right)$$
$$N = \frac{2k}{R} y_o \quad . \tag{D-4}$$

Now, set

$$M = P\cos\gamma$$
$$N = P\sin\gamma$$

to obtain

$$I = \int_0^{2\pi}\int_0^{\infty} e^{-\rho/a} \cos\left[\rho\sqrt{M^2+N^2}\cos(\varphi-\gamma)\right] \rho d\rho d\varphi \quad .$$

The term $(\varphi - \gamma)$ ranges from $-\gamma$ to $2\pi - \gamma$ as $\varphi$ goes through its range of o to $2\pi$; the integrand assumes all the values that it would if the value of $\gamma$ were zero. Thus,

$$I = \int_0^{2\pi}\int_0^{\infty} e^{-\rho/a} \cos\left[\rho\sqrt{M^2 + N^2}\cos\varphi\right]\rho d\rho d\varphi \quad .$$

From Gradshteyn and Ryzhik (integral 3.715-19, p. 402) one finds for the integral

$$\int_0^{2\pi} \cos\left[\rho\sqrt{M^2 + N^2}\cos\varphi\right] d\varphi = 2\pi J_o\left[\rho\sqrt{M^2 + N^2}\right] \quad ,$$

where $J_o$ is the zeroth ordered Bessel function. The expression for I becomes

$$I = 2\pi\int_0^{\infty} e^{-\rho/a}\,\rho J_o\left[\rho\sqrt{M^2 + N^2}\right] d\rho \quad .$$

Using an integral solution (6.623-2, p. 712) in Gradshteyn and Ryzhik, one obtains for I

$$I = \frac{2\pi}{a}\left[\frac{1}{\frac{1}{a^2} + \left(\frac{k\sin\theta}{R}\right)^2\left(x_o + \frac{\Delta_2}{2} - \frac{\Delta_1}{2}\right)^2 + \left(\frac{2k}{R}\right)^2 y_o^2}\right]^{3/2} \quad ; \text{(D-5)}$$

which gives for $J_+$

$$J_+ = \frac{2k^4\langle P^2\rangle \sin^4\theta}{\pi a R_{10}^2 R_{20}^2 A_o^2}$$

$$\times \int_0^{\frac{\Delta_2}{2}}\int_0^{\frac{\Delta_1}{2}} \frac{dx\,dy}{\left[\frac{1}{a^2} + \left(\frac{2k\sin\theta}{R}\right)^2\left(x_o + \frac{\Delta_2}{2} - \frac{\Delta_1}{2}\right)^2 + \left(\frac{2k}{R}\right)^2 y_o^2\right]^{3/2}} \quad . \quad \text{(D-6)}$$

Integrating over $y_o$ by employing the table of integrals by Gradshteyn and Ryzhik (integral 2.271-5, p. 86), one gets

$$J_+ = \frac{k\ell \left\langle F_o^2 \right\rangle R^3}{4\pi a R_{10}^2 R_{20}^2 A_o^2 \sin^2\psi} \times \int_o^{\Delta} \frac{dx_o}{\left[\left(x_o + \frac{\Delta_2}{2} - \frac{\Delta_1}{2}\right)^2 + \left(\frac{R}{2ka\sin^2\psi}\right)^2\right]\sqrt{\left(x_o + \frac{\Delta_2}{2} - \frac{\Delta_1}{2}\right)^2 + \left(\frac{R}{2ka\sin^2\psi}\right)^2 + \frac{\ell^2}{\sin^4\psi}}} \quad \text{(D-7)}$$

Set

$$v = x_o + \frac{\Delta_2}{2} - \frac{\Delta_1}{2}$$

to get for $J_+$

$$J_+ = \frac{k\ell \left\langle F_o^2 \right\rangle R^3}{4\pi a R_{10}^2 R_{20}^2 A_o^2 \sin^2\psi} \times \int_{\frac{\Delta_2-\Delta_1}{2}}^{\Delta_2} \frac{dv}{\left[v^2 + \left(\frac{R}{2ka\sin^2\psi}\right)^2\right]\sqrt{v^2 + \left(\frac{R}{2ka\sin^2\psi}\right)^2 + \frac{\ell^2}{\sin^4\psi}}} \quad \text{(D-8)}$$

Set

$$A = \left(\frac{R}{2ka\sin^2\psi}\right)^2 \quad \text{, and}$$

$$B = \left(\frac{R}{2ka\sin^2\psi}\right)^2 + \frac{\ell^2}{\sin^4\psi} \quad \text{(D-9)}$$

to get

$$J_+(\Delta_1,\Delta_2) = \frac{k\ell \left\langle F_o^2 \right\rangle R^3}{4\pi a R_{10}^2 R_{20}^2 A_o^2 \sin^2\psi} \int_{\frac{\Delta_2-\Delta_1}{2}}^{\Delta_2} \frac{dv}{(v^2 + A)\sqrt{v^2 + B}}$$

Integrating over $y_o$ by employing the table of integrals by Gradshteyn and Ryzhik (integral 2.271-5, p. 86), one gets

$$J_+ = \frac{k\ell \left\langle F_o^2 \right\rangle R^3}{4\pi a R_{10}^2 R_{20}^2 A_o^2 \sin^2\psi} \times \int_o^{\Delta} \frac{dx_o}{\left[\left(x_o + \frac{\Delta_2}{2} - \frac{\Delta_1}{2}\right)^2 + \left(\frac{R}{2ka\sin^2\psi}\right)^2\right]^2 \sqrt{\left(x_o + \frac{\Delta_2}{2} - \frac{\Delta_1}{2}\right)^2 + \left(\frac{R}{2ka\sin^2\psi}\right)^2 + \frac{\ell^2}{\sin^4\psi}}} \quad \text{(D-7)}$$

Set

$$v = x_o + \frac{\Delta_2}{2} - \frac{\Delta_1}{2}$$

to get for $J_+$

$$J_+ = \frac{k\ell \left\langle F_o^2 \right\rangle R^3}{4\pi a R_{10}^2 R_{20}^2 A_o^2 \sin^2\psi} \times \int_{\frac{\Delta_1-\Delta_1}{2}}^{\Delta_2} \frac{dv}{\left[v^2 + \left(\frac{R}{2ka\sin^2\psi}\right)^2\right]^2 \sqrt{v^2 + \left(\frac{R}{2ka\sin^2\psi}\right)^2 + \frac{\ell^2}{\sin^4\psi}}} \quad \text{(D-8)}$$

Set

$$A = \left(\frac{R}{2ka\sin^2\psi}\right)^2 \quad \text{, and}$$

$$B = \left(\frac{R}{2ka\sin^2\psi}\right)^2 + \frac{\ell^2}{\sin^4\psi} \quad \text{(D-9)}$$

to get

$$J_+(\Delta_1,\Delta_2) = \frac{k\ell \left\langle F_o^2 \right\rangle R^3}{4\pi a R_{10}^2 R_{20}^2 A_o^2 \sin^2\psi} \int_{\frac{\Delta_2-\Delta_1}{2}}^{\Delta_2} \frac{dv}{(v^2 + A)\sqrt{v^2 + B}}$$

From this equation one can write

$$J_+(\Delta_2,\Delta_1) = \frac{k\ell \left\langle F_o^2 \right\rangle R^3}{4\pi a R_{10}^2 R_{20}^2 A_o^2 \sin^2 \psi} \int_{\frac{\Delta_1-\Delta_2}{2}}^{\Delta_1} \frac{dv}{(v^2 + A)\sqrt{v^2 + B}}$$

and since

$$J_1 = J_+(\Delta_1,\Delta_2) + J_+(\Delta_2,\Delta_1)$$

one obtains

$$J_1 = \frac{k\ell \left\langle F_o^2 \right\rangle R^3}{4\pi a R_{10}^2 R_{20}^2 A_o^2 \sin^2 \psi} \int_{-\Delta_1}^{\Delta_2} \frac{dv}{(v^2 + A)\sqrt{v^2 + B}} .$$

$J_1$ can be written as

$$J_1 = \frac{k\ell \left\langle F_o^2 \right\rangle R^3}{4\pi a R_{10}^2 R_{20}^2 A_o^2 \sin^2 \psi}$$

$$\times \left[ \int_0^{\Delta_1} \frac{dv}{(v^2 + A)\sqrt{v^2 + B}} + \int_0^{\Delta_2} \frac{dv}{(v^2 + A)\sqrt{v^2 + B}} \right] .$$

Change the variable of integration to

$$w^2 = \frac{1}{B} + \frac{1}{v^2}$$

to get for $J_1$

$$J_1 = \frac{k\ell \left\langle F_o^2 \right\rangle R^3}{4\pi a R_{10}^2 R_{20}^2 A_o^2 \sin^2 \psi} \left(\frac{-1}{A\sqrt{B}}\right) \left[ \int_{\infty}^{w_1} \frac{dw}{w^2 + \left(\frac{1}{A} - \frac{1}{B}\right)} \right.$$

$$\left. + \int_{\infty}^{w_2} \frac{dw}{w^2 + \left(\frac{1}{A} - \frac{1}{B}\right)} \right]$$

where

$$w_1 = \sqrt{\frac{1}{B} + \frac{1}{\Delta_1^2}}$$

and

$$w_2 = \sqrt{\frac{1}{B} + \frac{1}{\Delta_2^2}}$$

With the use of

$$\int \frac{dx}{a + x^2} = \frac{1}{\sqrt{a}} \arctan\left(\frac{x}{\sqrt{a}}\right)$$

$J_1$ becomes

$$J_1 = \frac{k\ell \left\langle F_o^2 \right\rangle R^3}{4\pi a R_{10}^2 R_{20}^2 A_o^2 \sin^2 \psi} \left[\frac{1}{A}\left(\frac{A}{B - A}\right)^{1/2}\right] \left\{ \pi \right.$$

$$\left. - \arctan\left[\frac{(A)^{1/2}}{\Delta_1}\left(\frac{\Delta_1^2 - B}{B - A}\right)^{1/2}\right] - \arctan\left[\frac{(A)^{1/2}}{\Delta_2}\left(\frac{\Delta_2^2 - B}{B - A}\right)^{1/2}\right] \right\}$$

The substitution of the expressions for A and B, Eq. (D-9), and the expression for $A_o$, Eq. (C-10) of Appendix C, into $J_1$ gives

$$J_1 = \frac{2k^2 \left\langle F_o^2 \right\rangle \sin^2 \psi}{\pi \left\{ \left[ C_\ell \left( C_{\Delta_1} + C_{\Delta_2} \right) - S_\ell \left( S_{\Delta_1} + S_{\Delta_2} \right) \right]^2 + \left[ C_\ell \left( S_{\Delta_1} + S_{\Delta_2} \right) + S_\ell \left( C_{\Delta_1} + C_{\Delta_2} \right) \right]^2 \right\}}$$

$$\times \left\{ \operatorname{arccot} \left[ \frac{R}{2ka\Delta_1 \ell \sin^2 \psi} \left( \ell^2 + \Delta_1^2 \sin^4 \psi + \frac{R^2}{4k^2 a^2} \right)^{1/2} \right] \right. \qquad \text{(D-10)}$$

$$\left. + \operatorname{arccot} \left[ \frac{R}{2ka\Delta_2 \ell \sin^2 \psi} \left( \ell^2 + \Delta_2^2 \sin^4 \psi + \frac{R^2}{4k^2 a^2} \right)^{1/2} \right] \right\} .$$

where S and C are the Fresnel integrals defined by Eq. (C-9) in Appendix C.

For the special case where

$$\Delta_1 = \Delta_2 = \Delta_o$$

$J_1$ becomes

$$J_1 = \frac{k^2 \left\langle F_o^2 \right\rangle \sin^2 \psi}{\pi \left[ C_\ell^2 \Delta_o - S_\ell \Delta_o \right]^2 + \left[ C_\ell \Delta_o + S_\ell \Delta_o \right]^2} \qquad \text{(D-11)}$$

$$\times \operatorname{arccot} \left[ \frac{R}{2ka\Delta_o \ell \sin^2 \psi} \left( \ell^2 + \Delta_o^2 \sin^4 \psi + \frac{R^2}{4k^2 a^2} \right)^{1/2} \right] .$$

For values of the argument of the Fresnel integrals, S and C, much larger than unity

$$\Delta_o \sqrt{\frac{2}{\pi R}} \sin \psi \gg 1 ,$$

$$\ell \sqrt{\frac{2}{\pi R}} \gg 1 .$$

S and C both approach one-half, and Eq. (D-11) reduces to

$$J_1 = \frac{4k^2 \left\langle F_o^2 \right\rangle \sin^2 \psi}{\pi} \times \operatorname{arccot}\left[\frac{R}{2ka\ell\Delta_o \sin^2 \psi}\left(\ell^2 + \Delta_o^2 \sin^4 \psi + \frac{R^2}{4k^2a^2}\right)^{1/2}\right] , \tag{D-12}$$

which can be compared with the $J_1$ term obtained by Gulin (1962), the result of using a Gaussian covariance function.

APPENDIX E

## DISCUSSION OF $J_2$ TERM

In Chapter III, Eq. (69), we encountered the integral

$$J_2 = \frac{k^4 \langle F_o^2 \rangle \sin^4 \psi}{2\pi^2 R_{10}^2 R_{20}^2 A_o^2} \int_{-\Delta_1}^{\Delta_2} \int_{-\ell}^{\ell} \int_{-\Delta_1}^{\Delta_2} \int_{-\ell}^{\ell} e^{-\frac{1}{a}\left[(x_1-x_1')^2+(y-y')^2\right]^{1/2}}$$

$$\times \cos\left[\frac{k}{R}\sin^2\psi\left(x_1^2 + x_1'^2\right) + \frac{k}{R}\left(y^2 + y'^2\right) - 2\vartheta_o'\right] dx_1\,dy\,dx_1'\,dy' \quad . \tag{E-1}$$

Making the change of integration variables as depicted in Fig. 5, the author could not find an analytical expression for $J_2$, but approximate expressions showed $J_2$ to be very small compared to $J_1$.

The conclusion that $J_1$ is much less than $J_2$ is borne out by examining the work of Gulin (1962) who has evaluated the integrals $J_1$ and $J_2$ for the Gaussian form of the covariance function. Numerical evaluations of his expressions are illustrated in Fig. E-1 for the case

$$R_{10} = R_{20} = 60.0 \text{ in.} \quad ,$$

$$\sqrt{\langle F_o^2 \rangle} = 0.091 \text{ in.} \quad ,$$

$$a = 2.55 \text{ in.} \quad ,$$

$$k = 10.31 \text{ in.}^{-1} \quad ,$$

which correspond to a frequency of 95,800 mc and a wavelength of 0.608 inch. The values used for $\Delta_1$, $\Delta_2$, and $\ell$ are listed in Table E-I in Appendix B. At a Rayleigh parameter of 0.7 (the theory is valid only for Rayleigh parameters less than one) the amplitude fluctuations, $(J_1 + J_2)^{1/2}$, exceed the phase fluctuations, $(J_1 - J_2)^{1/2}$, by approximately 4 percent. Since for small Rayleigh parameters the amplitude and phase

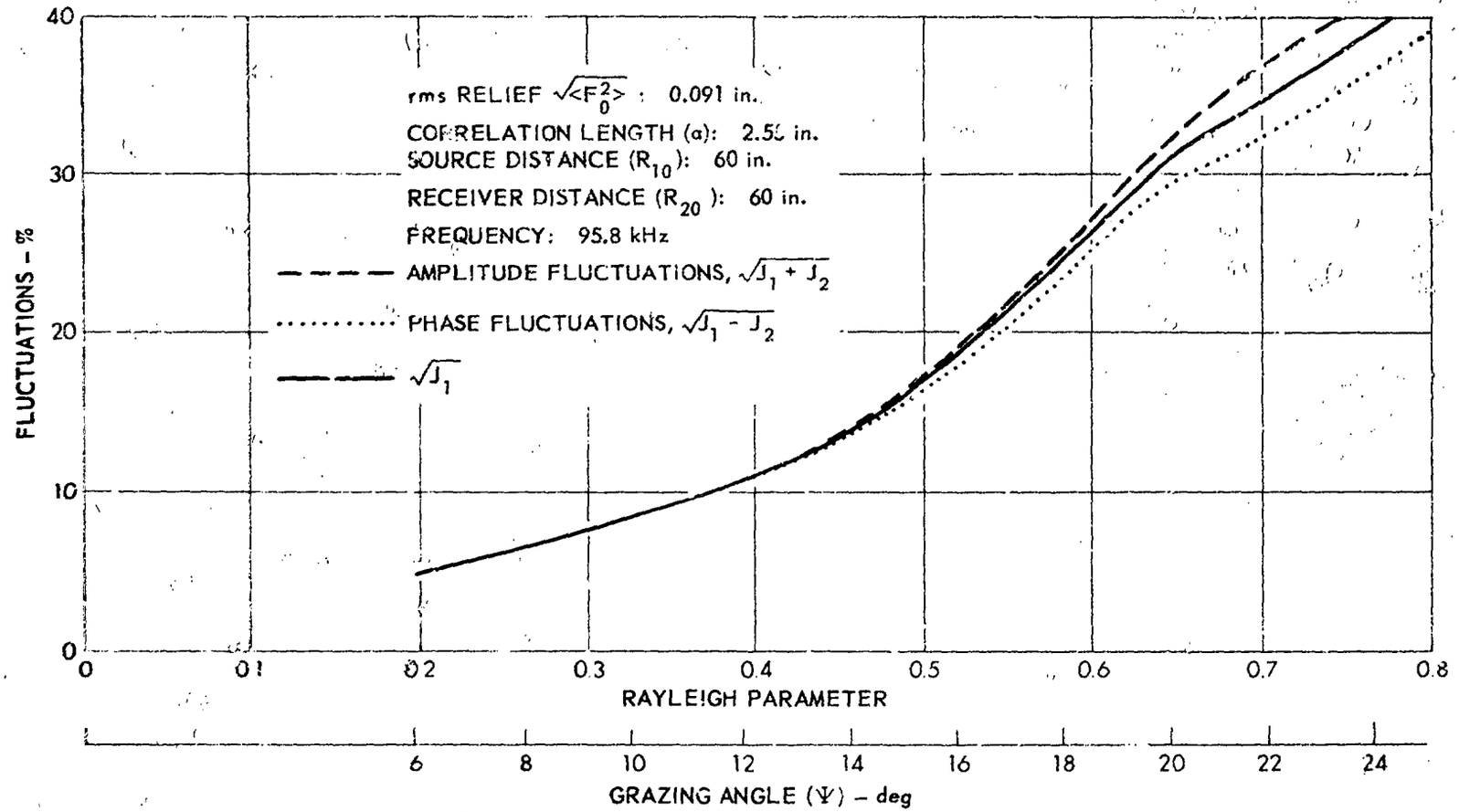


FIGURE E-1
THEORETICAL FLUCTUATIONS
IN THE SPECULAR DIRECTION
FOR A GAUSSIAN COVARIANCE FUNCTION

fluctuations are approximately of the same magnitude, Gulins' expressions for $J_1$ and $J_2$ show, for the example cited, that

$$J_2 \ll J_1 \quad .$$

Figure E-2 shows that the $J_1$ term for the case of an exponential covariance function does not differ much from the $J_1$ term for the case of an Gaussian covariance function, especially in the region of Rayleigh parameters less than one where the theory is valid. Thus, one concludes that the Gulin result of $J_2 \ll J_1$ for the Gaussian case is applicable also to the exponential case.

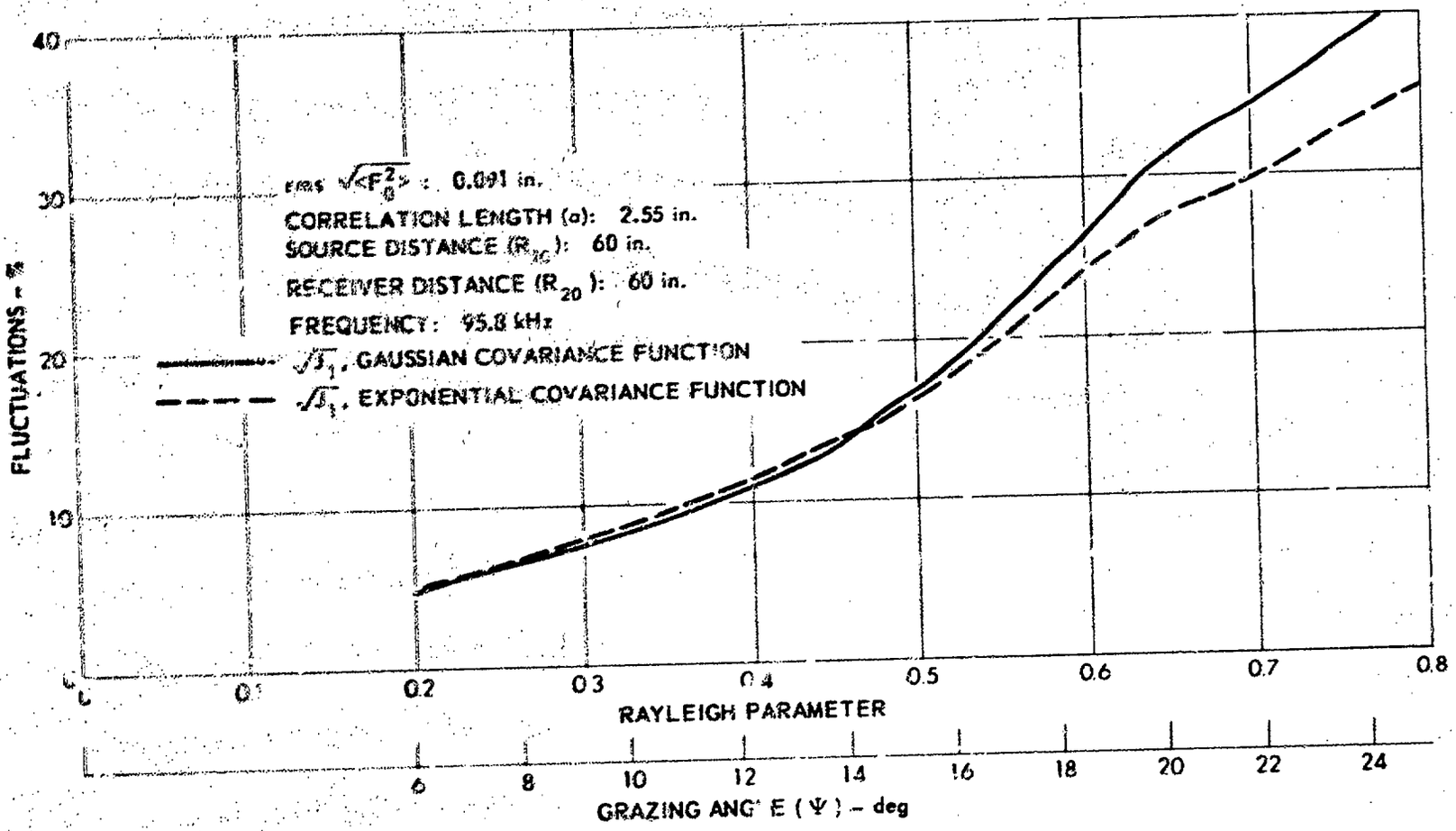


FIGURE E-2
COMPARISON OF FLUCTUATIONS BETWEEN
A GAUSSIAN AND EXPONENTIAL COVARIANCE
FUNCTION IN THE SPECULAR DIRECTION

BIBLIOGRAPHY


Baker, B. B., and E. T. Copson, The Mathematical Theory of Huygen's Principle, Oxford University Press, London, 1939, pp. 23-28.

Barnard, G. R., C. W. Horton, M. K. Miller, and F.R. Spitznogle, "Underwater-Sound Reflection from a Pressure-Release Sinusoidal Surface," J. Acoust. Soc. Am. 39, 1162-1169 (June 1966).

Beckmann, Petr, and A. Spizzichino, The Scattering of Electromagnetic Waves from Rough Surfaces, The MacMillan Company, New York, 1963.

Beckmann, Petr, "Scattering by Composite Rough Surfaces," Proc. IEEE 53, 1012-1015 (August 1965).

Brekhovskikh, L. M., "Wave Diffraction by an Uneven Surface - Part I," (in Russian). zh. éksp. i teor. fiz. 23, 275-289 (1952).

Brown, M. V., and James Ricard, "Fluctuations in Surface-Reflected Pulsed cw Arrivals," J. Acoust. Soc. Am. 32, 1551-1554 (December 1960).

Chernov, Lev A., Wave Propagation in a Random Medium, McGraw-Hill Book Company, Inc., New York, 1960, pp. 58-61.

Clay, C. S., "Fluctuations of Sound Reflected from the Sea Surface," J. Acoust. Soc. Am. 32, 1547-1551 (December 1960).

Eckart, C., "The Scattering of Sound from the Sea Surface," J. Acoust. Soc. Am. 25, 566-570 (May 1953).

Feinstein, Joseph, "Some Stochastic Problems in Wave Propagation-Part I," Trans. IRE AP-2, 23-30 (January 1954).

Gradshteyn, I. S., and I. M. Ryzhik, Table of Integrals Series and Products, Academic Press, New York, 1965.

Gulin, E. P., "Amplitude and Phase Fluctuations of a Sound Wave Reflected from a Statistically Uneven Surface," Akust. Zh. 8, 2, 175-182, (April-June 1962), [Soviet Physics-Acoustics 8, 2, 139-140 (October-November 1962)].

Gulin, E. P., and K. I. Malyshev, "Statistical Characteristics of Sound Signals Reflected from the Undulating Sea Surface," Akust. Zh. 8, 3, 292-300 (July-September 1962), [Soviet Physics-Acoustics 8, 3, 228-234 (January-March 1963)].

Horton, C. W., W. B. Hopkins, and A. A. J. Hoffman, "A Statistical Analysis of Some Aeromagnetic Maps from the Northwestern Canadian Shield," Geophysics 30, 582-601 (August 1964).

Horton, C. W., A. A. J. Hoffman, and W. B. Hempkins, "Mathematical Analysis of the Microstructure of an Area of the Bottom of Lake Travis," Jour. Tex. Acad. Sci. 26, 309-319 (June 1962).

Horton, Sr., C. W., S. K. Mitchell, and G. R. Barnard, "Model Studies on the Scattering of Acoustic Waves from a Rough Surface," J. Acoust. Soc. Am. 41, 635-643 (March 1967).

Horton, Sr., C. W., and G. T. Muir, "Theoretical Studies on the Scattering of Acoustic Waves from a Rough Surface," J. Acoust. Soc. Am. 41, 635-643 (March 1967).

Isakovick, M. A., "Scattering of Waves from a Statistically Rough Surface," (in Russian) Zh. éksp. i teor. fiz. 23, 305-314 (1952).

Kerr, Donald E., Ed., Propagation of Short Radio Waves, McGraw-Hill Book Company, Inc., New York, 1951, pp. 411-418.

Leizer, I. G., "Applicability of the Methods of Geometric Acoustics for the Calculation of Sound Reflection from Plane Surfaces," Akust. Zh. 12, 206-212 (April-June 1966), [Soviet Physics-Acoustics 12, 180-184 (October-December 1966)].

Medwin, Herman, "Specular Scattering of Underwater Sound from a Wind-Driven Surface," J. Acoust. Soc. Am. 41, 1485-1495 (June 1967).

Mitchell, S. K., "Underwater Sound Scattering from an Irregular Surface," Thesis, The University of Texas (1966).

Strutt, J. W. (Lord Rayleigh), The Theory of Sound, Dover Publications, New York, 1945, vol. II, pp. 89-96.

Uretsky, J. L., "Reflection of a Plane Sound Wave from a Sinusoidal Surface," J. Acoust. Soc. Am. 33, 1293-1294 (March 1961).

Uretsky, J. L., "The Scattering of Plane Waves from Periodic Surfaces," Ann. Phys. 33, 400-427 (July 1965).

# VITA

Daniel Rayburn Melton was born in Sulphur Springs, Texas, on November 30, 1938, the son of Rayburn Arlton and Nova Ollie Melton. After having graduated from La Vega High School, Bellmead, Texas, in 1956, he entered Baylor University, Waco, Texas and received the degree of Bachelor of Science in Physics in May 1960. He received the degree of Master of Science in Physics in January 1962 from Baylor University. In February 1962 he was employed in the Research and Technical Department of The Texas Company in Bellaire, Texas. On September 6, 1964, he was married to Celeste Thelma Lawrence in Fayetteville, Arkansas. On a leave of absence from The Texas Company, he entered the Graduate School of The University of Texas at Austin in September 1964.

Permanent address: 1203 Ashleman
Waco, Texas 76705

This dissertation was typed by Alice Kavanaugh.